UNIVERSIDADE FEDERAL DE SÃO CARLOS
CENTRO DE CIÊNCIAS EXATAS E DE TECNOLOGIA
PROGRAMA DE PÓS-GRADUAÇÃO EM MATEMÁTICA

Multilayer Graphene through quantum periodic graphs: Dirac cones

Vinícius Lourenço da Rocha

São Carlos

2020

UNIVERSIDADE FEDERAL DE SÃO CARLOS
CENTRO DE CIÊNCIAS EXATAS E DE TECNOLOGIA
PROGRAMA DE PÓS-GRADUAÇÃO EM MATEMÁTICA

Multilayer Graphene through quantum periodic graphs: Dirac cones

Vinícius Lourenço da Rocha

Supervisor: Prof. Dr. César Rogério de Oliveira

Dissertation submitted to PPGM/UFSCar as partial fulfillment of the requirements for the degree of Doctor of Science.

São Carlos

2020

UNIVERSIDADE FEDERAL DE SÃO CARLOS

Centro de Ciências Exatas e de Tecnologia
Programa de Pós-Graduação em Matemática

Folha de Aprovação

Assinaturas dos membros da comissão examinadora que avaliou e aprovou a Defesa de Tese de Doutorado do candidato Vinicius Lourenço da Rocha, realizada em 06/03/2020:

Prof Dr Cesar Rogerio de Oliveira
UFSCar

Profa. Dra. Alessandra Aparecida Verri
UFSCar

Prof Dr Luiz Roberto Hartmann Junior
UFSCar

Prof Dr Silas Luiz de Carvalho
UFMG

Prof Dr. Tiago Pereira da Silva
ICMC/USP

"If more people valued home, above gold, this world would be a merrier place..."

Thorin Oakenshield

Acknowledgements

First and foremost, I am grateful to God Almighty for giving me the strength, sustaenance, knowledge, ability and opportunity to complete this research study. It would not have been possible without His blessings.

I would like to thank my wife, Beatriz, for being my inconditional support, my love and my inspiration in every moment of my life; I love you.

I am thankful to my family for the love and support, and also for encouraging me to get where I am. It is comfortable to know that you will always be there for me.

I am grateful to my supervisor, Prof. César Rogério, for all the shared expertises, including the ones necessary to develop satisfactorily this research project.

To my friends, colleagues and professors of the Department of Mathematics of Universidade Federal of São Carlos, I owe you my gratitude for the contributions and, of course, the fun in the past four years.

This work had the indispensable financial support of CAPES, for which I am grateful.

Resumo

Neste trabalho, estudamos a caracterização espectral e existência de cones de Dirac, sempre utilizando modelos de grafos quânticos periódicos, em três situações. Na primeira, modelamos materiais bidimensionais e hexagonais, como o Grafeno e Nitreto de Boro. Neste caso, consideramos o operador de Dirac com condições de vértices de Robin. Na segunda situação, propomos uma modelagem de duas e três camadas de grafeno no empilhamento do tipo Bernal (também chamado de empilhamento do tipo AB). Utilizando o operador de Schrödinger com condições de vértice de Neumann, conseguimos expressões exatas para as relações de dispersão desses materiais. Na última situação, também considerando o operador de Schrödinger com condições de Neumann, propomos a modelagem do grafeno multicamada para n folhas, no empilhamento do tipo AA. Para $n = 2, 3$, expressões exatas para a relação de dispersão foram obtidas, enquanto que para $n \geq 4$, utilizamos aproximações para o estudo dos cones de Dirac. Ainda no empilhamento AA, um grafo quântico tridimensional foi proposto para a modelagem e estudo dos cones de Dirac do grafite.

Palavras-Chave: Grafeno, Nitreto de Boro, operador de Schrödinger, operador de Dirac, Grafeno Multicamadas, cones de Dirac, relação de dispersão.

Abstract

We study the spectral characterization and Dirac cones, always through periodic quantum graphs, in three situations. Firstly, we model bidimensional honeycomb materials, for instance, Graphene and Boron Nitride. We consider the Dirac operator with more general Robin vertex condition. Secondly, we propose a model for Bernal-stacked (also called AB-stacked) bilayer and trilayer graphene. Considering the Schrödinger operator with the standard Neumann vertex condition, we have obtained the exact expressions of the dispersion relation for these materials. Finally, also considering the Schrödinger operator with Neumann conditions, we propose the modelling of the AA-stacked multilayer graphene (for n any positive integer) and AA-stacked graphite (a 3D model). For $n = 2, 3$, exact expressions for the dispersion relations were obtained. For $n \geq 4$, approximations was employed for the study of the Dirac cones.

Keywords: Graphene, Boron Nitride, Schrödinger operator, Dirac operator, Multilayer Graphene, Dirac cones, dispersion relation.

List of Figures

1.1 A representation of AB-stacked bilayer graphene. Half of atoms lies over atoms and the other half of atoms lies over the center of a hexagon. 11

2.1 The hexagonal 2D lattice G and its lattice vectors E_1 and E_2; some type-A and type-B points are labeled. 17
2.2 The fundamental domain W. It contains three edges a_1, a_2 and a_3 and two vertices v_1 and v_2. 18
2.3 The reflection lines r_1 and r_2 and hexagons H_1 and H_2. 18
2.4 The four possibilities for $T(H)$. 19
2.5 The Dirac cones on the dispersion relation of the Dirac operator on the diagonal B_d; here, $\alpha_N = \alpha_B = 0$. The solid line for the conduction band and the dashed one for the valence band. 33
2.6 The dispersion relation of the Dirac operator with parameters $\alpha_N = 1$ and $\alpha_B = 0$. The solid line for the conduction band and the dashed one for the valence band. There is no Dirac cone. 34

3.1 The lattice structures of the AB-stacked multilayer graphene. Some type-A and type-B points are labelled. For simplicity, in (b) we present only a few links between sheets. 36
3.2 The fundamental domains $\mathcal{W}_2^{\mathrm{AB}}$ and $\mathcal{W}_3^{\mathrm{AB}}$. 37
3.3 The dispersion relation of the AB-stacked bilayer graphene operator restricted to $\mathcal{B}_d$ and $\theta_1 \in \left[\frac{2\pi}{3} - \frac{\pi}{4}, \frac{2\pi}{3} + \frac{\pi}{4}\right]$, with the parameter $t_0 = 0.3$. There are no Dirac cones, only quadratic touchings. 50

3.4 The dispersion relation of the AB-stacked trilayer graphene operator restricted to $\mathcal{B}_d$ and $\theta_1 \in \left[\frac{2\pi}{3} - \frac{\pi}{4}, \frac{2\pi}{3} + \frac{\pi}{4}\right]$, with the parameter $t_0 = 0.3$. There is a Dirac cone at $2\pi/3$. Note that there is also a quadratic touching at $2\pi/3$. 50

4.1 The lattice structure of AA-stacked multilayer graphene. 55

4.2 The fundamental domain $\mathcal{W}_n^{\mathrm{AA}}$ with two vertices and three edges of each graphene sheet and the connecting edges of consecutive layers. 56

4.3 Dispersion relation for AA-stacked bilayer graphene restricted to $\mathcal{B}_d$ and $\theta_1 \in [-\pi, \pi]$; the curves are calculated for $t_0 = 0.3$. 72

4.4 Dispersion relation for AA-stacked trilayer graphene restricted to $\mathcal{B}_d$ and $\theta_1 \in [\pi, \pi]$; the curves are calculated for $t_0 = 0.3$. 74

4.5 Dispersion relation for AA-stacked graphite restricted to $\mathcal{B}_{\mathrm{g}}^d$ and $\theta_1 \in [-\pi, \pi]$ with $t_0 = 0.3$. Three values of θ_3 were taken: $\theta_3 = 0, \pi/2$ and π. Any $\theta_3 \in (-\pi, \pi)$ generates a similar curve (in fact, interpolating). 76

Contents

1 Introduction **9**

2 Dirac Operator on hexagonal 2D lattice **16**

2.1 Dirac graph for single layer graphene 16

2.2 Spectral Analysis of the Dirac operator 21

2.3 Dirac cones 31

3 AB-Stacked Bilayer and Trilayer Graphene **35**

3.1 Quantum graphs for multilayer graphene structures 35

3.2 Spectral Analysis of the AB-stacked multilayer graphene operator 39

3.3 Study of Dirac cones 49

3.4 Comparison with physics literature 52

4 AA-stacked multilayer graphene and graphite **54**

4.1 Quantum graphs for finite and infinite numbers of graphene sheets 55

4.2 Spectral Analysis 58

4.3 Dirac cones 69

4.4 Conclusions 76

5 Final Conclusions **78**

Bibliography **79**

Chapter 1

Introduction

In practical terms, graphene is a two-dimensional material, a single layer of graphite, with carbon atoms arranged in the well-known honeycomb periodic structure [19, 9, 7]; it is the union of two triangular sublattices (see (2.1)), g_A (with atoms of type-A) and g_B (with atoms of type-B), each atom of type-A has exactly three nearest neighbors, all of type-B, and vice versa. From the spectral viewpoint, the presence of the so-called *Dirac cones*, at the *Dirac points* of the Brillouin zone of graphene, has outstanding physical consequences; for instance, the motion of an electron in this region is effectively described by a two-dimensional Dirac operator with effective zero mass and effective speed of light $c/300$; this Dirac operator was first identified in [11] (and experimentally in [45]).

The experimental isolation of graphene, in 2004, has triggered a large amount of research papers on the subject, mainly in the physics and chemistry literature. Usually such theoretical works are based on tight-binding approximations and numerical simulations, and it is interesting that the first tight-binding consideration was done in 1947 by Wallace [43] as a starting point for understanding the properties of bulk graphite (see also [8]), with the rather surprising result of a zero-gap semiconductor with a linear dispersion relation (Dirac cone), at a finite number of Dirac points. To be more precise, let $\theta = (\theta_1, \theta_2)$ denotes the quasimomentum in the first Brillouin zone $\mathcal{B} := [-\pi, \pi]^2$, and $\lambda(\theta)$ the associated dispersion relation; $\theta_D \in \mathcal{B}$ is a *Dirac point* candidate (*D-point*) if there is a constant $\gamma \neq 0$ so that

$$\lambda(\theta) - \lambda(\theta_D) + \mathcal{O}((\lambda(\theta) - \lambda(\theta_D))^2) = \pm\gamma|\theta - \theta_K| + \mathcal{O}(|\theta - \theta_K|^2),$$

and we have a *Dirac cone*, since valence (the "-" sign above) and conducting (the "+"

sign) bands touch linearly in lowest order approximation.

For mathematical studies of the spectrum and Dirac cones of models based on Schrödinger operators, we mention the works by Fefferman and Weinstein [14] and Kuchment and Post [23]. In [14] the Schrödinger operator with honeycomb periodic smooth potentials is considered and, under some conditions, the presence of Dirac cones was proved. In [23] the authors have considered an approach of a quantum graph model for the graphene and derive its spectral properties, including the presence of Dirac cones (see also [1, 8, 40]). An approach through quantum graphs seems to have been first proposed by Linus Pauling [37] to describe some chemical systems and implemented in [40]. Recall that, in quantum graph models, the electron is confined to the edges of the graph, and the model starts with Schrödinger operators on edges; the usual boundary conditions at the vertices are the Neumann conditions, characterized by continuity and zero total flux at the vertices [23] (it is also explicitly stated in (2.6)). Although the quantum honeycomb graph is an approximation as a model of graphene, it is possible to (rigorously) explicitly obtain the exact dispersion relation via the Floquet-Bloch theory [13, 38] of periodic Schrödinger operators.

Other works with a mathematical approach discuss self-adjoint extensions of the Dirac operator with specific boundary conditions [3, 16], the approximation of the Schrödinger dynamics by a massless Dirac operator [15], confinement of Dirac fermions in graphene [18], etc.

However, about 700 bidimensional materials have been predicted to be stable[1]! One outstanding material is the boron nitride BN[2], with the same honeycomb structure of graphene but with nitrogen atoms at type-A vertices and boron at type-B ones. We restrict ourselves to one or two kinds of atoms and use the BN as a practical paradigm in our discussion.

There is also theoretical and experimental interest in systems composed of finite layers of graphene (see, for instance [2, 6, 24, 26, 30, 32, 33, 35, 36, 39]), also as an approximation for the bulk graphite. There are two important remarks here; first, the strength of the bond between consecutive layers are much weaker than the bonds between neighbor carbon atoms in the same layer (see Remark 3.1.1); second, there are different possibilities for stacking layers of graphene, and it was experimentally found that physical properties depend on

[1] `https://en.wikipedia.org/wiki/Two-dimensional_materials`

[2] `https://en.wikipedia.org/wiki/Boron_nitride`

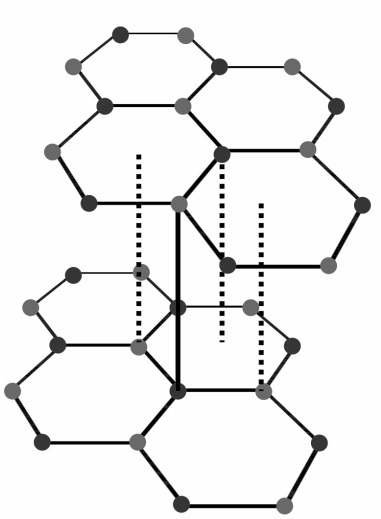

Figure 1.1: A representation of AB-stacked bilayer graphene. Half of atoms lies over atoms and the other half of atoms lies over the center of a hexagon.

how layers are stacked.

The main configurations of multilayer graphene are the AB-stacked form (also called Bernal-stacked), for which half of the atoms lie over an atom of the previous layer and half of the atoms lie directly over the center of a hexagon in the previous layer (see Figure 1.1), and the AA-stacked form, in which all layers are aligned. It has been physically observed that the AB-stacked configuration is more stable than the AA-stacked structure, and so the theoretical and experimental works are more abundant for AB-stacked systems (usually for bilayer and trilayer graphene); however, in some situations the presence of bilayer graphene with AA-stacking is also common [28, 2, 10, 33, 39]. It is expected that the increasing interest in theoretical AA-stacking, including this work, will trigger additional experimental research for this configuration. Here we also consider the AA-stacked bulk graphite as infinitely many layers indexed by the set of integer numbers.

This work is divided in three situations. The first one has a threefold motivation; always through the quantum graph model of a honeycomb structure with at most two different kinds of atoms. First, are there Dirac cones if the graphene is modelled directly by the (massive) Dirac operator, instead of the Schrödinger one? Would we have a possible "relativistic Dirac cone," or is it an artifact of the spectral theory of Schrödinger operators? Second, what is the result if graphene is modelled through the more general Robin boundary condition (see (2.6); which is reduced to the Neumann case when some parameters vanish)? Will Dirac cones be present? Third, we propose to model BN by using two different

parameter values in the Robin boundary conditions; is such model capable to rigorously reproduce basic BN results from the physics and chemistry literature? Note that the second and third motivations apply to the Schrödinger case as well.

In the second situation we investigate spectral properties and the possible presence of Dirac cones for bilayer and trilayer graphene systems, Bernal-stacked (AB-stacked) and modelled by quantum graphs, that is, we extend the mathematical analysis of [23] to two and three AB-stacked graphene sheets. In this setting, we need that all edges are of equal lengths, so the weak interaction between layers should be modelled in an alternative way. Note that we no longer will consider the Dirac operator. Instead, from this point we will consider the Schrödinger operator with the standard Neumann vertex condition; we require the continuity of wavefunctions at the vertices and propose to model the weak interaction between layers through a parameter $t_0 > 0$ in the total flux (i.e., sum of derivatives of wavefunctions) at each vertex (t_0 is the same for all vertices, see (1.4)). Details of the proposed model appear in Section 3.1.

In the last situation we perform a similar study to the case of AB-stacked multilayer graphene, but now for the AA-stacked multilayer graphene and AA-stacked graphite. As before, we suppose that all edges are of equal lengths and models the weak interaction between layers with the parameter t_0 in the Neumann vertex condition (see (1.4) and also (4.4) and (4.5)).

Now we summarize the main results in each situation described above. Details appear in other chapters. Recall that, in the usual quantum graph model, the Schrödinger operator in an edge e of the graph is

$$H_e u(x) = -\frac{\mathrm{d}^2 u}{\mathrm{d}x^2}(x) + q(x)u(x), \tag{1.1}$$

for an even potential $q(x)$, and the full operator is the sum of such operators over all edges with self-adjoint boundary conditions at each vertex v. The Robin vertex condition (also called δ-type condition) is given by

$$\begin{cases} u \text{ is continuous at } v \\ \sum_e \pm u'_e(v) = \delta_v u(v), \end{cases} \tag{1.2}$$

with real parameters δ_v. The first condition is just the continuity of domain elements at each vertex. In the second one, the sum of derivatives is over all edges connected to v, with the "+" sign if v is a initial point of the edge and "−" if it is a final point, the "total

flux at each edge," that here is proportional to the value of the own function at v; if the parameter $\delta_v = 0$ for all vertices v, we have the habitual Neumann condition (considered, e.g., in [23]). We suppose that δ_v may take two values, δ_A and δ_B, for atoms of type-A (e.g., nitrogen) and B (e.g., boron), respectively. Since for the hexagonal graph one may suppose that all type-A vertices are initial points of edges and all type-B vertices are final points, the second condition in (1.2) takes the form

$$\sum_e u'_e(v) = \delta_A u(v), \qquad \sum_e u'_e(v) = -\delta_B u(v), \tag{1.3}$$

if v is of type-A and type-B, respectively.

In Chapter 2, instead of the usual operator H_e above, we consider the Dirac operator D_e on each edge e, whose action is

$$D_e u(x) = -i\hbar c \frac{\mathrm{d}u(x)}{\mathrm{d}x}\alpha + mc^2 u(x)\beta + q(x)u(x)I,$$

where α and β are Pauli matrices (see Section 2.1), I the 2×2 identity matrix, $\hbar, m$ and c are Planck's constant, the mass of the electron and the speed of light, respectively. The above Robin vertex condition has a version for Dirac operators presented in (2.6), and here we again consider the two values δ_A and δ_B for the parameter δ_v.

In Section 2.1 we present details of the construction of the hexagonal graph model with Dirac operators and the Robin boundary conditions; a main difference is that each vector u has two components and the operator is of first order.

In Subsection 2.2 we adapt the spectral description of [23] (Schrödinger with Neumann condition) to the Dirac case with Robin vertex conditions; although we have got similar statements, the proofs require suitable adaptations for the Dirac case; however, we have not obtained eigenvalues of infinite multiplicity, since the construction in [23] does not adjust to the two-components Dirac case.

Then we investigate the possible presence of the Dirac cones in this setting of Dirac operator and more general boundary conditions at vertices; this is the contents of Section 2.3. Here we have (in our opinion) the most interesting results of that chapter; we have proved that Dirac cones may be present in this relativistic model, and they occur if, and only if, $\delta_A = \delta_B$, that is, the parameter δ_v is the same for all vertices (so the same kind of atoms in the honeycomb lattice; of course, including the Neumann case $\delta_v = 0$ for all v discussed in [23]); see Theorem 2.3.1. More precisely, if $\delta_A \neq \delta_B$, there is a (positive) gap between the valence and conduction bands and no point in the dispersion relation is (approximately) linear.

It is worth mentioning that these results also hold true for the Schrödinger case (i.e., Dirac cones do exist if and only if $\delta_A = \delta_B$), although we do not present technicalities since they may be adapted from the proof of Theorem 2.3.1 ahead. So, in Section 2.3 we are able to conclude that, from the point of view of the proposed model with honeycomb symmetry, Dirac cones and their physical consequences, as ballistic electron motion [19, 9, 7], occur only for the graphene and not for BN where a gap in the dispersion relation is found [1, 17, 44, 27]; this is exactly the results from the physics and chemistry literature, where the gap in the BN dispersion relation is usually considered a consequence of electronegativity difference between B and N atoms, here modelled by different Robin parameters.

In Chapter 3, we propose a quantum graph model that is supposed to represent the AB-stacked bilayer and trilayer graphene. We consider the Schrödinger operator described in (1.1) with the usual Neumann vertex condition,

$$\begin{cases} u \text{ is continuous at } v \\ \sum_e u'_e(v) + \sum_f t_0 u'_f(v) = 0, \end{cases} \tag{1.4}$$

where "e" represent the edges on layers and "f" the edges between two consecutive layers, and the parameter t_0 models the weak interaction between consecutive layers of graphene; see details in Section 3.1. In Section 3.2 we perform the spectral analysis of the Schrödinger operator for the AB-stacked bilayer and trilayer graphene. For both bilayer and trilayer cases, the spectra have eigenvalues of infinite multiplicity (the eigenvalues of the Dirichlet Hamiltonian in a single edge). Moreover, an absolutely continuous component built of closed intervals (bands). The singular continuous spectrum is always absent.

In Section 3.3, we prove our main result about Dirac cones for such situation. We show that the bilayer graphene model has no Dirac cones, whereas such cones are present in trilayer graphene dispersion relation. However, the bilayer dispersion relation is gapless and with quadratic touching. Finally, in Section 3.4, we see that the obtained results are consistent with the physics literature.

In Chapter 4, we perform a similar study from Chapter 3. Here we summarize the main differences from both cases. For bilayer and trilayer systems, we have got the presence and exact descriptions of Dirac cones (there are no higher order corrections). For the n-layer graphene, $n \geq 4$, we employ an approximation for general model determinants so that we need to consider small values of $t_0 > 0$, and we have also shown the presence of Dirac cones. It was observed that, for our argument, the higher the number of layers n the closer to

zero t_0 needs to be. Here is a important remark about considering AB-stacked multilayer graphene with n layers of graphene: by employing approximations (and further physical literature) we had evidence that, for n even, the dispersion relation has no Dirac cones. However, we did not managed to prove, in this model, that the approximated parabolic touch does not turns into a Dirac cone for the original problem.

The AA-model for graphite is also shown to present Dirac cones; no approximate model is employed in this situation. Note that Dirac fermions (a consequence of Dirac cones) have also been experimentally reported in graphite [45]. We compare our findings with results obtained in the physics literature for small values of n and graphite. Our work seems to be the first one that considers any finite number of graphene layers, and in a mathematically rigorous approach.

In Section 4.1 we present the construction of the quantum periodic graph that models the AA-stacked multilayer graphene and AA-stacked graphite. In Section 4.2 we study the spectra of the Schrödinger operator in each case. The presence of Dirac cones is proved in Section 4.3 and the obtained results are compared with the physics literature in Section 4.4.

Chapter 2

Dirac Operator on hexagonal 2D lattice

In this chapter, we perform the spectral analysis for the Dirac operator D defined on the hexagonal 2D structure, represented by a quantum periodic graph (see Figure 2.1). The main goal here is to check that we are able to extend some results of [23] about spectral characterization of D and Dirac cones.

In Section 2.1 we present the construction of the quantum periodic graph that is proposed to represent one single layer of a hexagonal 2D material. Examples of hexagonal 2D materials are *Graphene* and *Boron Nitride*, but about 700 two-dimensional materials have been predicted to be stable[1]!

The study of the spectrum of D is presented in Subsection 2.2. Finally, in Section 2.3 we prove our main result about Dirac cones (see Theorem 2.3.1).

2.1 Dirac graph for single layer graphene

Let G be the hexagonal 2D lattice defined as the union of two triangular sublattices g_A and g_B,

$$g_A := \mathbb{Z}E_1 \oplus \mathbb{Z}E_2 \quad \text{and} \quad g_B := (1,0) + \mathbb{Z}E_1 \oplus \mathbb{Z}E_2$$

where

$$E_1 = (3/2, \sqrt{3}/2) \quad \text{and} \quad E_2 = (0, \sqrt{3}) \tag{2.1}$$

[1] https : //en.wikipedia.org/wiki/Two − dimensional_materials

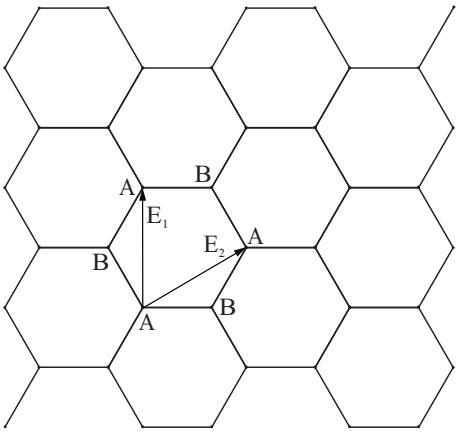

Figure 2.1: The hexagonal 2D lattice G and its lattice vectors E_1 and E_2; some type-A and type-B points are labeled.

are the *lattice vectors*. It is supposed that atoms are situated at the vertices of G and the covalent bonds are represented by edges of length 1 (see Figure 2.1). We denote by $E(G)$ and $V(G)$ the set of edges and set of vertices of G, respectively.

Consider the action of group $\mathbb{Z}^2$ on G defined by the *shift* of $x \in G$ by a vector $p = (p_1, p_2) \in \mathbb{Z}^2$, that is,

$$\mathbb{Z}^2 \times G \ni (p, x) \longmapsto x + p_1 E_1 + p_2 E_2. \tag{2.2}$$

As *fundamental domain* of this action, we choose the set W, as shown in Figure 2.2. It contains two vertices v_1, v_2 and three edges a_1, a_2 and a_3, which are conveniently directed as in Figure 2.2.

Since G is supposed to be embedded into the Euclidean space $\mathbb{R}^2$, we can naturally identify each edge $e \in E(G)$ with the segment $[0, 1]$, which identifies the end points of e with 0 and 1. The arc length metric induces a measure, denoted by dx, which permits to integrate functions on G. We denote a function on G by $u = \{u_e\}_{E(G)}$, where $u_e = \begin{bmatrix} u_e^1 & u_e^2 \end{bmatrix}^\intercal$. Then we can define the Hilbert space of all square integrable functions on G,

$$\mathrm{L}^2(G, \mathbb{C}^2) = \bigoplus_{e \in E(G)} \mathrm{L}^2(e, \mathbb{C}^2),$$

with norm $\|u\|_{L^2(G,\mathbb{C}^2)}$ given by

$$\|u\|^2_{L^2(G,\mathbb{C}^2)} = \sum_{e \in E(G)} \|u_e\|^2_{L^2(e,\mathbb{C}^2)}.$$

Now we define the *Dirac operator* acting on functions of $\mathrm{L}^2(G, \mathbb{C}^2)$. Let q_0 be a real even continuous function on $[0, 1]$, that is, $q_0(x) = q_0(1 - x)$, for all $x \in [0, 1]$. Since each edge

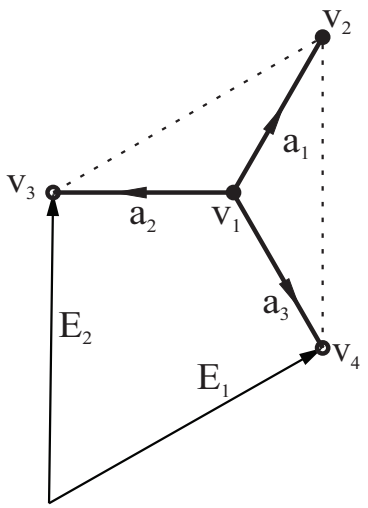

Figure 2.2: The fundamental domain W. It contains three edges a_1, a_2 and a_3 and two vertices v_1 and v_2.

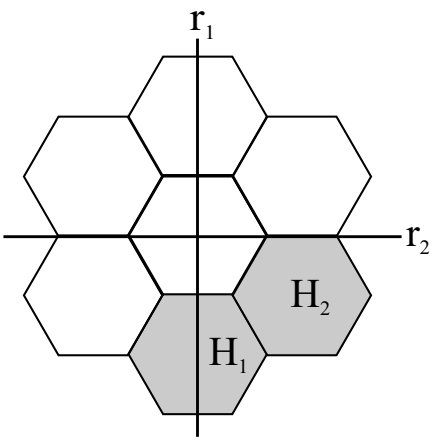

Figure 2.3: The reflection lines r_1 and r_2 and hexagons H_1 and H_2.

$e \in E(G)$ is identified with the segment $[0, 1]$, we can define a *potential* q on G acting in each edge of G as q_0. Note that due the evenness assumption on q_0, the potential q does not depend on the orientations chosen along the edges. We have the following result:

Lemma 2.1.1. *The potential q defined as above is invariant with respect to the symmetry group of the G.*

Proof. The proof of this lemma is analogous to the one presented in [12]. For completeness, we present here the arguments.

Let T_p denote the shift by the integer vector $p_1E_1 + p_2E_2$, where $p = (p_1, p_2) \in \mathbb{Z}^2$ and let R_1 and R_2 denote the reflections with respect to the lines r_1 and r_2 in the Figure 2.3,

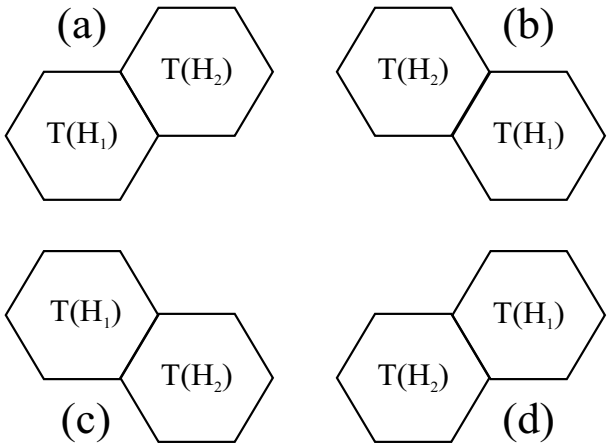

Figure 2.4: The four possibilities for $T(H)$.

respectively. First we prove that the symmetry group of the graph G is generated by T_p, R_1 and R_2, and then show that q is invariant under each of these transformations.

Let $F : G \to G$ be an isometry from the symmetry group of the graph G. Let H_1 and H_2 be the shaded hexagons in the Figure 2.3 and denote $H := H_1 \cup H_2$. Let $p_0 = (p_1^0, p_2^0) \in \mathbb{Z}^2$ such that

$$T(H_1) := T_{p_0}(F(H_1))$$

coincides with H_1, as hexagons. Since T preserves distances, then $T(H)$ is one of the four possibilities of the Figure 2.4.

In the case (a), $T = \mathrm{Id}$, then $F = T_{p_0}$. In the case (b), we have that $T = R_1$, thus $F = T_{p_0}R_1$. In the case (c), $F = T_{p_0}R_2R_1$, since $T = R_2R_1$. Finally, in the case (d), $T = R_2$ which implies $F = T_{p_0}R_2$. Therefore, we can represent any isometry of the symmetry group of G as a combination of T_p, R_1 and R_2.

Now we prove that the potential q is invariant with respect of each of the transforms T_p, R_1 and R_2. Let $M \in e$, $e \in E(G)$, be some point of the graph G. Let $x_e(M)$ be the point in the interval $[0, 1]$ that is identified with M. Since the directions of the edges of G are defined periodically from the directions of the edges a_1, a_2 and a_3 of the fundamental domain W (see Figure 2.2), it follows that $x_e(M) = x_{T_p(e)}(T_p(M))$, $p \in \mathbb{Z}^2$. Then,

$$q(M) = q_0(x_e(M)) = q_0(x_{T_p(e)}(T_p(M))) = q(T_p(M)). \tag{2.3}$$

Thus the potential q is invariant with respect to the shifts T_p, $p \in \mathbb{Z}^2$. For the reflections R_1, and R_2, due the directions of the edges we have

$$x_e(M) = 1 - x_{R_1(e)}(R_1(M))$$

and

$$x_e(M) = x_{R_2(e)}(R_2(M)).$$

Analogous to (2.3), we see that $q(M) = q(R_2(M))$, and since q_0 is even on $[0, 1]$, it follows that

$$\begin{aligned} q(M) &= q_0(x_e(M)) = q_0(1 - x_{R_1(e)}(R_1(M))) \\ &= q_0(x_{R_1(e)}(R_1(M))) = q((R_1(M))). \end{aligned}$$

Therefore, the potential q is invariant with respect to the symmetry group of the graph G. □

Let D be the *Dirac operator* [42] which acts along each edge $e \in E(G)$ as

$$Du_e(x) = -i\hbar c\frac{\mathrm{d}u_e(x)}{\mathrm{d}x}\alpha + mc^2u_e(x)\beta + q(x)u_e(x)I, \tag{2.4}$$

where

$$u_e(x) = \begin{bmatrix} u_e^1(x) \\ u_e^2(x) \end{bmatrix}, \ \alpha = \begin{bmatrix} 0 & 1 \\ 1 & 0 \end{bmatrix}, \ \beta = \begin{bmatrix} 1 & 0 \\ 0 & -1 \end{bmatrix}, \ I = \begin{bmatrix} 1 & 0 \\ 0 & 1 \end{bmatrix} \tag{2.5}$$

and $\hbar$, m and c are Planck's constant, the mass of the electron and the speed of light, respectively. The matrices α and β are *Pauli matrices* and satisfy the algebraic relations

$$\alpha^2 = \beta^2 = I \ \text{ and } \ \alpha\beta + \beta\alpha = 0,$$

The domain of the Dirac operator is the subspace $\operatorname{dom} D$ that consists the functions u on G such that:

(i) $u_e \in H^1(e, \mathbb{C}^2)$, for all $e \in E(G)$, where $H^1(e, \mathbb{C}^2)$ is the usual *Sobolev Space* in the edge e and u_e is the restriction of u to e;

(ii) $\sum_{e\in E(G)} \|u_e\|^2_{H^1(e,\mathbb{C}^2)} < \infty$;

(iii) The *Robin condition* at vertex v (adapted from (1.2)-(1.3)), is defined as

$$\begin{cases} u^1 \text{ is continuous at } v \\ \sum_{e\in E_v(G)} \pm u_e^2(v) = \delta_v u^1(v), \end{cases} \tag{2.6}$$

were $E_v(G)$ is the set of edges of G that contains the vertex v, δ_v is a fixed real number, and the "+" sign in $\pm u_e^2(v)$ if v is the initial point of the edge e and "−"

sign if it is an end point. In the graphene we may take (and we do) type-A vertex as initial points and type-B as final points of vertices, so that the second equation in (2.6) takes the form

$$\sum_{e\in E_v(G)} u_e^2(v) = \pm\delta_v u^1(v),$$

with "+" for type-A vertices and "−" for type-B vertices. The particular case when $\delta_v = 0$, for all $v \in V(G)$, is called *Neumann vertex condition* and it is usually considered the "standard" one.

Remark 2.1.1. *Graphene is composed by a hexagonal 2D lattice such that the carbon atoms are situated at the vertices. In [23], the graphene was modeled by the Schrödinger periodic graph G with Neumann vertex condition, that is, $\delta_v = 0$ for all vertices. A more general suitable boundary condition is to consider a constant $\delta_v = \delta_C$, for all $v \in V(G)$, as we do.*

Boron nitride is a 2D material with hexagonal structure composed by nitrogen and boron atoms; here, nitrogen atoms are situated at type-A vertices whereas the boron atoms are located at type-B vertices. We propose to use different values of the parameter δ_v in Robin condition (2.6) *as a way to differentiate such atoms in the model: if v is a type-A (type-B) vertex, we choose $\delta_v = \delta_N$ ($\delta_v = \delta_B$), with $\delta_N \neq \delta_B$.*

Remark 2.1.2. *If we consider the Robin vertex condition* (2.6) *for the Schrödinger operator (instead the Neumann vertex condition presented in [23]), we see that the first u^1 and second u^2 components of $u \in \operatorname{dom} D$ play the role of the function $u \in \operatorname{dom} H$ and its derivative u', respectively.*

This definition makes D an unbounded self-adjoint operator ([22, Theorem 1.4.19] is easily adapted for the Dirac operator) and, by the evenness condition on the potential and Lemma 2.1.1, its action is invariant with respect to all symmetries of G.

2.2 Spectral Analysis of the Dirac operator

In this section we use the Floquet-Bloch theory [5, 13, 21, 25, 5, 38] to study the spectrum $\sigma(D)$ of D. This theory also holds in the quantum graph case ([23] and references therein). For each *quasimomentum* $\theta = (\theta_1, \theta_2)$ in the *Brillouin zone* $B := [-\pi, \pi]^2$, let

$D(\theta)$ be the *Bloch Dirac operator* acting as in (2.4) on functions of $H^1(W, \mathbb{C}^2)$ that satisfy the conditions (i), (ii) and (iii) of $\operatorname{dom} D$ and also the *cyclic condition* (or *Floquet condition*)

$$u(x + p_1E_1 + p_2E_2) = e^{i(p_1\theta_1 + p_2\theta_2)}u(x), \tag{2.7}$$

for any $p = (p_1, p_2) \in \mathbb{Z}^2$ and $x \in G$. It is known that $D(\theta)$ has purely discrete spectrum $\sigma(D(\theta)) = \{\lambda_n(\theta)\}_n$. The function $\theta \mapsto \{\lambda_n(\theta)\}_n$ is called the *dispersion relation of* D and it determines its spectrum [5]

$$\sigma(D) = \bigcup_{\theta \in B} \sigma(D(\theta)). \tag{2.8}$$

Thus, we need to determine the spectra of $D(\theta)$, for $\theta \in B$, by solving the eigenvalue problem

$$D(\theta)u = \lambda u, \quad u \in \operatorname{dom} D(\theta), \tag{2.9}$$

for $\lambda \in \mathbb{R}$ and $u \neq 0$.

Let us write out the vertex conditions (iii) and the cyclic condition (2.7) on the fundamental domain W. As we identify each edge $e \in E(G)$ with the interval $[0, 1]$, it follows that $v_1 \sim 0$ and $v_i \sim 1$, for $i = 2, 3, 4$ (see Figure 2.2). Thus,

$$\begin{cases} u_{a_1}(1) = u(v_2) = u(v_3 + E_1) = e^{i\theta_1}u(v_3) = e^{i\theta_1}u_{a_2}(1) \\ u_{a_1}(1) = u(v_2) = u(v_4 + E_2) = e^{i\theta_2}u(v_4) = e^{i\theta_2}u_{a_3}(1) \end{cases}. \tag{2.10}$$

Hence, by (2.10), the conditions (iii) and (2.7) on W are equivalent to

$$\begin{cases} u^1_{a_1}(0) = u^1_{a_2}(0) = u^1_{a_3}(0) := \beta_1 \\ u^1_{a_1}(1) = e^{i\theta_1}u^1_{a_2}(1) = e^{i\theta_2}u^1_{a_3}(1) := \beta_2 \\ u^2_{a_1}(0) + u^2_{a_2}(0) + u^2_{a_3}(0) = \delta_N\beta_1 \\ u^2_{a_1}(1) + e^{i\theta_1}u^2_{a_2}(1) + e^{i\theta_2}u^2_{a_3}(1) = -\delta_B\beta_2 \end{cases}. \tag{2.11}$$

We will use now an auxiliary operator. Let D^D denote the *Dirichlet Dirac operator* acting as in (2.4) on functions of $\mathrm{L}^2([0, 1], \mathbb{C}^2)$ that satisfy the *Dirichlet boundary conditions*, that is,

$$u^1(0) = u^2(0) \quad \text{and} \quad u^1(1) = u^2(1). \tag{2.12}$$

It is well known (see [41]) that D^D has pure point spectrum, denoted here by $\sigma(D^D) = \{\lambda^D_n\}_n$. Let $\lambda \notin \sigma(D^D)$. Then there exists two linearly independent solutions $\varphi_{\lambda,0} = \begin{bmatrix} \varphi^1_{\lambda,0} & \varphi^2_{\lambda,0} \end{bmatrix}^\intercal$ and $\varphi_{\lambda,1} = \begin{bmatrix} \varphi^1_{\lambda,1} & \varphi^2_{\lambda,1} \end{bmatrix}^\intercal$ of the eigenvalue problem

$$D\varphi = \lambda\varphi$$

such that

$$\begin{cases} \varphi^1_{\lambda,0}(0) = 1 \\ \varphi^1_{\lambda,0}(1) = 0 \end{cases} \qquad \begin{cases} \varphi^1_{\lambda,1}(0) = 0 \\ \varphi^1_{\lambda,1}(1) = 1 \end{cases} \tag{2.13}$$

and

$$\varphi^2_{\lambda,1}(x) = -\varphi^2_{\lambda,0}(1-x), \quad \forall x \in [0,1]. \tag{2.14}$$

In fact, it is easy to show that $\varphi_{\lambda,0} = \begin{bmatrix} \varphi^1_{\lambda,0} & \varphi^2_{\lambda,0} \end{bmatrix}^\intercal$ exists, then we just take $\varphi_{\lambda,1} = \begin{bmatrix} \varphi^1_{\lambda,1} & \varphi^2_{\lambda,1} \end{bmatrix}^\intercal$ as $\varphi^1_{\lambda,1}(x) = \varphi^1_{\lambda,0}(1-x)$ and $\varphi^2_{\lambda,1}(x) = -\varphi^2_{\lambda,0}(1-x)$, for all $x \in [0,1]$. We can define $\varphi_{\lambda,0}$ and $\varphi_{\lambda,1}$ in each edge $e \in E(G)$ as $(\varphi_{\lambda,i})_e = \varphi_{\lambda,i}$, for $i = 0, 1$, since each edge of the graph G is identified with the interval $[0,1]$. We will keep the same notation $\varphi_{\lambda,i}$ for such functions.

Remark 2.2.1. *In [23], the Schrödinger-Dirichlet operator considered was H^D, which acts on functions $u \in \mathrm{L}^2[0,1]$ as*

$$H^D u(x) = -\frac{\mathrm{d}^2 u(x)}{\mathrm{d}x^2} + q_0(x)u(x)$$

and satisfies the Dirichlet boundary condition $u(0) = u(1) = 0$. Note that there is no condition on the derivative $u'(x)$, differently from the Dirac case that ties the first and second components of u, as we see in (2.12)*. This leads to some technical differences between the Schrödinger and Dirac cases. For instance, in the latter, we can not construct eigenfunctions with infinite multiplicity by following the process presented in [23] (see Remark 2.2.4).*

For each $\lambda \notin \sigma(D^D)$, let

$$\begin{cases} u_{a_1} = \beta_1\varphi_{\lambda,0} + \beta_2\varphi_{\lambda,1} \\ u_{a_2} = \beta_1\varphi_{\lambda,0} + e^{-i\theta_1}\beta_2\varphi_{\lambda,1} \\ u_{a_3} = \beta_1\varphi_{\lambda,0} + e^{-i\theta_2}\beta_2\varphi_{\lambda,1} \end{cases}. \tag{2.15}$$

With the representation (2.15), the continuity (first two) conditions in (2.11) and the eigenvalue problem (2.9) are satisfied. It remains to impose the third and fourth conditions in (2.11). By substituting (2.15) into (2.11),

$$\begin{cases} 3\varphi^2_{\lambda,0}(0)\beta_1 + \bar{F}(\theta)\varphi^2_{\lambda,1}(0)\beta_2 = \delta_N\beta_1 \\ F(\theta)\varphi^2_{\lambda,0}(1)\beta_1 + 3\varphi^2_{\lambda,1}(1)\beta_2 = -\delta_B\beta_2 \end{cases}, \tag{2.16}$$

where $F(\theta) := 1+e^{i\theta_1}+e^{i\theta_2}$ and $\bar{F}(\theta)$ is its complex conjugate. Since $\varphi^2_{\lambda,1}(x) = -\varphi^2_{\lambda,0}(1-x)$ for all $x \in [0,1]$, by (2.14) we have that (2.16) is equivalent to

$$\begin{cases} -3\varphi^2_{\lambda,1}(1)\beta_1 + \bar{F}(\theta)\varphi^2_{\lambda,1}(0)\beta_2 = \delta_N\beta_1 \\ -F(\theta)\varphi^2_{\lambda,1}(0)\beta_1 + 3\varphi^2_{\lambda,1}(1)\beta_2 = -\delta_B\beta_2 \end{cases}. \tag{2.17}$$

Since $\varphi^2_{\lambda,1}(0) \neq 0$, the quotients

$$\eta(\lambda) := \varphi^2_{\lambda,1}(1)/\varphi^2_{\lambda,1}(0), \quad \alpha_N := \delta_N/\varphi^2_{\lambda,1}(0), \quad \alpha_B := \delta_B/\varphi^2_{\lambda,1}(0)$$

are well defined. Hence, after dividing the system (2.17) by $\varphi^2_{\lambda,1}(0)$ and multiplying the second equation by -1, we obtain

$$\begin{cases} (-3\eta(\lambda) - \alpha_N)\beta_1 + \bar{F}(\theta)\beta_2 = 0 \\ F(\theta)\beta_1 + (-3\eta(\lambda) - \alpha_B)\beta_2 = 0 \end{cases}. \tag{2.18}$$

Write (2.18) in matrix form, that is

$$\mathcal{M}(\lambda,\theta)\begin{bmatrix}\beta_1\\ \beta_2\end{bmatrix} = \begin{bmatrix}0\\ 0\end{bmatrix},$$

where

$$\mathcal{M}(\lambda,\theta) = \begin{bmatrix} -3\eta(\lambda) - \alpha_N & \bar{F}(\theta) \\ F(\theta) & -3\eta(\lambda) - \alpha_B \end{bmatrix}. \tag{2.19}$$

Hence, if there exists $\theta \in B$ such that $\det \mathcal{M}(\lambda,\theta) = 0$, then the representation (2.15) solves the eigenvalue problem (2.9) and, by (2.8), it follows that $\lambda \in \sigma(D)$. Such arguments prove the following result:

Proposition 2.2.1. *Let $\lambda \notin \sigma(D^D)$. Then $\lambda \in \sigma(D)$ if and only if there exists $\theta \in B$ such that*

$$9\eta^2(\lambda) + 3(\alpha_N + \alpha_B)\eta(\lambda) + \alpha_N\alpha_B - F(\theta)\bar{F(\theta)} = 0. \tag{2.20}$$

Proposition 2.2.1 says that, in order to obtain the spectrum of the Dirac operator D, except for the countable set $\sigma(D^D)$, we need to know the range of the roots of (2.20), which are given by

$$\eta_\pm(\lambda,\theta) = \frac{-(\alpha_N + \alpha_B) \pm \sqrt{(\alpha_N - \alpha_B)^2 + 4F(\theta)\bar{F}(\theta)}}{6}. \tag{2.21}$$

Remark 2.2.2. *Note that the range of the function*

$$F(\theta)\bar{F}(\theta) = |F(\theta)|^2 = 1 + 8\cos\left(\frac{\theta_1 - \theta_2}{2}\right)\cos\left(\frac{\theta_1}{2}\right)\cos\left(\frac{\theta_2}{2}\right)$$

is $[0, 9]$ *with maximum and minimum attained at* $(0, 0)$ *and* $\pm(2\pi/3, -2\pi/3)$*, respectively. Hence, the functions* $\pm\sqrt{F(\theta)\bar{F}(\theta)}$ *touch each other at* 0 *if and only if* $F(\theta)\bar{F}(\theta) = 0$*, that is, if and only if* $\theta = \pm(2\pi/3, -2\pi/3)$*. Since these points belongs to the diagonal*

$$B_d := \{\theta \in B : \theta_1 = -\theta_2\}, \tag{2.22}$$

in order to analyze the range and maximum/minimum points of (2.21)*, it suffices to consider* $\theta \in B_d$*.*

Now, the proof of the following result is straightforward:

Lemma 2.2.1. *Let* $\lambda \notin \sigma(D^D)$*. Then* $\eta_\pm(\lambda, \theta)$ *given by* (2.21) *are not constant functions in* $\theta \in B$ *and their ranges are given by*

$$\operatorname{img}\eta_+(\lambda, \theta) = [a_+, b_+] \quad \textit{and} \quad \operatorname{img}\eta_-(\lambda, \theta) = [b_-, a_-]\,,$$

where

$$\begin{aligned} a_\pm &= \frac{-(\alpha_N + \alpha_B) \pm |\alpha_N - \alpha_B|}{6} \\ b_\pm &= \frac{-(\alpha_N + \alpha_B) \pm \sqrt{(\alpha_N - \alpha_B)^2 + 36}}{6}. \end{aligned}$$

Moreover,

(i) $\max_{\theta\in B}\eta_+(\lambda, \theta) = b_+$ *and* $\min_{\theta\in B}\eta_+(\lambda, \theta) = a_+$ *which are attained at* $(0, 0)$ *and* $\pm(2\pi/3, -2\pi/3)$*, respectively.*

(ii) $\max_{\theta\in B}\eta_-(\lambda, \theta) = a_-$ *and* $\min_{\theta\in B}\eta_-(\lambda, \theta) = b_-$*, which are attained at* $\pm(2\pi/3, -2\pi/3)$ *and* $(0, 0)$*, respectively.*

It will be convenient to consider the *Dirac Periodic operator* D^{per} acting on functions $u \in H^1(\mathbb{R}, \mathbb{C}^2)$ as

$$D^{\text{per}}u(x) = -i\hbar c\frac{du(x)}{dx}\alpha + mc^2u(x)\beta + q(x)u(x)I, \tag{2.23}$$

where α and β are the Pauli matrices given by (2.5) and $q(x)$ is the potential obtained by extending periodically the even potential q_0 (see Section 2.1) to the whole axis $\mathbb{R}$.

For the spectral problem

$$D^{\text{per}}\varphi = \lambda\varphi, \tag{2.24}$$

let $M(\lambda)$ be the *monodromy matrix* of D^{per}, given by the equation

$$\begin{bmatrix}\varphi^1(1)\\ \varphi^2(1)\end{bmatrix} = M(\lambda)\begin{bmatrix}\varphi^1(0)\\ \varphi^2(0)\end{bmatrix}, \tag{2.25}$$

where φ is any solution of (2.24). The monodromy matrix shifts a solution φ of (2.24) by the period of the potential. In our case, the period is 1. Let

$$d(\lambda) := \operatorname{tr}(M(\lambda))$$

be the *discriminant* of the periodic Dirac operator D^{per}. It is known that $d(\lambda)$ plays the major role in the spectral theory of the periodic Dirac operator (see [5]). In the following, we gather well-known results about the relation between the spectra of D^{per} and its discriminant $d(\lambda)$.

Proposition 2.2.2.

(i) The spectrum $\sigma(D^{\text{per}})$ of periodic Dirac operator is purely absolutely continuous.

(ii) $\sigma(D^{\text{per}}) = \{\lambda \in \mathbb{R} : |d(\lambda)| \leq 2\}$.

(iii) Let $\{\alpha_n\}_n$ and $\{\beta_n\}_n$ be the spectra of the Dirac operator with periodic and semi-periodic conditions on $[0,1]$, respectively, and let

$$B_{2n} = [\alpha_{2n}, \beta_{2n}] \text{ and } B_{2n+1} = [\beta_{2n+1}, \alpha_{2n+1}].$$

Here,

$$\ldots \leq \alpha_n < \beta_n \leq \beta_{k+1} < \alpha_{k+1} \leq \alpha_{k+2} < \ldots,$$

*with $\lim_{n\to\pm\infty} \alpha_n = \pm\infty$. Therefore, $\sigma(D^{\text{per}}) = \cup_n B_n$. The closed non-overlapping intervals B_n are called **spectral bands** (or just **bands**) of $\sigma(D^{\text{per}})$ and the segments (α_n, α_{n+1}) and (β_n, β_{n+1}) are called **spectral gaps** (or just **gaps**).*

(iv) Let $\lambda_k^D \in \sigma(D^D)$ the k^{th} Dirichlet eigenvalue. Then λ_k^D belongs to the closure of $(k+1)^{th}$ gap. If the gap closes, λ_k^D is the intersection point of two bands.

(v) Let B_k be the k^{th} band of $\sigma(D^{\text{per}})$ and let $\lambda \in B_k$. Then $d'(\lambda) \neq 0$ and $d(\lambda) : B_k \longrightarrow [-2,2]$ is a homeomorphism. Moreover, $d(\lambda)$ is decreasing on B_{2k}, increasing on B_{2k+1} and has a single extremum in each spectral gap.

(vi) If $q_0 = 0$, the dispersion relation for D^{per} is given by

$$d(\lambda) = 2\cos\left(\sqrt{\frac{\lambda^2 - (mc^2)^2}{\hbar^2 c^2}}\right). \tag{2.26}$$

Proof. *(i)-(v)* is a collection of well-known results concerning the spectra of periodic Dirac operators (see [13, 21, 25, 5, 38]). Here we present the proof of the item *(vi)*. First, note that, if $q_0 = 0$, then

$$\bar{\psi}_0(x) = e^{i\frac{p}{\hbar}x}\begin{bmatrix} 1 \\ \frac{cp}{\lambda + mc^2} \end{bmatrix} \text{ and } \bar{\psi}_1(x) = e^{-i\frac{p}{\hbar}x}\begin{bmatrix} -\frac{cp}{\lambda - mc^2} \\ 1 \end{bmatrix},$$

are two linearly independent solutions of the eigenvalue problem (2.24). It is easy to see that

$$\phi_0(x) := \frac{1}{2}\bar{\psi}_0(x) - \frac{1}{2}\frac{cp}{\lambda + mc^2}\bar{\psi}_1(x)$$

and

$$\phi_1(x) := \frac{1}{2}\frac{cp}{\lambda - mc^2}\bar{\psi}_0(x) + \frac{1}{2}\bar{\psi}_1(x)$$

are also solutions of (2.24) such that

$$\phi_0(0) = \begin{bmatrix} 1 \\ 0 \end{bmatrix} \text{ and } \phi_1(0) = \begin{bmatrix} 0 \\ 1 \end{bmatrix}.$$

Hence the monodromy matrix is given by (see [5])

$$M(\lambda) = \begin{bmatrix} \phi_0^1(1) & \phi_1^1(1) \\ \phi_0^2(1) & \phi_1^2(1) \end{bmatrix}. \tag{2.27}$$

Calculating $\phi_0^1(1)$ we have:

$$\phi_0^1(1) = \frac{1}{2}e^{i\frac{p}{\hbar}} - \frac{1}{2}\frac{cp}{\lambda + mc^2}\frac{-cp}{\lambda - mc^2}e^{-i\frac{p}{\hbar}} = \cos\left(\frac{p}{\hbar}\right),$$

since

$$\frac{(cp)^2}{\lambda^2 - (mc^2)^2} = 1$$

by the energy-momentum relation

$$\lambda^2 = (cp)^2 + (mc^2)^2. \tag{2.28}$$

Similarly we have that $\phi_1^2(1) = \cos\left(\frac{p}{\hbar}\right)$. Hence, by (2.28) it follows that

$$\frac{p}{\hbar} = \pm\sqrt{\frac{\lambda^2 - (mc^2)^2}{c^2\hbar^2}},$$

and (2.26) is proved. □

Now we check that one is able to extend some results of [23] in order to characterize the spectrum of D. First, we relate the roots $\eta(\lambda)$ of (2.20) to the discriminant $d(\lambda)$ of the periodic Dirac operator D^{per} (see Lemma 2.2.2). Next, we present two lemmas that give conditions on the parameters α_N and α_B in order to obtain $|\eta_\pm(\lambda,\theta)| \leq 1$, for $\theta \in B$. The proofs of these two results are straightforward from Lemma 2.2.1. This is important to relate the spectra of the Dirac operator D to the Dirac-periodic operator D^{per}, given by (2.4) and (2.23), respectively (see Remark 2.2.6).

Lemma 2.2.2. *Let $\lambda \notin \sigma(D^D)$ and $d(\lambda)$ be the discriminant of the periodic Dirac operator D^{per}. Then, we have*

$$\eta(\lambda) = \frac{d(\lambda)}{2}, \tag{2.29}$$

where $\eta(\lambda)$ is a root of (2.20).

Proof. First, we have that $d(\lambda) = \phi_0^1(1) + \phi_1^2(1)$, by (2.27). Since (2.25) holds for any solution of eigenvalue problem (2.24), it is still valid for $\varphi_{0,\lambda}$ and $\varphi_{1,\lambda}$. Then, by (2.25) and (2.27),

$$\begin{aligned}
\varphi_{0,\lambda}^1(1) &= \phi_0^1(1) + \varphi_{0,\lambda}^2(0)\phi_1^1(1) && (2.30)\\
\varphi_{0,\lambda}^2(1) &= \phi_0^2(1) + \varphi_{0,\lambda}^2(0)\phi_1^2(1) && (2.31)\\
\varphi_{1,\lambda}^1(1) &= \varphi_{1,\lambda}^2(0)\phi_1^1(1) && (2.32)\\
\varphi_{2,\lambda}^1(1) &= \varphi_{1,\lambda}^2(0)\phi_1^2(1) && (2.33)
\end{aligned}$$

By (2.13), (2.14) and (2.31), we have that $\phi_0^1(1) = \varphi_{1,\lambda}^2(1)\phi_1^1(1)$. Since $\phi_1^1(1) = 1/\varphi_{1,\lambda}^2(0)$, by (2.33), it follows that $\phi_0^1(1) = \eta(\lambda)$. Finally, (2.33) implies immediately that $\phi_1^2(1) = \eta(\lambda)$. Therefore, (2.29) is proved. □

Lemma 2.2.3. *Let $\alpha_B = \alpha_N$. Then* (2.21) *turns to*

$$\eta_\pm(\lambda,\theta) = \frac{-\alpha_N \pm \sqrt{F(\theta)\bar{F}(\theta)}}{3}. \tag{2.34}$$

Moreover,

(i) If $\alpha_N \in [0,3]$, then $|\eta_+(\lambda,\theta)| \leq 1$, for all $\theta \in B$.

(ii) If $\alpha_N \in [-3,0]$, then $|\eta_-(\lambda,\theta)| \leq 1$, for all $\theta \in B$.

(iii) If $\alpha_N \in (-3, 3)$*, then the touch*

$$\eta_+(\lambda, \pm\theta_D) = \eta_-(\lambda, \pm\theta_D) = \frac{-\alpha_N}{3}, \tag{2.35}$$

with $\theta_D = (2\pi/3, -2\pi/3)$*, lies in* $(-1, 1)$*. The unique case that*

$$|\eta_+(\lambda, \theta)| \leq 1 \quad \textit{and} \quad |\eta_-(\lambda, \theta)| \leq 1$$

simultaneously is when $\alpha_N = \alpha_B = 0$*, representing the standard Neumann vertex condition and the Graphene material (see* (2.6)*).*

Remark 2.2.3. *In Theorem 2.3.1 we shall prove that the touch* (2.35) *is, in fact, a Dirac cone (see Definition 2.3.1).*

The proof of this lemma is analogous to the presented in [12]

Lemma 2.2.4. *Let* $\alpha_N \neq \alpha_B$*. Then* (2.21) *satisfies:*

(i) $|\eta_+(\lambda, \theta)| \leq 1$*, for all* $\theta \in B$*, if* $\alpha_B \in (-3, +\infty)$ *and* $\frac{-3\alpha_B}{3+\alpha_B} \leq \alpha_N \leq 3$*.*

(ii) $|\eta_-(\lambda, \theta)| \leq 1$*, for all* $\theta \in B$*, if* $\alpha_B \in (-\infty, +3)$ *and* $-3 \leq \alpha_N \leq \frac{-3\alpha_B}{3-\alpha_B}$*.*

Remark 2.2.4. *We shall have a look at a spectral difference between* D *and the Schrödinger operator* H*, presented in [23]. It was shown that every Schrödinger-Dirichlet eigenvalue is an eigenvalue of infinite multiplicity of the Schrödinger operator* H*. Moreover, each of the corresponding eigenfunctions vanishes at the vertices of* G *and are supported on a single hexagon of* G *(see Lemma 3.5 of [23]).*

However, for the Dirac operator D *and* $\lambda \in \sigma(D^D)$*, we cannot construct an eigenfunction* ψ_λ *of* D*, supported on a single hexagon, with the Robin vertex boundary conditions* (2.6)*. Indeed, the continuity condition of* (2.6) *implies that the first component* ψ_λ^1 *of* ψ_λ *must vanish at the vertices of* G*; then, since* ψ_λ *is an eigenfunction of* D^D*, it follows that the second component* ψ_λ^2 *of* ψ_λ *must vanish at all vertices of* G*, by* (2.12)*. Hence, necessarily,* $\psi_\lambda = 0$*.*

Finally, we can describe the spectral structure of the Dirac operator D on the hexagonal 2D structure G.

Theorem 2.2.1. *Let* D *be the Dirac operator given by* (2.4)*. Then:*

(i) The singular continuous spectrum of D *is empty.*

(ii) Except possibly for λ in a countable set, the dispersion relation of D is given by

$$d(\lambda) = \frac{-(\alpha_N + \alpha_B) \pm \sqrt{(\alpha_N - \alpha_B)^2 + 4F(\theta)\bar{F}(\theta)}}{3}, \tag{2.36}$$

where α_N and α_B are taken such that $|\eta_\pm(\lambda, \theta)| \leq 1$, for all $\theta \in B$ (see Lemmas 2.2.3 and 2.2.4), and $\eta_\pm(\lambda, \theta)$ are given by (2.21).

(iii) The absolutely continuous spectrum $\sigma_{\mathrm{ac}}(D)$ coincides, as a set, with $\sigma(D^{\mathrm{per}})$, that is, it has band-gap structure and

$$\sigma_{\mathrm{ac}}(D) = \{\lambda \in \mathbb{R} : |d(\lambda)| \leq 2\}. \tag{2.37}$$

Remark 2.2.5. *The countable set considered in Theorem 2.2.1(ii) is, in fact, the eigenvalues of the Dirac operator D^D with Dirichlet boundary conditions.*

Proof. The proof of this theorem is based on Theorem 3.6 of [23] and Theorem 7 of [12]. In the following we present the arguments for *(ii)* and *(iii)*.

(ii) Let $\lambda \notin \sigma(D^D)$. Then, by Proposition 2.2.1, (λ, θ) lies in the dispersion surface of D if and only if, $\eta(\lambda)$ is a root of (2.20), that is,

$$\eta(\lambda) = \frac{-(\alpha_N + \alpha_B) \pm \sqrt{(\alpha_N - \alpha_B)^2 + 4F(\theta)\bar{F}(\theta)}}{6}.$$

By Lemma 2.2.2, $d(\lambda) = 2\eta(\lambda)$. Now, take the parameters α_N and α_B such that $|\eta_+(\lambda, \theta)| \leq 1$ and/or $|\eta_-(\lambda, \theta)| \leq 1$, for all $\theta \in B$, that is, α_N and α_B according to Lemma 2.2.3 or 2.2.4. Hence, (λ, θ) is in the dispersion surface of D if and only if (2.36) holds. This proves *(ii)*.

(iii) Let $\lambda \notin \sigma(D^D)$ and α_N and α_B according to Lemmas 2.2.3 or 2.2.4. Then $\lambda \in \sigma(D)$ if and only if (2.36) holds. By Lemma 2.2.1, we see that $\lambda \in \sigma(D)$ if and only if $|\eta(\lambda)| \leq 1$ (for appropriate α_N and α_B). Since $d(\lambda) = 2\eta(\lambda)$, it follows that $\lambda \in \sigma(D)$ if and only if $|d(\lambda)| \leq 2$, that is, $\lambda \in \sigma(D^{\mathrm{per}})$, by Proposition 2.2.2. Hence

$$\sigma(D) = \sigma(D^{\mathrm{per}}) = \{\lambda \in \mathbb{R} : |d(\lambda)| \leq 2\}.$$

Again by Lemma 2.2.1, $\eta_\pm(\lambda, \theta)$ are not constant functions in $\theta \in B$, for all $\lambda \notin \sigma(D^D)$. Therefore, (2.37) holds. □

Remark 2.2.6. *We underline the importance of Lemmas 2.2.3 and 2.2.4. The Proposition 2.2.1 and Lemma 2.2.2 shown that if $\lambda \notin \sigma(D^D)$, then $\lambda \in \sigma(D)$ if and only if $d(\lambda) = \frac{1}{2}\eta(\lambda)$ is a root of* (2.20). *However, with only this information we can not describe the spectrum*

$\sigma(D)$. Since Proposition 2.2.2 has a complete spectral characterization of D^{per} in terms of $d(\lambda)$ (see item (ii)), then it is convenient to ensure that

$$|\eta(\lambda)| \leq 1, \tag{2.38}$$

in order to be able to compare the spectra $\sigma(D)$ and $\sigma(D^{\mathrm{per}})$. The conditions imposed on δ_B and δ_N in Lemmas 2.2.3 and 2.2.4 implies (2.38) *and the spectral characterization of D is guaranteed.*

2.3 Dirac cones

In this section, we prove our results about existence of *Dirac cones* for the dispersion relation $d(\lambda)$, given by (2.36). As mentioned in the Introduction, roughly, a *Dirac cone* is a point where two spectral bands linearly touch each other, at least in lowest order approximation. Precisely, we have:

Definition 2.3.1. *A point (λ, θ_D) in the dispersion relation, for $\lambda \in \mathbb{R}$ and $\theta_D \in B$, is called a Dirac cone if there is a constant $\gamma \neq 0$ so that*

$$\lambda(\theta) - \lambda(\theta_D) + \mathcal{O}((\lambda(\theta) - \lambda(\theta_D))^2) = \pm\gamma\,|\theta - \theta_D| + \mathcal{O}(|\theta - \theta_D|^2). \tag{2.39}$$

In this case, the quasimomentum θ_D is called a D-point. In (2.39)*, the "$-$" and "$+$" are signs for the valence and conducting bands, respectively.*

Theorem 2.3.1 presents necessary and sufficient conditions on the parameters α_N and α_B to obtain a Dirac cone in the dispersion relation of the Dirac operator D.

Theorem 2.3.1. *Let D be the Dirac operator on the hexagonal 2D lattice G with Robin vertex condition* (2.6)*. Suppose that α_N and α_B are according to Lemmas 2.2.3/2.2.4. Then,*

(i) If $\alpha_N = \alpha_B$, the dispersion relation of D has Dirac cones at the Dirac points $\pm(2\pi/3, -2\pi/3)$ (see Figure 2.5).

(ii) If $\alpha_N \neq \alpha_B$, the dispersion relation of D does not have Dirac points (see Figure 2.6).

Proof. Recall that it suffices to consider θ in the diagonal $B_d = \{\theta \in B : \theta_1 = -\theta_2\}$ of the Brillouin zone, since the possible D-points of the function $F(\theta)\bar{F}(\theta)$, $\pm(2\pi/3, -2\pi/3)$, belongs to B_d (see Remark 2.2.2). In B_d, we have that

$$F(\theta) = \bar{F}(\theta) = 1 + 2\cos(\theta_1).$$

Let $\alpha_N = \alpha_B \in (-3, 3)$ (Lemma 2.2.3*(iii)*). Then by Theorem 2.2.1*(ii)*, it follows that the dispersion relation of D is given by $d(\lambda) = 2\eta_\pm(\lambda, \theta)$, for $\lambda \notin \sigma(D^D)$, where

$$\eta_\pm(\lambda, \theta) = \frac{-\alpha_N \pm |F(\theta)|}{3}. \tag{2.40}$$

In order to prove (2.39), we expand in Taylor's series $d(\lambda)$ around $\lambda(\pm\theta_D)$ and $\eta_\pm(\lambda, \theta)$ around $\pm\theta_D$, where $\theta_D = 2\pi/3$. Expanding $F(\theta)$ around θ_D, we obtain

$$1 + 2\cos(\theta_1) = -\sqrt{3}(\theta_1 - \theta_D) + \mathcal{O}((\theta_1 - \theta_D)^2).$$

Hence,

$$|F(\theta)| = \sqrt{3}|\theta_1 - \theta_D| + \mathcal{O}(|\theta_1 - \theta_D|^2). \tag{2.41}$$

Since $\eta_\pm(\lambda, \theta_D) = -\alpha_N/3$, after substituting (2.41) on (2.40), it follows that

$$\eta_\pm(\lambda, \theta) = \frac{-\alpha_N}{3} \pm \frac{\sqrt{3}}{3}|\theta_1 - \theta_D| + \mathcal{O}(|\theta_1 - \theta_D|^2),$$

which implies

$$\eta_\pm(\lambda, \theta) - \eta_\pm(\lambda, \theta_D) = \pm\frac{\sqrt{3}}{3}|\theta_1 - \theta_D| + \mathcal{O}(|\theta_1 - \theta_D|^2). \tag{2.42}$$

Now we expand $d(\lambda)$ around $\lambda(\theta_D)$. Since we are considering $\lambda \notin \sigma(D^D)$, then $d'(\lambda) \neq 0$ by Proposition 2.2.2*(v)*. Hence,

$$d(\lambda(\theta)) - d(\lambda(\theta_D)) = d'(\lambda(\theta_D))(\lambda(\theta) - \lambda(\theta_D)) + \mathcal{O}((\lambda(\theta) - \lambda(\theta_D))^2). \tag{2.43}$$

In particular, if $q_0 = 0$, then by Proposition 2.2.2*(vi)*,

$$d(\lambda) = 2\cos\sqrt{\frac{\lambda^2 - (mc^2)^2}{\hbar^2 c^2}}. \tag{2.44}$$

Hence,

$$d'(\lambda(\theta)) = -\frac{2\lambda(\theta_D)}{\hbar c\sqrt{\lambda(\theta_D)^2 - (mc^2)^2}}\ \sin\left(\sqrt{\frac{\lambda(\theta_D)^2 - (mc^2)^2}{(\hbar c)^2}}\right). \tag{2.45}$$

Combining (2.42) and (2.43), we obtain

$$\lambda(\theta) - \lambda(\theta_D) + \mathcal{O}((\lambda(\theta) - \lambda(\theta_D))^2) = \pm\frac{2}{\sqrt{3}}\frac{1}{d'(\lambda(\theta_D))}|\theta - \theta_D| + \mathcal{O}(|\theta - \theta_D|^2),$$

that is, (2.39) holds for

$$\gamma = \frac{2}{\sqrt{3}d'(\lambda(\theta_D))}. \tag{2.46}$$

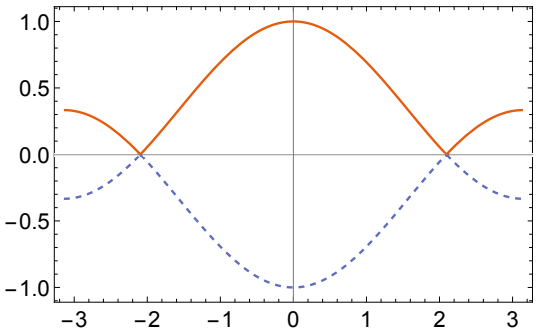

Figure 2.5: The Dirac cones on the dispersion relation of the Dirac operator on the diagonal B_d; here, $\alpha_N = \alpha_B = 0$. The solid line for the conduction band and the dashed one for the valence band.

If we consider $-\theta_D$, the proof is analogous. Therefore, *(i)* is proved.

Now, suppose that $\alpha_N \neq \alpha_B$ and recall Lemmas 2.2.1 and 2.2.4. Let $\theta \in B_d$, as before. By Lemma 2.2.1,

$$\eta_\pm(\lambda, \theta_D) = \frac{-(\alpha_N + \alpha_B) \pm |\alpha_N - \alpha_B|}{6},$$

and so $\eta_+(\lambda, \theta)$ and $\eta_-(\lambda, \theta)$ never touch each other in this case. Furthermore, we will show that $\eta_\pm(\lambda, \theta)$ does not have a linear behavior around $\pm\theta_D$. In fact, expanding in Taylor's series, we obtain

$$\eta_\pm(\lambda, \theta) - \eta_\pm(\lambda, \pm\theta_D) = \frac{d\eta_\pm(\lambda, \pm\theta_D)}{d\theta_1}(\theta_1 - (\pm\theta_D)) + \mathcal{O}((\theta - (\pm\theta_D))^2);$$

however,

$$\frac{d\eta_\pm(\lambda, \pm\theta_D)}{d\theta_1} = \frac{4F(\pm\theta_D)\frac{dF(\pm\theta_D)}{d\theta}}{\sqrt{(\alpha_N + \alpha_B)^2 + 4F(\pm\theta_D)^2}} = 0,$$

since $F(\pm\theta_D) = 0$. Therefore, $\eta_\pm(\lambda, \theta)$ is not linear around $\pm\theta_D$. Therefore, the dispersion relation of the Dirac operator does not have any Dirac points if $\alpha_N \neq \alpha_B$. □

Therefore, we conclude that

Corollary 2.3.1. *The dispersion relation of the Dirac operator D modelling the boron nitride, that is, $\delta_N \neq \delta_B$ in the Robin vertex condition* (2.6) *(see Remark 2.1.1), does not have Dirac cones. On the other hand, if one has just one kind of atom on all vertices, then Dirac cones are present.*

Remark 2.3.1. *We had a quick look at the formal nonrelativistic limit of the discriminant* (2.44)*, used to derive the dispersion relation for the (graphene) quantum graph model*

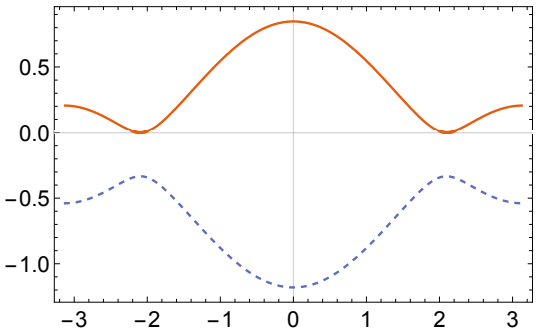

Figure 2.6: The dispersion relation of the Dirac operator with parameters $\alpha_N = 1$ and $\alpha_B = 0$. The solid line for the conduction band and the dashed one for the valence band. There is no Dirac cone.

through Dirac operator with zero potential, that is,

$$d_D(\lambda_D) = 2\cos\left(\sqrt{\frac{\lambda_D^2 - (mc^2)^2}{\hbar^2 c^2}}\right).$$

We have appended the subindex D to indicate the relativistic version, for both, d_D and energy λ_D. We have then computed such quantity for the Schrödinger case, also with zero potential, but taking into account the physical constants, so that

$$H_e u(x) = -\frac{\hbar^2}{2m}\frac{\mathrm{d}^2 u}{\mathrm{d}x^2}(x),$$

and have got

$$d_S(\lambda_S) = 2\cos\left(\sqrt{\frac{2m}{\hbar^2}}\lambda_S\right), \tag{2.47}$$

with the subindex S to indicate the nonrelativistic version. Let's assume that the electron is in a regime so that the nonrelativistic energy $0 < \lambda_S \ll mc^2$ and that the relativistic one is $\lambda_D = mc^2 + \lambda_S$, that is, the nonrelativistic energy plus the electron rest mass energy. So, after inserting

$$\lambda_D^2 - (mc^2)^2 = \lambda_S^2 + 2\lambda_S mc^2 \approx 2\lambda_S mc^2$$

into (2.44)*, the nonrelativistic version* (2.47) *is recovered. Furthermore, for the important slope γ of the Dirac cones we have (see* (2.46)*)*

$$\gamma_D = \frac{2}{\sqrt{3}}\frac{1}{d'_D(\lambda_D)}, \qquad \gamma_S = \frac{2}{\sqrt{3}}\frac{1}{d'_S(\lambda_S)},$$

and, under the above conditions, the nonrelativistic γ_S is recovered from the relativistic one γ_D as well.

Chapter 3

AB-Stacked Bilayer and Trilayer Graphene

In this chapter, we propose a quantum graph model that is supposed to represent the Bernal-stacked (also called AB-stacked) bilayer and trilayer graphene. This approach is based on the quantum graph model for a single layer of graphene, proposed by Kuchment and Post in [23]. We investigate the spectral properties of the Schrödinger operator H_n^{AB}, $n = 2, 3$, defined on this structure (see (3.2)). Also, we study the possible presence of Dirac cones in the dispersion relation of H_n^{AB} (see Definition 2.3.1). We decided to consider here (as well in Chapter 4), the Schrödinger operator instead the Dirac operator, since the obtained results in Chapter 2 are similar to those obtained in [23].

In Section 3.1 we present the proposed quantum graph geometry and the Schrödinger operators that represent the variations of Bernal-stacked graphene. A spectral analysis of the bilayer and trilayer Schrödinger operator is performed in Section 3.2. The possible presence of Dirac cones is presented in Section 3.3. Finally, in Section 3.4, some comparisons with the physics literature are done.

3.1 Quantum graphs for multilayer graphene structures

Now we introduce the periodic quantum graphs that is proposed to represent the *AB-stacked bilayer/trilayer graphene*; we need a metric graph structure and a suitable Hamil-

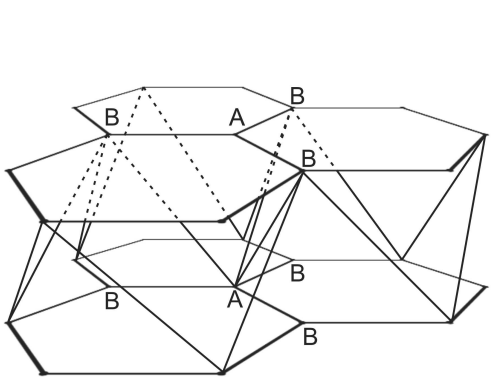

(a) Bilayer graphene.

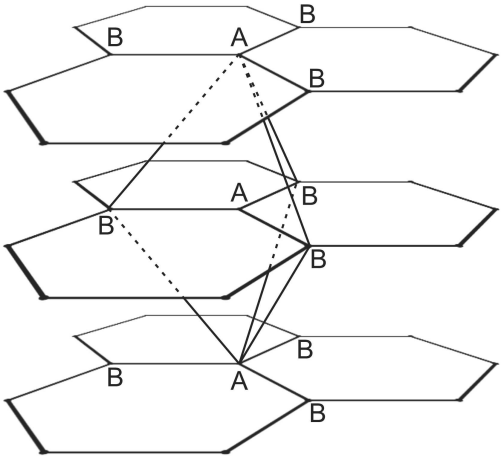

(b) Trilayer graphene.

Figure 3.1: The lattice structures of the AB-stacked multilayer graphene. Some type-A and type-B points are labelled. For simplicity, in (b) we present only a few links between sheets.

tonian.

In following, G_i always denote a single layer of graphene, defined in Chapter 2 (see Figure 2.1) . The structure of the bilayer graphene, denoted by $\mathcal{G}_2^{AB}$, consists of two sheets of graphene, G_1 and G_2 stacked such that a type-A vertex of G_1 is located exactly above the corresponding type-A vertex of G_2 and alike for type-B vertices; that is, the sheets are alined. The only connections between G_1 and G_2 are that each type-A vertex of G_1 is connected with the nearest three type-B vertices of G_2 (see Figure 3.1(a)); such connections are performed through additional edges.

The trilayer graphene, denoted by $\mathcal{G}_3^{\mathrm{AB}}$, consists of three graphene sheets, G_1, G_2 and G_3, in an analogous alined stacking of the bilayer case, but now each type-B vertex of G_2 is linked up (only) with the nearest three type-A vertices of G_1 and the nearest three type-A vertices of G_3, a total of six additional connections (see Figure 3.1(b)). In both cases, the distance between two consecutive graphene sheets is taken in such way that every edges in $\mathcal{G}_n^{\mathrm{AB}}$ have length 1, for $n = 2, 3$; ahead we describe how we control the interaction intensity between consecutive graphene sheets.

Consider the action of group $\mathbb{Z}^2$ on $\mathcal{G}_n^{\mathrm{AB}}$,

$$\mathcal{S} : \mathbb{Z}^2 \times \mathcal{G}_n^{\mathrm{AB}} \to \mathcal{G}_n^{\mathrm{AB}}, \quad \mathcal{S}(p, x) := x + p_1 E_1 + p_2 E_2, \tag{3.1}$$

where E_1 and E_2 are given by (2.1) and $x = x_1 E_1 + x_2 E_2$, that is, $\mathcal{S}$ shifts $x \in \mathcal{G}_n^{\mathrm{AB}}$ by

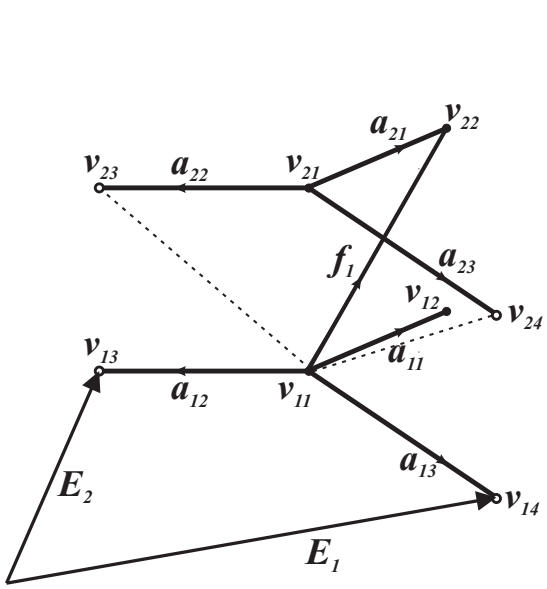

(a) $\mathcal{W}_2^{\mathrm{AB}}$ of the bilayer graphene.

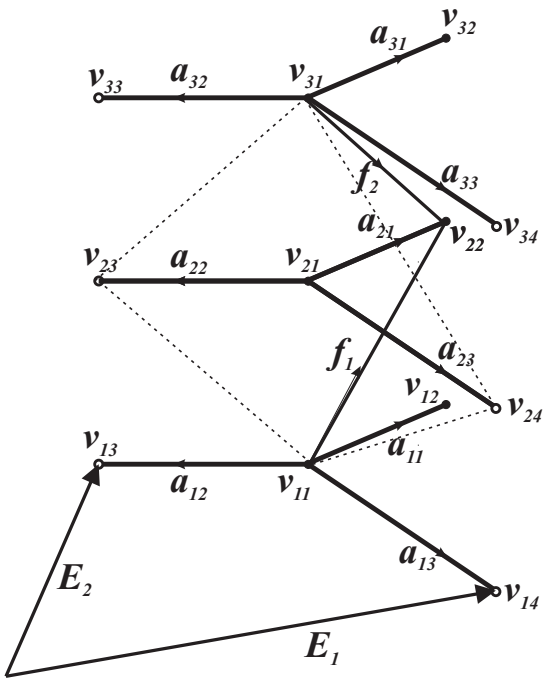

(b) $\mathcal{W}_3^{\mathrm{AB}}$ of the trilayer graphene.

Figure 3.2: The fundamental domains $\mathcal{W}_2^{\mathrm{AB}}$ and $\mathcal{W}_3^{\mathrm{AB}}$.

$p_1E_1 + p_2E_2$, $p = (p_1, p_2) \in \mathbb{Z}^2$. As fundamental domain of $\mathcal{S}$, we choose the set $\mathcal{W}_n^{\mathrm{AB}}$ as shown in Figure 3.2, which contains two points and three edges of each graphene sheet G_k, and the edges that connect consecutive layers (as discussed above). It will be convenient to direct the edges as in Figure 3.2. We label the sheet's edges by the letter "a" whereas the edges between two consecutive sheets are labeled by "f". Let $E(\mathcal{G}_n^{\mathrm{AB}})$ denote the set of edges of $\mathcal{G}_n^{\mathrm{AB}}$. Moreover, let $\bar{E}(\mathcal{G}_n^{\mathrm{AB}})$ and $\tilde{E}(\mathcal{G}_n^{\mathrm{AB}})$ denote the set of edges of graphene sheets and between the graphene sheets, respectively. Hence, $E(\mathcal{G}_n^{\mathrm{AB}}) = \bar{E}(\mathcal{G}_n^{\mathrm{AB}}) \cup \tilde{E}(\mathcal{G}_n^{\mathrm{AB}})$.

Since $\mathcal{G}_n^{\mathrm{AB}}$ is supposed to be embedded into the Euclidean space $\mathbb{R}^3$, we identify each edge $e \in E(\mathcal{G}_n^{\mathrm{AB}})$ with the segment $[0, 1]$, which identifies the end points of e with 0 and 1. Hence, we can define, derivate and integrate functions on $\mathcal{G}^{\mathrm{AB}}$. We denote a function on $\mathcal{G}_n^{\mathrm{AB}}$ by $u = \{u_e\}_{e \in E(\mathcal{G}_n^{\mathrm{AB}})}$, where u_e is a function defined on the edge e. One can naturally define the Hilbert space of all square integrable functions on $\mathcal{G}_n^{\mathrm{AB}}$,

$$\mathrm{L}^2(\mathcal{G}_n^{\mathrm{AB}}) = \bigoplus_{e \in E(\mathcal{G}_n^{\mathrm{AB}})} \mathrm{L}^2(e),$$

with norm

$$\|u\|^2_{L^2(\mathcal{G}^{\mathrm{AB}})} := \sum_{e \in E(\mathcal{G}_n^{\mathrm{AB}})} \|u_e\|^2_{L^2(e)}.$$

To see $\mathcal{G}_n^{\mathrm{AB}}$ as a periodic quantum graph, it remains to introduce the Schrödinger operator acting in $\mathrm{L}^2(\mathcal{G}_n^{\mathrm{AB}})$. Let $q_0 : [0,1] \to \mathbb{R}$ be an even continuous function, that is, $q_0(x) = q_0(1-x)$ for all $x \in [0,1]$. As we have identified the edges of $\mathcal{G}_n^{\mathrm{AB}}$ with the segment $[0,1]$, we can define a *potential* $q = \{q_e\}_{e \in E(\mathcal{G}_n^{\mathrm{AB}})}$ on $\mathcal{G}_n^{\mathrm{AB}}$, where $q_e = q_0$, for all $e \in E(\mathcal{G}_n^{\mathrm{AB}})$. Note that due the evenness assumption on q_0, the potential q does not depend on the orientations chosen along the edges; an even potential is a consequence of the fact that we have the same kind of atoms at the vertices. The following result is easily extended from Lemma 2.1.1 for this case.

Lemma 3.1.1. *The above potential q is invariant with respect to the symmetry group of $\mathcal{G}_n^{\mathrm{AB}}$.*

Finally, we introduce the *Bernal-stacked multilayer graphene Schrödinger operator* H_n^{AB}, $n = 2, 3$, which acts on a function $u \in \mathrm{dom}\,(H_n^{\mathrm{AB}})$ as

$$H_n^{\mathrm{AB}} u_e(x_e) := (-\Delta + q(x))u_e(x_e) = -\frac{\mathrm{d}^2 u_e(x_e)}{\mathrm{d}x^2} + q_e(x_e)u_e(x_e)\,, \tag{3.2}$$

for all $e \in E(\mathcal{G}_n^{\mathrm{AB}})$. When the context is clear, the subscript "e" will be omitted. The domain $\mathrm{dom}\,(H_n^{\mathrm{AB}})$ consists of the functions u on $\mathcal{G}_n^{\mathrm{AB}}$ such that

(i) $u_e \in H^2(e)$, for all $e \in E(\mathcal{G}_n^{\mathrm{AB}})$, where $H^2(e)$ is the usual *Sobolev Space* in the edge e;

(ii) $\displaystyle\sum_{e \in E(\mathcal{G}_n^{\mathrm{AB}})} \|u_e\|^2_{H^2(e)} < \infty$;

(iii) The *Neumann vertex conditions* (or *Kirchhoff vertex conditions*), which requires the continuity of the functions (3.3) at each vertex $v \in V(\mathcal{G}_n^{\mathrm{AB}})$ and the vanishing of the total flux (3.4) at v, that is,

$$u_{e_1}(v) = u_{e_2}(v), \text{ for all } e_1, e_2 \in E_v(\mathcal{G}_n^{\mathrm{AB}}), \tag{3.3}$$

$$\sum_{a \in \bar{E}_v(\mathcal{G}_n^{\mathrm{AB}})} u'_a(v) + \sum_{f \in \tilde{E}_v(\mathcal{G}_n^{\mathrm{AB}})} t_0\, u'_f(v) = 0, \tag{3.4}$$

where $\bar{E}_v(\mathcal{G}_n^{\mathrm{AB}})$ is the set of edges of the graphene sheets that contains the vertex v, $\tilde{E}_v(\mathcal{G}_n^{\mathrm{AB}})$ is the set of edges between consecutive sheets of graphene sheets that contains v, $u'_e(v)$ is the derivate of u_e directed from v to the other vertex of e and $0 < t_0$ is an interaction (real) parameter between consecutive layers.

This definition makes H_n^{AB} an unbounded self-adjoint operator [22, 20, 4] and, by the evenness condition on the potential and Lemma 3.1.1, it is invariant with respect to all symmetries of the graph $\mathcal{G}_n^{\mathrm{AB}}$.

Remark 3.1.1. *A word on the role of the interaction parameter t_0. The interaction between consecutive layers of graphene is weaker than the interaction between neighboring carbon atoms in the same layer. If $t_0 = 1$ we would have no distinction between the interactions; so we have proposed to take $0 < t_0 < 1$ as a way to control the influence of an atom in a different sheet to the flux through a vertex; the smaller t_0 smaller the influence. However, the general results here (Theorems 3.2.1 and 4.3.1) hold true for all positive values of the interaction parameter $t_0 > 0$, and so it is natural to ask whether such property is shared with other models, as the tight-binding one; we don't know the answer.*

3.2 Spectral Analysis of the AB-stacked multilayer graphene operator

In this section we use Floquet-Bloch theory [13, 21, 38, 5] to study the spectrum of H_n^{AB}; we extend results of [23]. We begin with general remarks, then we specialize to bilayer ad trilayer graphene.

For each *quasimomentum* $\theta = (\theta_1, \theta_2)$ in the Brillouin zone $\mathcal{B} = [-\pi, \pi]^2$, let $H_n^{\mathrm{AB}}(\theta)$ be the *Bloch Hamiltonian* acting in $\mathrm{L}^2(\mathcal{W}_n^{\mathrm{AB}})$ as in (3.2), but with a different domain: $\mathrm{dom}\,(H_n^{\mathrm{AB}}(\theta))$ is the subspace of functions u that satisfy (i), (ii) and (iii) in $\mathrm{dom}\,(H_n^{\mathrm{AB}})$, and also the following *Floquet condition*

$$u(x + p_1E_1 + p_2E_2) = e^{ip\theta}u(x) = e^{i(p_1\theta_1 + p_2\theta_2)}u(x), \tag{3.5}$$

for all $p = (p_1, p_2) \in \mathbb{Z}^2$ and all $x \in \mathcal{G}_n^{\mathrm{AB}}$. It is well known that $H_n^{\mathrm{AB}}(\theta)$ has purely discrete spectrum [22], denoted by $\sigma(H_n^{\mathrm{AB}}(\theta)) = \{\lambda_k(\theta)\}_{k\geq 1}$. The function $\theta \mapsto \{\lambda_k(\theta)\}$ is called the *dispersion relation* of H_n^{AB} and it determines its spectrum [13, 21, 38, 5]

$$\sigma(H_n^{\mathrm{AB}}) = \bigcup_{\theta\in\mathcal{B}} \sigma(H_n^{\mathrm{AB}}(\theta)). \tag{3.6}$$

The goal now is to determine the spectra of $\sigma(H_n^{\mathrm{AB}}(\theta))$, $\theta \in \mathcal{B}$, by solving the eigenvalue problem

$$H_n^{\mathrm{AB}}(\theta)u = \lambda u, \quad \lambda \in \mathbb{R}, \quad u \in \mathrm{dom}\,(H_n^{\mathrm{AB}}(\theta)). \tag{3.7}$$

Consider two auxiliary operators. The first one is the *Dirichlet Schrödinger operator* H^D that acts in $\mathrm{L}^2([0,1])$ as

$$H^D u(x) = -\frac{\mathrm{d}^2 u(x)}{\mathrm{d}x^2} + q_0(x)u(x), \tag{3.8}$$

where u satisfies the Dirichlet boundary condition, that is,

$$u(0) = u(1) = 0. \tag{3.9}$$

It is well known that H^D has purely discrete spectrum, denoted by $\sigma(H^D) = \{\lambda_k^D\}_{k\geq 1}$ (see, for instance, [5]).

In order to describe the second operator, let q_p be the *potential function* obtained by extending periodically q_0 to the whole real axis $\mathbb{R}$. The *Hill operator* H^{per} acts in $\mathrm{L}^2(\mathbb{R})$ as

$$H^{\mathrm{per}} u(x) = -\frac{\mathrm{d}^2 u(x)}{\mathrm{d}x^2} + q_p(x)u(x). \tag{3.10}$$

For the spectral problem

$$H^{\mathrm{per}}\varphi = \lambda\varphi, \tag{3.11}$$

consider the *monodromy matrix* $M(\lambda)$ of H^{per} given by (see [5])

$$\begin{bmatrix} \varphi(1) \\ \varphi'(1) \end{bmatrix} = M(\lambda) \begin{bmatrix} \varphi(0) \\ \varphi'(0) \end{bmatrix}, \tag{3.12}$$

where φ is any solution of the problem (3.11). The matrix $M(\lambda)$ shifts $\begin{bmatrix} \varphi(0) & \varphi'(0) \end{bmatrix}^{\mathsf{T}}$ by the period of q_p (in our case, 1). Let

$$\mathcal{D}(\lambda) := \mathrm{tr}(M(\lambda))$$

be the *discriminant* of the Hill operator H^{per}. There are many results and properties about the spectrum of the Hill operator H^{per} and its discriminant $\mathcal{D}(\lambda)$ (similar to the Proposition 2.2.2 for periodic Dirac operator). The next proposition is a collection of well-known results concerning the Hill operator and its discriminant (see [13, 21, 25, 5, 38]).

Proposition 3.2.1. *Let H^{per} be the Hill operator given by* (3.10)*. Then:*

(i) The spectrum $\sigma(H^{\mathrm{per}})$ of the Hill operator is purely absolutely continuous.

(ii) $\sigma(H^{\mathrm{per}}) = \{\lambda \in \mathbb{R} : |\mathcal{D}(\lambda)| \leq 2\}$.

(iii) *Let $\{\alpha_n\}_n$ and $\{\beta_n\}_n$ be the spectra of the Hill operator with periodic and anti-periodic conditions on $[0,1]$, respectively, and let*

$$B_{2k} = [\alpha_{2k}, \beta_{2k}] \text{ and } B_{2k+1} = [\beta_{2k+1}, \alpha_{2k+1}].$$

Here,

$$\alpha_0 < \beta_0 \leq \beta_1 < \alpha_1 \leq \alpha_2 < \dots,$$

with $\lim_{k\to\infty} \alpha_k = \infty$. Therefore, $\sigma(H^{\text{per}}) = \cup_k B_k$. The closed non-overlapping intervals B_k are called bands of $\sigma(H^{\text{per}})$ and the segments (α_k, α_{k+1}) and (β_k, β_{k+1}) are called spectral gaps.

(iv) *Let $\sigma(H^D) = \{\lambda_k^d\}_k$ and let $\lambda_j^d \in \sigma(H^D)$ the j^{th} Dirichlet eigenvalue. Then λ_j^d belongs to the closure of the j^{th} gap. If q_0 is symmetric, then λ_j^d is one of the two edges of the gap. If the gap closes (to a single point), λ_j^d is the intersection point of two bands.*

(v) *Let B_j be the j^{th} band of $\sigma(H^{\text{per}})$ and let $\lambda \in B_j$. Then $\mathcal{D}'(\lambda) \neq 0$ and $\mathcal{D}(\lambda) : B_j \longrightarrow [-2,2]$ is a homeomorphism. Moreover, $\mathcal{D}(\lambda)$ is decreasing on $(-\infty, \beta_0)$ and B_{2k}, increasing on B_{2k+1} and has a single extremum in each spectral gap.*

(vi) *If $q_0 = 0$, the dispersion relation for H^{per} is given by*

$$\mathcal{D}(\lambda) = 2\cos(\theta), \tag{3.13}$$

where θ is the one-dimensional quasimomentum.

Bilayer graphene

The structure that represents the AB-stacked bilayer graphene $\mathcal{G}_2^{\text{AB}}$ consists of two graphene sheets, as described in Section 3.1; see Figures 3.1(a) and 3.2(a). Let us write out the conditions (3.3), (3.4) and (3.5) on the fundamental domain $\mathcal{W}_2^{\text{AB}}$ (Figure 3.2(a)). As we identify each edge e with the interval $[0,1]$, it follows that $v_{i1} \sim 0$ and $v_{i2} \sim 1$, for $i = 1, 2$. By the continuity condition (3.3),

$$\begin{cases} u_{a_{11}}(0) = u_{a_{12}}(0) = u_{a_{13}}(0) = u_{f_1}(0) =: A_1 \\ u_{a_{21}}(0) = u_{a_{22}}(0) = u_{a_{23}}(0) =: A_2 \end{cases}. \tag{3.14}$$

The Floquet condition (3.5) implies that

$$u_{a_{i1}}(1) = e^{i\theta_1} u_{a_{i2}}(1) \quad \text{and} \quad u_{a_{i1}}(1) = e^{i\theta_2} u_{a_{i3}}(1), \quad i = 1, 2, \tag{3.15}$$

so by (3.3),

$$\begin{cases} u_{a_{11}}(1) = e^{i\theta_1} u_{a_{12}}(1) = e^{i\theta_2} u_{a_{13}}(1) =: B_1 \\ u_{a_{21}}(1) = e^{i\theta_1} u_{a_{22}}(1) = e^{i\theta_2} u_{a_{23}}(1) = u_{f_1}(1) =: B_2 \end{cases} . \tag{3.16}$$

Similarly, by the zero-flux condition (3.4),

$$\begin{cases} u'_{a_{11}}(0) + u'_{a_{12}}(0) + u'_{a_{13}}(0) + t_0\, u'_{f_1}(0) = 0 \\ u'_{a_{11}}(1) + e^{i\theta_1} u'_{a_{12}}(1) + e^{i\theta_2} u'_{a_{13}}(1) = 0 \\ u'_{a_{21}}(0) + u'_{a_{22}}(0) + u'_{a_{23}}(0) = 0 \\ u'_{a_{21}}(1) + e^{i\theta_1} u'_{a_{22}}(1) + e^{i\theta_2} u'_{a_{23}}(1) + t_0\, u'_{f_1}(1) = 0 \end{cases} . \tag{3.17}$$

Let $\lambda \notin \sigma(H^D)$. Then there exists two linearly independent solutions $\varphi_{\lambda,0}, \varphi_{\lambda,1}$ of the problem

$$-\frac{\mathrm{d}^2\varphi(x)}{\mathrm{d}x^2} + q(x)\varphi(x) = \lambda\varphi(x), \tag{3.18}$$

such that

$$\begin{cases} \varphi_{\lambda,0}(0) = 1 \\ \varphi_{\lambda,0}(1) = 0 \end{cases} \qquad \begin{cases} \varphi_{\lambda,1}(0) = 0 \\ \varphi_{\lambda,1}(1) = 1 \end{cases} \tag{3.19}$$

and

$$\varphi'_{\lambda,1}(x) = -\varphi'_{\lambda,0}(1-x), \quad x \in [0,1]. \tag{3.20}$$

Since each edge of $\mathcal{W}_2^{\mathrm{AB}}$ is identified with the interval $[0,1]$, we can define $\varphi_{\lambda,i}$ in each edge and we will keep the same notation $\varphi_{\lambda,i}$ for such functions. Hence, for each $\lambda \notin \sigma(H^D)$, we can represent

$$\begin{cases} u_{a_{i1}} = A_i\varphi_{\lambda,0} + B_i\varphi_{\lambda,1} \\ u_{a_{i2}} = A_i\varphi_{\lambda,0} + e^{-i\theta_1} B_i\varphi_{\lambda,1} \\ u_{a_{i3}} = A_i\varphi_{\lambda,0} + e^{-i\theta_2} B_i\varphi_{\lambda,1} \\ u_{f_1} = A_1\varphi_{\lambda,0} + B_2\varphi_{\lambda,1} \end{cases} \qquad i = 1, 2. \tag{3.21}$$

It is easy to see that the function defined by (3.21) satisfies the continuity conditions (3.14) and (3.16) and solves the eigenvalue problem (3.7). It remains to verify condition (3.17).

By substituting (3.21) into (3.17), we get

$$\begin{cases} (3+t_0)A_1\varphi'_{\lambda,0}(0) + \bar{F}(\theta)B_1\varphi'_{\lambda,1}(0) + t_0\, B_2\varphi'_{\lambda,1}(0) = 0 \\ F(\theta)A_1\varphi'_{\lambda,0}(1) + 3B_1\varphi'_{\lambda,1}(1) = 0 \\ 3A_2\varphi'_{\lambda,0}(0) + \bar{F}(\theta)B_2\varphi'_{\lambda,1}(0) = 0 \\ t_0A_1\varphi'_{\lambda,0}(1) + F(\theta)A_2\varphi'_{\lambda,0}(1) + (3+t_0)B_2\varphi'_{\lambda,1}(1) = 0 \end{cases}, \tag{3.22}$$

where $F(\theta) := 1 + e^{-i\theta_1} + e^{-i\theta_2}$ and $\bar{F}(\theta)$ is its complex conjugate. By (3.20), we have that $\varphi'_{\lambda,0}(1) = -\varphi'_{\lambda,1}(0)$ and $\varphi'_{\lambda,0}(0) = -\varphi'_{\lambda,1}(1)$. Thus the system (3.22) is equivalent to

$$\begin{cases} -(3+t_0)A_1\varphi'_{\lambda,1}(1) + \bar{F}(\theta)B_1\varphi'_{\lambda,1}(0) + t_0\, B_2\varphi'_{\lambda,1}(0) = 0 \\ -F(\theta)A_1\varphi'_{\lambda,1}(0) + 3B_1\varphi'_{\lambda,1}(1) = 0 \\ -3A_2\varphi'_{\lambda,1}(1) + \bar{F}(\theta)B_2\varphi'_{\lambda,1}(0) = 0 \\ -t_0A_1\varphi'_{\lambda,1}(0) - F(\theta)A_2\varphi'_{\lambda,1}(0) + (3+t_0)B_2\varphi'_{\lambda,1}(1) = 0 \end{cases}. \tag{3.23}$$

Since $\varphi'_{\lambda,1}(0) \neq 0$, the quotient

$$\eta(\lambda) := \frac{\varphi'_{\lambda,1}(1)}{\varphi'_{\lambda,1}(0)} \tag{3.24}$$

is well defined. Hence, dividing the system (3.23) by $\varphi'_{\lambda,1}(0)$ and multiplying the second and fourth lines by -1, we obtain

$$\begin{cases} -T_0\eta A_1 + \bar{F}B_1 + t_0B_2 = 0 \\ F\, A_1 - 3\eta B_1 = 0 \\ -3\eta A_2 + \bar{F}B_2 = 0 \\ t_0A_1 + F\, A_2 - T_0\eta B_2 = 0 \end{cases}, \tag{3.25}$$

where $T_0 = 3 + t_0$, $\eta = \eta(\lambda)$ and $F = F(\theta)$. The matrix form of the system (3.25) is

$$\mathcal{M}_2^{\mathrm{AB}}(\lambda,\theta)X = 0, \tag{3.26}$$

where $X = \begin{bmatrix} A_1 & B_1 & A_2 & B_2 \end{bmatrix}^{\intercal}$ and

$$\mathcal{M}_2^{\mathrm{AB}}(\lambda,\theta) = \begin{bmatrix} -T_0\eta & \bar{F} & 0 & t_0 \\ F & -3\eta & 0 & 0 \\ 0 & 0 & -3\eta & \bar{F} \\ t_0 & 0 & F & -T_0\eta \end{bmatrix}. \tag{3.27}$$

From now on, we will omit the dependence on θ in the matrix $\mathcal{M}_2^{\mathrm{AB}}(\lambda,\theta)$. Note that $\det(\mathcal{M}_2^{\mathrm{AB}}(\lambda))=0$ is a quartic polynomial in $\eta(\lambda)$. Hence, if there exists a $\theta\in\mathcal{B}$ such that $\det(\mathcal{M}_2^{\mathrm{AB}}(\lambda))=0$, that is, $\eta(\lambda)$ is one of the four roots of $\det(\mathcal{M}_2^{\mathrm{AB}}(\lambda))=0$, it follows that the representation (3.21) solves the eigenvalue problem (3.7) and so $\lambda\in\sigma(H_2^{\mathrm{AB}})$, by (3.6).

Trilayer graphene

We now analyze the case $n=3$; $\mathcal{G}_3^{\mathrm{AB}}$ consists of three graphene sheets G_1, G_2 and G_3. Similarly to the case $n=2$, lets write out the conditions (3.3), (3.4) and (3.5) on the fundamental domain $\mathcal{W}_3^{\mathrm{AB}}$ (see Figure 3.2(b)). Since

$$u_{a_{i1}}(1)=e^{i\theta_1}u_{a_{i2}}(1)\quad\text{and}\quad u_{a_{i1}}(1)=e^{i\theta_2}u_{a_{i3}}(1),\quad i=1,2,3,$$

it follows that the continuity condition (3.3) is equivalent to

$$\begin{cases} u_{a_{11}}(0)=u_{a_{12}}(0)=u_{a_{13}}(0)=u_{f_1}(0)=:A_1\\ u_{a_{11}}(1)=e^{i\theta_1}u_{a_{12}}(1)=e^{i\theta_2}u_{a_{13}}(1)=:B_1\\ u_{a_{21}}(0)=u_{a_{22}}(0)=u_{a_{23}}(0)=:A_2\\ u_{a_{21}}(1)=e^{i\theta_1}u_{a_{22}}(1)=e^{i\theta_2}u_{a_{23}}(1)=u_{f_1}(1)=u_{f_2}(1)=:B_2\\ u_{a_{31}}(0)=u_{a_{32}}(0)=u_{a_{33}}(0)=u_{f_2}(0)=:A_3\\ u_{a_{31}}(1)=e^{i\theta_1}u_{a_{32}}(1)=e^{i\theta_2}u_{a_{33}}(1)=:B_3 \end{cases}, \tag{3.28}$$

and the zero-flux condition (3.4) is equivalent to

$$\begin{cases} u'_{a_{11}}(0)+u'_{a_{12}}(0)+u_{a_{13}}(0)+t_0\,u'_{f_1}(0)=0\\ u'_{a_{11}}(1)+e^{i\theta_1}u'_{a_{12}}(1)+e^{i\theta_2}u'_{a_{13}}(1)=0\\ u'_{a_{21}}(0)+u'_{a_{22}}(0)+u'_{a_{23}}(0)=0\\ u'_{a_{21}}(1)+e^{i\theta_1}u'_{a_{22}}(1)+e^{i\theta_2}u'_{a_{23}}(1)+t_0\,u'_{f_1}(1)+t_0\,u'_{f_2}(1)=0\\ u'_{a_{31}}(0)+u'_{a_{32}}(0)+u'_{a_{33}}(0)+t_0\,u'_{f_2}(0)=0\\ u'_{a_{31}}(1)+e^{i\theta_1}u'_{a_{32}}(1)+e^{i\theta_2}u'_{a_{33}}(1)=0 \end{cases}. \tag{3.29}$$

Let $\lambda \notin \sigma(H^D)$ and let $\varphi_{\lambda,0}$ and $\varphi_{\lambda,1}$ be the two linearly independent solutions of the problem (3.18) that satisfies (3.19) and (3.20). If we write

$$\begin{cases} u_{a_{i1}} = A_i\varphi_{\lambda,0} + B_i\varphi_{\lambda,1} \\ u_{a_{i2}} = A_i\varphi_{\lambda,0} + e^{-i\theta_1}B_i\varphi_{\lambda,1} \\ u_{a_{i3}} = A_i\varphi_{\lambda,0} + e^{-i\theta_2}B_i\varphi_{\lambda,1} \qquad i = 1,2,3, \\ u_{f_1} = A_1\varphi_{\lambda,0} + B_2\varphi_{\lambda,1} \\ u_{f_2} = A_3\varphi_{\lambda,0} + B_2\varphi_{\lambda,1} \end{cases} \tag{3.30}$$

the continuity condition (3.28), as well problem (3.7), are satisfied. It remains to verify the zero-flux condition (3.29). Similar to the bilayer graphene case, the matrix form of the obtained system in this case is

$$\mathcal{M}_3^{\mathrm{AB}}(\lambda)X = 0,$$

with $X = \begin{bmatrix} A_1 & B_1 & A_2 & B_2 & A_3 & B_3 \end{bmatrix}^{\intercal}$ and

$$\mathcal{M}_3^{\mathrm{AB}}(\lambda) = \begin{bmatrix} M_{T_0\tilde{T}_0} & \tilde{m}_{t_0}^{\intercal} \\ \tilde{m}_{t_0} & N_{T_0} \end{bmatrix}, \tag{3.31}$$

where $T_0 = 3 + t_0$, $\tilde{T}_0 = 3 + 2t_0$, $F = F(\theta) = 1 + e^{i\theta_1} + e^{i\theta_2}$,

$$M_{T_0\tilde{T}_0} = \begin{bmatrix} -T_0\eta & \bar{F} & 0 & t_0 \\ F & -3\eta & 0 & 0 \\ 0 & 0 & -3\eta & \bar{F} \\ t_0 & 0 & F & -\tilde{T}_0\eta \end{bmatrix}, \tag{3.32}$$

$$\tilde{m}_{t_0} = \begin{bmatrix} 0 & 0 & 0 & t_0 \\ 0 & 0 & 0 & 0 \end{bmatrix} \quad \text{and} \quad N_{T_0} = \begin{bmatrix} -T_0\eta & \bar{F} \\ F & -3\eta \end{bmatrix}. \tag{3.33}$$

Note that $\mathcal{M}_2^{\mathrm{AB}}(\lambda) = M_{T_0T_0}$. Thus, if there exists $\theta \in \mathcal{B}$ such that $\det(\mathcal{M}_3^{\mathrm{AB}}(\lambda)) = 0$, the representation (3.30) solves the eigenvalue problem (3.7) and so $\lambda \in \sigma(H_3^{\mathrm{AB}})$.

Joint spectral analysis

Therefore, we have the following result (as before, we keep the dependence of $\mathcal{M}_n^{\mathrm{AB}}(\lambda)$ on θ implicit):

Proposition 3.2.2. *Let $\lambda \notin \sigma(H^D)$. Then, for $n = 2, 3$ and $t_0 > 0$, the real number $\lambda \in \sigma(H_n^{\mathrm{AB}})$ if and only if there exists $\theta \in \mathcal{B}$ such that*

$$\det\left(\mathcal{M}_n^{\mathrm{AB}}(\lambda)\right) = 0\,. \tag{3.34}$$

Note that $\det(\mathcal{M}_n^{\mathrm{AB}}(\lambda)) = 0$ is a polynomial of degree $2n$ in $\eta(\lambda)$, for $n = 2, 3$. By Proposition 3.2.2, the spectra $\sigma(H_n^{\mathrm{AB}})$ are basically determined if we know the range of all $2n$ roots $\eta(\lambda, \theta)$ of $\det(\mathcal{M}_n^{\mathrm{AB}}(\lambda))$. For the case $n = 2$ we can easily calculate the roots of (3.34). We use the *Laplace's expansion formula* for matrix determinants in $\mathcal{M}_2^{\mathrm{AB}}(\lambda)$, given by (3.27), to obtain

$$\begin{aligned} \det(\mathcal{M}_2^{\mathrm{AB}}(\lambda)) &= 9T_0^2\eta^4(\lambda) - (9t_0^2 + 6T_0F(\theta)\bar{F}(\theta))\eta^2(\lambda) \\ &+ \left(F(\theta)\bar{F}(\theta)\right)^2 = 0. \end{aligned} \tag{3.35}$$

Note that we can easily turn the quartic equation (3.35) into a quadratic one (just introduce $\delta = \eta(\lambda)^2$ and calculate the two roots for δ). Thus, the four roots are

$$\eta_{\pm}^{\pm}(\lambda, \theta) = \pm\sqrt{\frac{G_2(t_0, \theta) \pm \sqrt{G_2(t_0, \theta)^2 - 36T_0^2(F\bar{F})^2}}{18T_0^2}}, \tag{3.36}$$

where $G_2(t_0, \theta) = 9t_0^2 + 6T_0F\bar{F}$. Here, the subscript $\pm$ refers to the outside " $\pm$ " of the first square root symbol while the superscript $\pm$ refers to the inside one.

For $n = 3$, applying Laplace's formula to (3.31), we obtain

$$\begin{aligned} \det(\mathcal{M}_3^{\mathrm{AB}}(\lambda)) &= 27T_0^2\tilde{T}_0\eta^6 - (54T_0t_0^2 + 9(T_0^2 + 2T_0\tilde{T}_0)F\bar{F})\eta^4 \\ &+ (18t_0^2F\bar{F} + 3(2T_0 + \tilde{T}_0)(F\bar{F})^2)\eta^2 - (F\bar{F})^3. \end{aligned} \tag{3.37}$$

The six roots of $\det(\mathcal{M}_3^{\mathrm{AB}}(\lambda))$ are the following:

$$\tilde{\eta}_{\pm}^{\pm}(\lambda, \theta) = \pm\sqrt{\frac{G_3(t_0, \theta) \pm \sqrt{G_3(t_0, \theta)^2 - 36T_0\tilde{T}_0(F\bar{F})^2}}{18T_0\tilde{T}_0}}, \tag{3.38}$$

$$\bar{\eta}_{\pm}(\lambda, \theta) = \pm\sqrt{\frac{F\bar{F}}{3T_0}}, \tag{3.39}$$

where $G_3(t_0, \theta) = 18t_0^2 + 3(T_0 + \tilde{T}_0)F\bar{F}$.

Remark 3.2.1. *To calculate the exact roots* (3.38) *and* (3.39) *of* $\det(\mathcal{M}_3^{\mathrm{AB}}(\lambda)) = 0$*, we have first replaced, in $\mathcal{M}_3^{\mathrm{AB}}(\lambda)$, the matrices $\tilde{m}_{t_0}$ and $\tilde{m}_{t_0}^{\intercal}$ by zero, to obtain a block matrix $\tilde{\mathcal{M}}_3^{\mathrm{AB}}(\lambda)$, so that*

$$\det(\tilde{\mathcal{M}}_3^{\mathrm{AB}}(\lambda)) = \det(M_{T_0\tilde{T}_0}) \det N_{T_0}.$$

Hence, the six roots of $\det(\tilde{\mathcal{M}}_3^{\mathrm{AB}}(\lambda)) = 0$ *are composed by the four roots of* $\det(M_{T_0\tilde{T}_0}) = 0$ *and the two roots of* $\det N_{T_0} = 0$. *Since the two determinants*

$$\det(\mathcal{M}_3^{\mathrm{AB}}(\lambda)) = 0 \quad \textit{and} \quad \det(\tilde{\mathcal{M}}_3^{\mathrm{AB}}(\lambda)) = 0 \tag{3.40}$$

have similar expressions, it was observed that the six roots of the original determinant should be similar to the roots of $\det(\tilde{\mathcal{M}}_3^{\mathrm{AB}}(\lambda)) = 0$. *Then,* (3.38) *was obtained from inspection and suitable modifications on the roots of* $\det M_{T_0\tilde{T}_0}$*;* (3.39) *are the roots of* $\det N_{T_0} = 0$ *(the latter resembles the single layer case [23]).*

So far, we have considered $\lambda \notin \sigma(H^D)$. In this case, we managed to establish a relationship between such λ's with the spectrum of H_n^{AB} (see Proposition 3.2.2). Now, let $\lambda \in \sigma(H^D)$, i.e., an eigenvalue of the Dirichlet operator H^D. For $n = 2, 3$, the proof of next lemma is analogous to the proof Lemma 3.5 of [23] and Lemma 6 of [12].

Lemma 3.2.1. *Each* $\lambda \in \sigma(H^D)$ *is an eigenvalue of infinite multiplicity of* H_n^{AB}.

Before we state the spectral characterization theorem of the Bernal-stacked multilayer graphene Schrödinger operator, let us discuss details of the relation between the roots $\eta(\lambda)$ of $\det(\mathcal{M}_n^{\mathrm{AB}}(\lambda)) = 0$ and the discriminant $\mathcal{D}(\lambda)$ of the Hill operator H^{per}, for $n = 2, 3$ ([23], page 813). As in Chapter 2, this is important to relate the spectrum of H^{per} to the spectrum of H_n^{AB}. The proof of the following lemma is analogous to Lemma 2.2.2; we just consider the monodromy matrix $M(\lambda)$ of Hill operator H^{per} instead the monodromy matrix of the periodic Dirac operator D^{per}.

Lemma 3.2.2. *Let* $\lambda \notin \sigma(H^D)$ *and* $\mathcal{D}(\lambda)$ *be the discriminant of the Hill operator* H^{per}. *Then for* H_2^{AB} *and* H_3^{AB}, *we have*

$$\eta(\lambda) = \frac{1}{2}\mathcal{D}(\lambda). \tag{3.41}$$

We are ready to characterize the spectra. The following result is proved with the same arguments presented in the proof of Theorem 2.2.1. Also, see [12], Theorem 7, and [23], Theorem 3.6.

Theorem 3.2.1. *For the Bernal-stacked graphene Schrödinger operators* H_n^{AB}, $n = 2, 3$, *we have:*

(i) The singular continuous spectrum of the H_n^{AB} *is empty.*

(ii) The dispersion relation of H_n^{AB} *consists of two parts:*

- *the pairs* (λ, θ) $(\lambda \notin \sigma(H^D))$ *such that*

$$\mathcal{D}(\lambda) = 2\eta(\lambda), \tag{3.42}$$

  where $\eta(\lambda)$ *are the* $2n$ *solutions of the equation* $\det(\mathcal{M}_n^{\mathrm{AB}}(\lambda)) = 0$*;*

- *the collection of flat branches* $\lambda \in \sigma(H^D)$*, that is, the pairs* (λ, θ) *for any* $\theta \in \mathcal{B}$*.*

(iii) Its absolutely continuous spectrum $\sigma_{\mathrm{ac}}(H_n^{\mathrm{AB}})$ *coincides, as a set, with* $\sigma(H^{\mathrm{per}})$*, that is, it has a band-gap structure and*

$$\sigma_{\mathrm{ac}}(H_n^{\mathrm{AB}}) = \{\lambda \in \mathbb{R} : |\mathcal{D}(\lambda)| \leq 2\}. \tag{3.43}$$

(iv) The pure point spectrum of H_n^{AB} *coincides with* $\sigma(H^D)$*, and each* $\lambda \in \sigma(H^D)$ *is an eigenvalue of infinite multiplicity of* H_n^{AB}*.*

(v) The absolutely continuous spectrum of H_n^{AB} *has gaps if and only if* $\sigma(H^{\mathrm{per}})$ *has gaps.*

For the bilayer graphene operator H_2^{AB}, the four curves of the dispersion relation (3.42) reduces to

$$\mathcal{D}(\lambda) = \pm 2\sqrt{\frac{G_2(t_0,\theta) \pm \sqrt{G_2(t_0,\theta)^2 - 36T_0^2(F\bar{F})^2}}{18T_0^2}},$$

where $G_2(t_0,\theta) = 9t_0^2 + 6T_0F\bar{F}$, and to obtain the six curves of the dispersion relation of the trilayer graphene operator H_3^{AB}, (3.42) takes the form (recall (3.38) and (3.39))

$$\mathcal{D}(\lambda) \;=\; \pm 2\sqrt{\frac{G_3(t_0,\theta) \pm \sqrt{G_3(t_0,\theta)^2 - 36T_0\tilde{T}_0(F\bar{F})^2}}{18T_0\tilde{T}_0}}$$

and

$$\mathcal{D}(\lambda) \;=\; \pm 2\sqrt{\frac{F\bar{F}}{3T_0}},$$

where $G_3(t_0,\theta) = 18t_0^2 + 3(T_0 + \tilde{T}_0)F\bar{F}$.

3.3 Study of Dirac cones

Now we present our main result about Dirac cones (recall Definition 2.3.1) in the dispersion relation of the Bernal-stacked multilayer graphene Schrödinger operator (see Theorem 3.2.1*(ii)*).

Theorem 3.3.1. *For the Bernal-stacked bilayer and trilayer graphene Schrödinger operators H_2^{AB} and H_3^{AB}, respectively, and each $t_0 > 0$, we have:*

(i) The dispersion relation of H_2^{AB} presents parabolic touchings at the points $\pm(2\pi/3, -2\pi/3)$ in the Brillouin zone, but no Dirac cone (see Figure 3.3).

(ii) The dispersion relation of H_3^{AB} presents (see Figure 3.4):

- *two Dirac cones at the D-points $\pm(2\pi/3, -2\pi/3)$, and*
- *two parabolic touchings at the same points $\pm(2\pi/3, -2\pi/3)$.*

Proof. (i) By Theorem 3.2.1(ii), the non-constant part of the dispersion relation for the AB-stacked bilayer graphene is given by $\mathcal{D}(\lambda) = 2\eta_{\pm}^{\pm}(\lambda, \theta)$, where

$$\eta_{\pm}^{\pm}(\lambda, \theta) = \pm\sqrt{\frac{G_2 \pm \sqrt{G_2^2 - 36T_0^2(F\bar{F})^2}}{18T_0^2}}, \tag{3.44}$$

with $G_2 = G_2(t_0, \theta) = 9t^2 + 6T_0F\bar{F}$ and $F = F(\theta) = 1 + e^{i\theta_1} + e^{i\theta_2}$. It is easy to show that

Lemma 3.3.1. *As functions of $\theta \in \mathcal{B}$, $\eta_{\pm}^{\pm}(\lambda, \theta)$ satisfies:*

(i) $\max \eta_{+}^{+}(\lambda, \theta) = 1$ and $\min \eta_{+}^{+}(\lambda, \theta) = t_0/(3 + t_0)$, which are attained at $(0, 0)$ and $\pm(2\pi/3, -2\pi, 3)$, respectively.

(ii) $\max \eta_{+}^{-}(\lambda, \theta) = 3/(3 + t_0)$ and $\min \eta_{+}^{-}(\lambda, \theta) = 0$, which are attained at $(0, 0)$ and $\pm(2\pi/3, -2\pi, 3)$, respectively.

(iii) $\max \eta_{-}^{+}(\lambda, \theta) = -t_0/(3+t_0)$ and $\min \eta_{-}^{+}(\lambda, \theta) = -1$, which are attained at $\pm(2\pi/3, -2\pi, 3)$ and $(0, 0)$, respectively.

(iv) $\max \eta_{-}^{-}(\lambda, \theta) = 0$ and $\min \eta_{-}^{-}(\lambda, \theta) = -3/(3+t_0)$, which are attained at $\pm(2\pi/3, -2\pi, 3)$ and $(0, 0)$, respectively.

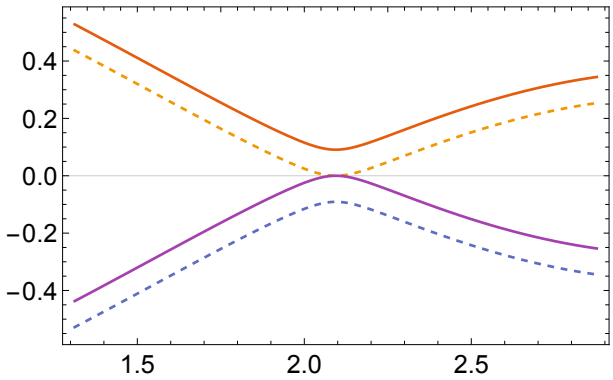

Figure 3.3: The dispersion relation of the AB-stacked bilayer graphene operator restricted to $\mathcal{B}_d$ and $\theta_1 \in \left[\frac{2\pi}{3} - \frac{\pi}{4}, \frac{2\pi}{3} + \frac{\pi}{4}\right]$, with the parameter $t_0 = 0.3$. There are no Dirac cones, only quadratic touchings.

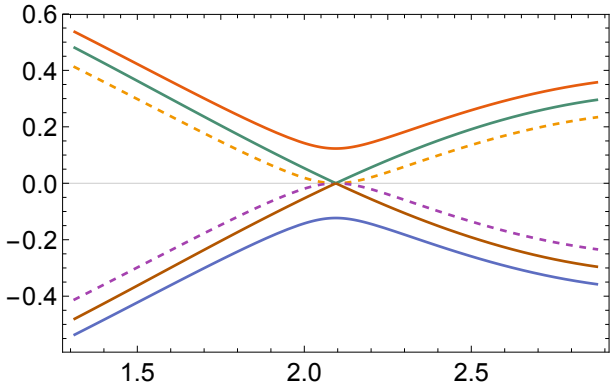

Figure 3.4: The dispersion relation of the AB-stacked trilayer graphene operator restricted to $\mathcal{B}_d$ and $\theta_1 \in \left[\frac{2\pi}{3} - \frac{\pi}{4}, \frac{2\pi}{3} + \frac{\pi}{4}\right]$, with the parameter $t_0 = 0.3$. There is a Dirac cone at $2\pi/3$. Note that there is also a quadratic touching at $2\pi/3$.

Note that the possible Dirac cones in this case depend on the function

$$F(\theta)\bar{F}(\theta) = |F(\theta)|^2 = 1 + 8\cos\left(\frac{\theta_1 - \theta_2}{2}\right)\cos\left(\frac{\theta_1}{2}\right)\cos\left(\frac{\theta_2}{2}\right).$$

We have that $|F(\theta)| = 0$ if and only if $\theta = \pm\theta_D$, where $\theta_D := (2\pi/3, -2\pi/3)$, and since these points belong to the diagonal

$$\mathcal{B}_d := \{\theta \in \mathcal{B} : \theta_1 = -\theta_2\}$$

of the Brillouin zone $\mathcal{B}$, it suffices to study $\eta_{\pm}^{\pm}$ restricted to $\mathcal{B}_d$. Note the touching at $\pm\theta_D$ given by Lemma 3.3.1, items (ii) and (iv), where $\min \eta_{+}^{-}(\lambda, \pm\theta_D) = \max \eta_{-}^{-}(\lambda, \pm\theta_D) = 0$ (that is, $\mathcal{D}(\lambda)$ vanishes).

For $\theta \in \mathcal{B}_d$, $F(\theta) = 1 + 2\cos(\theta_1)$ and then (3.44) takes the form

$$\eta_{\pm}^{\pm}(\lambda,\theta) = \pm\sqrt{\frac{G_2 \pm \sqrt{G_2^2 - 36T_0^2F^4}}{18T_0^2}}. \tag{3.45}$$

Calculating $d\eta_{\pm}^{\pm}/d\theta$, we get

$$\frac{d\eta_{\pm}^{\pm}(\lambda,\theta)}{d\theta} = \pm\frac{G_2' \pm \frac{2G_2G_2' - 144T_0^2F^3F'}{2(G_2^2-36T_0^2F^4)^{1/2}}}{2(18T_0^2)^{1/2}(G_2 \pm (G_2^2 - 36T_0^2F^4)^{1/2})^{1/2}}, \tag{3.46}$$

where $G_2' = 12T_0FF'$. Thus, $d\eta_{\pm}^{+}/d\theta$ do exist for every $\theta \in \mathcal{B}_d$ and vanish at $\pm 2\pi/3$, since $F(\pm 2\pi/3) = 0$; so the branches $\eta_{\pm}^{+}$ have a quadratic behaviour close to $\pm 2\pi/3$ and do not present Dirac cones. However, we have an indetermination (i.e., $0/0$) for $d\eta_{\pm}^{-}/d\theta$ in $\pm 2\pi/3$ (otherwise they are well behaved); the behaviour of these functions around $\pm 2\pi/3$ can be obtained by recalling that, for small x, we have

$$(1+x)^{1/2} \approx 1 + \frac{x}{2} - \frac{x^2}{8}.$$

Then, for θ close to $\pm 2\pi/3$,

$$\begin{aligned}
\eta_{\pm}^{-}(\lambda,\theta) &= \pm\sqrt{\frac{9t_0^2 + 6T_0F^2 - \sqrt{(9t_0^2 + 6T_0F^2)^2 - 36T_0^2F^4}}{18T_0^2}} \\
&= \pm\sqrt{\frac{9t_0^2 + 6T_0F^2 - 9t_0\left(1 + \frac{4T_0}{3t_0^2}F^2\right)^{1/2}}{18T_0^2}} \\
&\approx \pm\sqrt{\frac{9t_0^2 + 6T_0F^2 - 9t_0\left(1 + \frac{2T_0}{3t_0^2}F^2 - \frac{2T_0^2}{9t_0^4}F^4\right)}{18T_0^2}} \\
&= \pm\frac{F^2}{3t_0}.
\end{aligned}$$

Thus, $\eta_{\pm}^{-}(\lambda,\theta)$ also have quadratic behaviour near $\pm 2\pi/3$. Therefore, the dispersion relation of the AB-stacked bilayer graphene does not present Dirac cones and have two parabolic touchings at $\pm\theta_D = \pm(2\pi/3, -2\pi/3)$.

(ii) By Theorem 3.2.1(ii), the non-constant part of the dispersion relation for the AB-stacked trilayer graphene is given by $\mathcal{D}(\lambda) = 2\eta(\lambda,\theta)$, where $\eta(\lambda,\theta)$ are the six roots of $\det M_3^{\mathrm{AB}}(\lambda)$, which are given by (3.38) and (3.39). Analogously to the bilayer graphene case, it is sufficient to consider $\theta \in \mathcal{B}_d$. Thus, (3.38) turns to

$$\tilde{\eta}_{\pm}^{\pm}(\lambda,\theta) = \pm\sqrt{\frac{G_3 \pm \sqrt{G_3^2 - 36T_0\tilde{T}_0F^4}}{18T_0\tilde{T}_0}}, \tag{3.47}$$

where $G_3 = G_3(t_0, \theta) = 9t_0^2 + 3(T_0 + \tilde{T}_0)F^2$ and $F = F(\theta) = 1 + 2\cos(\theta_1)$, and (3.39) takes the form

$$\bar{\eta}_{\pm}(\lambda, \theta) = \pm \frac{|F(\theta)|}{\sqrt{3T_0}}. \tag{3.48}$$

The proofs that (3.47) does not have Dirac points and have two parabolic touching at $\pm\theta_D$ are analogous to the proof presented for item (i). It remains to show that $\mathcal{D}(\lambda) = 2\bar{\eta}_{\pm}(\lambda, \theta)$ satisfies (2.39) (recall Definition 2.3.1).

Expanding (3.48) in Taylor's series around $\pm\bar{\theta}$, where $\bar{\theta} = \pm 2\pi/3$, we get

$$\bar{\eta}_{\pm}(\lambda, \theta) - \bar{\eta}_{\pm}(\lambda, \bar{\theta}) = \pm\bar{\gamma}|\theta_1 - \bar{\theta}| + \mathcal{O}(|\theta_1 - \bar{\theta}|^2), \tag{3.49}$$

where $\bar{\gamma} = \sqrt{\frac{1}{T_0}}$, since $\bar{\eta}_{\pm}(\lambda, \bar{\theta}) = 0$ and

$$\cos\theta_1 = -\frac{1}{2} \mp \frac{\sqrt{3}}{2}(\theta_1 - \bar{\theta}) + \mathcal{O}((\theta_1 - \bar{\theta})^2).$$

We have $\bar{\gamma} \neq 0$, since $t_0 > 0$. It remains to analyze $\mathcal{D}(\lambda) = \mathcal{D}(\lambda(\theta))$. Since $\mathcal{D}'(\lambda(\theta)) \neq 0$ in the spectral bands of $\sigma(H_3^{\mathrm{AB}})$ (see [23], Proposition 3.4), then we can expand $\mathcal{D}(\lambda(\theta))$ in Taylor's series around $\lambda(\bar{\theta})$, to obtain

$$\mathcal{D}(\lambda(\theta)) - \mathcal{D}(\lambda(\bar{\theta})) = \mathcal{D}'(\lambda(\bar{\theta}))(\lambda(\theta) - \lambda(\bar{\theta})) + \mathcal{O}((\lambda(\theta) - \lambda(\bar{\theta}))^2). \tag{3.50}$$

In particular, when $q_0 = 0$, that is, in the free case, since $\mathcal{D}(\lambda(\theta)) = 2\cos\sqrt{\lambda(\theta)}$, it follows that

$$\mathcal{D}'(\lambda(\theta)) = -\frac{\sin(\sqrt{\lambda(\bar{\theta})})}{\sqrt{\lambda(\bar{\theta})}}.$$

Combining (3.49) and (3.50), we obtain (2.39), with $\gamma = \bar{\gamma}/\mathcal{D}'(\lambda(\bar{\theta}))$. Therefore, the dispersion relation of the AB-stacked trilayer graphene have two Dirac cones, precisely at $\pm(2\pi/3, -2\pi/3)$ in the Brillouin zone $\mathcal{B}$, and the proof of the theorem is complete. □

3.4 Comparison with physics literature

Our study about the spectrum and the dispersion relation of the AB-stacked bi- and trilayer graphene is based on a limit model, using periodic quantum graph structures. The advantage of this method is that the dispersion relation has an explicit analytical expression.

The obtained results are consistent with the physics literature. For instance, bi- and trilayer models have a gapless band component and thus may be characterized as a semimetal.

The rigorous non-existence of Dirac cones on the dispersion relation for our model of AB-stacked bilayer graphene and with gapless parabolic bands touching at two points, illustrated in Figure 3.3, are similar to results obtained

(i) through tight-binding calculations [39, 30, 32],

(ii) by an effective two-dimensional Hamiltonian [31] that acts in a space of two-component wave functions (à la Dirac equation),

(iii) by using a π-orbital continuum model with nearest-neighbor tunneling [33].

This opens the possibility of chiral particles with a parabolic nonrelativistic energy spectrum [34, 32]; a subject to be investigated.

For the trilayer graphene with AB-stacking, the presence of Dirac cones was observed in [26, 2, 33] through tight-binding calculations; this is compatible with Theorem 4.3.1(ii) for our graph model and illustrated in Figure 3.4. Another point of agreement with the physics literature is that, for the trilayer case, the Dirac cones come from just one pair of curves in the dispersion relation, and they are absent in the other two pairs [33]; it can be seen as a combination [7] of features of a single graphene sheet with the bilayer one, exactly what our results reveal (see, e.g., Remark 3.2.1).

For the trilayer graphene, we have found that the existence and location of D-points is independent of the value of the interlayer interaction parameter t_0. It would be interesting to investigate whether this occurs for, say, tight-binding models, at least for a range of interaction parameters; we have not found any result in this direction in the literature.

Finally, a natural question is whether other models and/or experiments also provide Dirac cones for the trilayer case for any interaction intensity between layers.

Chapter 4

AA-stacked multilayer graphene and graphite

In this chapter we perform a similar study to Chapter 3; we propose a quantum graph model to represent the AA-stacked multilayer graphene and graphite. We shall notice the differences with respect to Chapter 3:

- While the quantum graph geometry, that models the AB-stacked bilayer and trilayer graphene, was obtained by connecting the type-A points with type-B points of two different sheets of graphene (see Section 3.1), in the AA-stacking of graphene layers every type-A point of a graphene sheet is connected to the type-A points of consecutive sheets of graphene, and similarly for type-B points (see Figure 4.1).

- In the Chapter 3, we explicitly studied the cases with two and three graphene sheets. It was concluded that for the AB-stacked bilayer graphene, the dispersion relation of the Schrödinger operator do not have Dirac cones (see Section 3.3), while for the trilayer case, there are two pairs of Dirac cones in the Brillouin zone. However, by modeling the AA-stacked multilayer graphene, it was possible to, besides explicitly study the bilayer and trilayer cases, study the case with n layers of graphene sheets under some controlled approximation, for any number of layers. Also, the AA-stacked graphite was modeled by a 3D quantum graph. In all these cases, it was observed Dirac cones in the dispersion relation of the Schrödinger operator (see Section 4.3).

This chapter is structured as follows. In Section 4.1, we present the construction of

the periodic quantum graphs and the Schrödinger operator that models the AA-stacked multilayer graphene and graphite. In Section 4.2, we perform the spectral analysis of the Schrödinger operator. The study of Dirac cones is in Section 4.3 and we finish the chapter with a comparison of obtained results with the physics literature, in Section 4.4.

4.1 Quantum graphs for finite and infinite numbers of graphene sheets

We begin introducing the periodic quantum graphs that are herein proposed to represent the *AA-stacked multilayer graphene*, for any (finite) number of layers, and the *AA-stacked graphite*. The metric graph structure that models the AA-stacked multilayer graphene is defined as follows. Let $\{G_k\}_{k=1}^n$ be n sheets of graphene, each one as defined in Section 2.1, stacked so that a type-A vertex of G_k is located exactly above the corresponding type-A vertex of G_{k-1}, $2 \leq k \leq n$. In this structure of multilayer graphene, denoted by $\mathcal{G}_n^{\mathrm{AA}}$, is that type-A (type-B) vertices of G_k are linked up (only) with their respective type-A (type-B) vertices of G_{k+1}, for $k = 1, \ldots, n-1$, as shown in Figure 4.1. We assume that all edges in $\mathcal{G}_n^{\mathrm{AA}}$ have length 1 for all n. The way how we control the interaction intensity between (consecutive) graphene sheets is described in Remark 3.1.1, in Section 3.1.

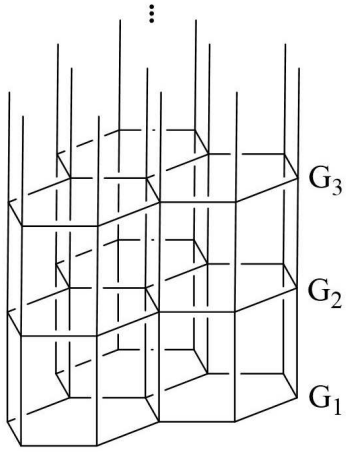

Figure 4.1: The lattice structure of AA-stacked multilayer graphene.

The action of the group $\mathbb{Z}^2$ on $\mathcal{G}_n^{\mathrm{AA}}$ is the same for the AB-stacked multilayer graphene (see (3.1) in Section 3.1), that is, is the shift

$$\mathbb{Z}^2 \times \mathcal{G}_n^{\mathrm{AA}} \ni (p, x) \mapsto x + p_1 E_1 + p_2 E_2, \tag{4.1}$$

where E_1, E_2 are given the lattice vectors, given by (2.1), and $x = x_1E_1 + x_2E_2 \in \mathcal{G}_n^{\mathrm{AA}}$. As fundamental domain of this action, we choose the set $\mathcal{W}_n^{\mathrm{AA}}$ shown in Figure 4.2, which contains two (consecutive) points and three edges of each graphene sheet G_k, and also the edges that connect consecutive layers (as discussed above).

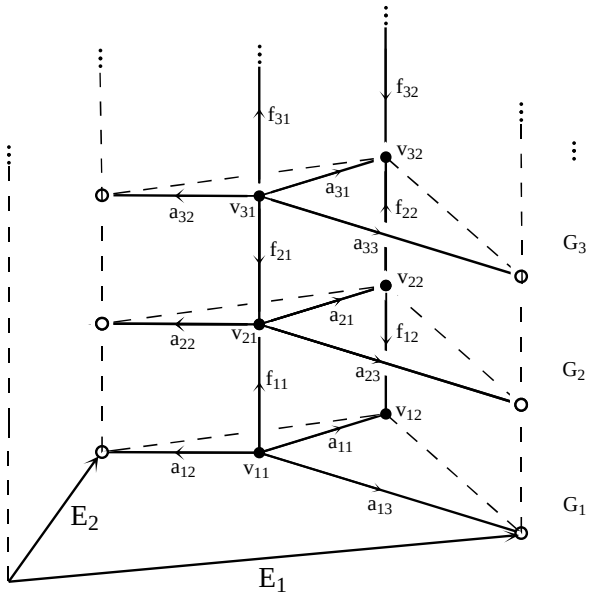

Figure 4.2: The fundamental domain $\mathcal{W}_n^{\mathrm{AA}}$ with two vertices and three edges of each graphene sheet and the connecting edges of consecutive layers.

Now we define the 3D periodic quantum graph that is proposed to model the *AA-stacked graphite*, denoted by $\mathcal{G}_{\mathrm{g}}^{\mathrm{AA}}$. Let $\{G_k\}_{k\in\mathbb{Z}}$, where G_k is a graphene sheet, for each $k \in \mathbb{Z}$, each one defined as in Section 2.1, stacked up in the same way that $\mathcal{G}_n^{\mathrm{AA}}$ is and, again, we assume that all edges in $\mathcal{G}_{\mathrm{g}}^{\mathrm{AA}}$ have length 1. The action of the group $\mathbb{Z}^3$ on $\mathcal{G}_{\mathrm{g}}^{\mathrm{AA}}$ is defined by

$$\mathcal{S}_{\mathrm{g}} : \mathbb{Z}^3 \times \mathcal{G}_{\mathrm{g}}^{\mathrm{AA}} \to \mathcal{G}_{\mathrm{g}}^{\mathrm{AA}}, \quad \mathcal{S}_{\mathrm{g}}(p, x) := x + \sum_{i=1}^{3} p_i E_i, \tag{4.2}$$

where $E_1 = (3/2, \sqrt{3}/2, 0)$, $E_2 = (0, \sqrt{3}, 0)$ and $E_3 := (0, 0, 1)$ are the lattice vectors; its fundamental domain $\mathcal{W}_{\mathrm{g}}^{\mathrm{AA}}$ is similar to $\mathcal{W}_n^{\mathrm{AA}}$ and is presented in Figure 4.2. It contains only two vertices $\{v_1, v_2\}$ and three edges $\{a_1, a_2, a_3\}$ of one graphene sheet and four edges $\{f_{1,\pm}, f_{2,\pm}\}$ that connect this layer to the others. It will be convenient to direct the edges in both $\mathcal{W}_{\mathrm{n}}^{\mathrm{AA}}$ and $\mathcal{W}_{\mathrm{g}}^{\mathrm{AA}}$ as in Figures 4.2. We label the sheet's edges by the letter "a" whereas the edges between two consecutive sheets are labeled by "f". We denote both quantum graphs by $\mathcal{G}_{\varrho}^{AA}$, where $\varrho = n$ represents the AA-stacked (n-)multilayer graphene and $\varrho = \mathrm{g}$

represents the AA-stacked graphite. We recall some notations:

1. $E(\mathcal{G}_\varrho^{\mathrm{AA}})$ denote the set of edges of $\mathcal{G}_\varrho^{AA}$;
2. $\bar{E}(\mathcal{G}_\varrho^{\mathrm{AA}})$ denote the set of graphene sheets edges of $\mathcal{G}_\varrho^{AA}$;
3. $\tilde{E}(\mathcal{G}_\varrho^{\mathrm{AA}})$ denote the set of edges of $\mathcal{G}_\varrho^{AA}$ that connect the sheets of graphene;
4. $V(\mathcal{G}_\varrho^{AA})$ the set of vertices of $\mathcal{G}_\varrho^{AA}$.

Since $\mathcal{G}_\varrho^{\mathrm{AA}}$ is supposed to be embedded into the Euclidean space $\mathbb{R}^3$, we identify each edge $e \in E(\mathcal{G}_\varrho^{\mathrm{AA}})$ with the segment $[0,1]$, which identifies the end points of e with 0 and 1. This allows us to define and differentiate functions along the edges. The arc length metric induces a measure, denoted by $\mathrm{d}x$, which permits to integrate functions on $\mathcal{G}_\varrho^{\mathrm{AA}}$. In particular, we can naturally define the Hilbert space of all square integrable functions on $\mathcal{G}_\varrho^{\mathrm{AA}}$,

$$\mathrm{L}^2(\mathcal{G}_\varrho^{\mathrm{AA}}) = \bigoplus_{e\in E(\mathcal{G}_\varrho^{\mathrm{AA}})} \mathrm{L}^2(e).$$

We denote functions on $\mathcal{G}_\varrho^{\mathrm{AA}}$ by $u = \{u_e\}_{e\in E(\mathcal{G}_\varrho^{\mathrm{AA}})}$, where u_e is a function acting on the edge e.

To see $\mathcal{G}_\varrho^{\mathrm{AA}}$ as a periodic quantum graph, it remains to define the Schrödinger operator acting in $\mathrm{L}^2(\mathcal{G}_\varrho^{\mathrm{AA}})$. It is defined in an analogous way to Section 3.1 and we repeat here the procedure. Let $q_0 : [0,1] \to \mathbb{R}$ be an even continuous function, that is, $q_0(x) = q_0(1-x)$ for all $x \in [0,1]$. As we have identified the edges of $\mathcal{G}_\varrho^{\mathrm{AA}}$ with the segment $[0,1]$, we can define a *potential* $q = \{q_e\}_{e\in E(\mathcal{G}_\varrho^{\mathrm{AA}})}$ on $\mathcal{G}_\varrho^{\mathrm{AA}}$, where $q_e = q_0$, for all $e \in E(\mathcal{G}_\varrho^{\mathrm{AA}})$. Note that due the evenness assumption on q_0, the potential q does not depend on the orientations chosen along the edges; an even potential is a consequence of the fact that we have the same kind of atoms at the vertices. We have (see Lemma 2.1.1):

Lemma 4.1.1. *The potential q above defined is invariant with respect to the symmetry group of $\mathcal{G}_\varrho^{\mathrm{AA}}$, for both $\varrho = n, \mathrm{g}$.*

Finally, we define the AA-stacked multilayer graphene and AA-stacked graphite Schrödinger operator H_ϱ^{AA}, which acts on a function $u \in \mathrm{dom}\,(H_\varrho^{\mathrm{AA}})$ as

$$H_\varrho^{\mathrm{AA}} u_e(x_e) := (-\Delta + q(x))u_e(x_e) = -\frac{\mathrm{d}^2 u_e(x_e)}{\mathrm{d}x^2} + q_e(x_e)u_e(x_e) \tag{4.3}$$

for all $e \in E(\mathcal{G}_\varrho^{\mathrm{AA}})$. When the context is clear, the subscript "e" will be omitted. The domain $\mathrm{dom}\,(H_\varrho^{\mathrm{AA}})$ consists of the functions u on $\mathcal{G}_\varrho^{\mathrm{AA}}$ such that

(i) $u_e \in H^2(e)$, for all $e \in E(\mathcal{G}_\varrho^{\mathrm{AA}})$, where $H^2(e)$ is the usual *Sobolev Space* in the edge e.

(ii) $\displaystyle\sum_{e\in E(\mathcal{G}_\varrho^{\mathrm{AA}})} \|u_e\|^2_{H^2(e)} < \infty.$

(iii) The *Neumann vertex conditions* (also called *Kirchhoff vertex conditions*), which requires the continuity of the functions at each vertex v, and the vanishing of the total flux at v, that is,

$$u_{e_1}(v) = u_{e_2}(v), \quad \text{for all} \quad e_1, e_2 \in E_v(\mathcal{G}_\varrho^{\mathrm{AA}}), \tag{4.4}$$

$$\sum_{a\in\bar{E}_v(\mathcal{G}_\varrho^{\mathrm{AA}})} u'_a(v) + \sum_{f\in\tilde{E}_v(\mathcal{G}_\varrho^{\mathrm{AA}})} t_0\, u'_f(v) = 0, \tag{4.5}$$

where $E_v(\mathcal{G}_\varrho^{\mathrm{AA}})$ is the set of edges that contains v (analogous to $\bar{E}_v(\mathcal{G}_\varrho^{\mathrm{AA}})$ and $\tilde{E}_v(\mathcal{G}_\varrho^{\mathrm{AA}})$), $u'_e(v)$ is the derivate of u_e directed from v to the other vertex of e and $0 < t_0 < 1$ is an interaction parameter between consecutive layers.

Recall Remark 3.1.1 in Section 3.1 for details about the justification of the parameter t_0 in (4.5). The operator H_ϱ^{AA} is an unbounded self-adjoint operator [22, 20, 4] and, by the evenness condition on the potential and Lemma 4.1.1, it is invariant with respect to all symmetries of the graph $\mathcal{G}_\varrho^{\mathrm{AA}}$.

4.2 Spectral Analysis

In this section we perform a similar study to Section 4.2; we use Floquet-Bloch theory [13, 21, 38, 5] to study the spectrum of H_ϱ^{AA}; we extend results of [23]. We begin with general remarks, then we specialize to bilayer, trilayer, the general n-layer graphene and, finally, to graphite.

Let $\mathcal{B}_n = [-\pi, \pi]^2$ and $\mathcal{B}_{\mathrm{g}} = [-\pi, \pi]^3$ be the *Brillouin zone* of $\mathcal{G}_n^{\mathrm{AA}}$ and $\mathcal{G}_{\mathrm{g}}^{\mathrm{AA}}$, respectively. For each *quasimomentum* $\theta \in \mathcal{B}_\varrho$, let $H_\varrho^{\mathrm{AA}}(\theta)$ be the *Bloch Hamiltonian* acting in $\mathrm{L}^2(\mathcal{W}_\varrho^{\mathrm{AA}})$ as in (4.3), with (different from H_ϱ^{AA}) domain $\mathrm{dom}\,(H_\varrho^{\mathrm{AA}}(\theta))$ which is the subspace of functions u that satisfies (i), (ii) and (iii) in $\mathrm{dom}\,(H_\varrho^{\mathrm{AA}})$ and also the following *cyclic condition* (or *Floquet condition*):

$$u(x + pE) = e^{ip\theta}u(x), \tag{4.6}$$

where $pE = \sum_{j=1}^{i} p_j E_j$, $p\theta = \sum_{j=1}^{i} p_j\theta_j$, for all $p \in \mathbb{Z}^i$ and all $x \in \mathcal{G}_\varrho^{\mathrm{AA}}$, with $i = 2$ for $\varrho = n$ and $i = 3$ for $\varrho = \mathrm{g}$. It is well known that $H_\varrho^{\mathrm{AA}}(\theta)$ has purely discrete spectrum [22],

denoted by $\sigma(H_\varrho^{\mathrm{AA}}(\theta)) = \{\lambda_k^\varrho(\theta)\}_{k\geq 1}$. The function $\theta \mapsto \{\lambda_k^\varrho(\theta)\}$ is called the *dispersion relation* of H_ϱ^{AA} and it determines its spectrum [13, 21, 38, 5]

$$\sigma(H_\varrho^{\mathrm{AA}}) = \bigcup_{\theta\in\mathcal{B}_\varrho} \sigma(H_\varrho^{\mathrm{AA}}(\theta)). \tag{4.7}$$

The goal now is to determine the spectra of $\sigma(H_\varrho^{\mathrm{AA}}(\theta))$, $\theta \in \mathcal{B}_\varrho$, by solving the eigenvalue problem

$$H_\varrho^{\mathrm{AA}}(\theta)u = \lambda u, \quad \lambda \in \mathbb{R}, \quad u \in D(H_\varrho^{\mathrm{AA}}(\theta)). \tag{4.8}$$

As in Section 3.2, we consider two auxiliary operators. The *Dirichlet Schrödinger operator* H^D, given (3.8) and satisfying the *Dirichlet boundary condition* (3.9), that is, a function $u \in L^2[0,1]$ is in $\operatorname{dom} H^D$ if and only if

$$u(0) = u(1) = 0. \tag{4.9}$$

The second operator is the *Hill operator* H^{per} defined in (3.10). We recall that for the spectral problem

$$H^{\mathrm{per}}\varphi = \lambda\varphi, \tag{4.10}$$

we consider the *monodromy matrix* $M(\lambda)$ of H^{per} given by (see [5])

$$\begin{bmatrix} \varphi(1) \\ \varphi'(1) \end{bmatrix} = M(\lambda) \begin{bmatrix} \varphi(0) \\ \varphi'(0) \end{bmatrix},$$

where φ is any solution of the problem (4.10). For the spectral properties of the Hill operator H^{per} and its discriminant $\mathcal{D}(\lambda)$, see Proposition 3.2.1.

Bilayer graphene

Now we consider the AA-stacked bilayer graphene $\mathcal{G}_2^{\mathrm{AA}}$, as described in Section 4.1. Let us write out the conditions (4.4), (4.5) and (4.6) on the fundamental domain $\mathcal{W}_2^{\mathrm{AA}}$ (see Figure 4.2). As we identify every edge e with the interval $[0,1]$, it follows that $v_{i1} \sim 0$ and $v_{i2} \sim 1$, for $i = 1, 2$. The cyclic Floquet condition (4.6) implies that

$$u_{a_{i2}}(1) = e^{i\theta_1}u_{a_{i1}}(1) \quad \text{and} \quad u_{a_{i3}}(1) = e^{i\theta_2}u_{a_{i1}}(1), \quad i = 1, 2. \tag{4.11}$$

So the continuity condition (4.4) is equivalent to

$$\begin{cases} u_{a_{11}}(0) = u_{a_{12}}(0) = u_{a_{13}}(0) = u_{f_1}(0) := A_1 \\ u_{a_{11}}(1) = e^{i\theta_1} u_{a_{12}}(1) = e^{i\theta_2} u_{a_{13}}(1) = u_{f_2}(1) := B_1 \\ u_{a_{21}}(0) = u_{a_{22}}(0) = u_{a_{23}}(0) = u_{f_1}(1) := A_2 \\ u_{a_{21}}(1) = e^{i\theta_1} u_{a_{22}}(1) = e^{i\theta_2} u_{a_{23}}(1) = u_{f_2}(0) := B_2 \end{cases} . \tag{4.12}$$

Similarly, the zero-flux condition (4.5) turns to

$$\begin{cases} u'_{a_{11}}(0) + u'_{a_{12}}(0) + u'_{a_{13}}(0) + t_0 u'_{f_1}(0) = 0 \\ u'_{a_{11}}(1) + e^{i\theta_1} u'_{a_{12}}(1) + e^{i\theta_2} u'_{a_{13}}(1) + t_0 u'_{f_2}(1) = 0 \\ u'_{a_{21}}(0) + u'_{a_{22}}(0) + u'_{a_{23}}(0) - t_0 u'_{f_1}(1) = 0 \\ u'_{a_{21}}(1) + e^{i\theta_1} u'_{a_{22}}(1) + e^{i\theta_2} u'_{a_{23}}(1) - t_0 u'_{f_2}(0) = 0 \end{cases} . \tag{4.13}$$

Let $\lambda \notin \sigma(H^D)$ (recall Section 3.2). Then there exists two linearly independent solutions $\varphi_{\lambda,0}, \varphi_{\lambda,1}$ of the problem

$$-\frac{\mathrm{d}^2\varphi(x)}{dx^2} + q(x)\varphi(x) = \lambda\varphi(x), \tag{4.14}$$

such that

$$\begin{cases} \varphi_{\lambda,0}(0) = 1 \\ \varphi_{\lambda,0}(1) = 0 \end{cases}, \qquad \begin{cases} \varphi_{\lambda,1}(0) = 0 \\ \varphi_{\lambda,1}(1) = 1 \end{cases} \tag{4.15}$$

and

$$\varphi'_{\lambda,1}(x) = -\varphi'_{\lambda,0}(1-x), \quad x \in [0,1]. \tag{4.16}$$

Since each edge of $\mathcal{W}_2^{\mathrm{AA}}$ is identified with the interval $[0,1]$, we can define $\varphi_{\lambda,i}$ in each edge and we will keep the same notation $\varphi_{\lambda,i}$. Hence, for each $\lambda \notin \sigma(H^D)$, we can represent

$$\begin{cases} u_{a_{i1}} = A_i\varphi_{\lambda,0} + B_i\varphi_{\lambda,1} \\ u_{a_{i2}} = A_i\varphi_{\lambda,0} + e^{-i\theta_1} B_i\varphi_{\lambda,1} \\ u_{a_{i3}} = A_i\varphi_{\lambda,0} + e^{-i\theta_2} B_i\varphi_{\lambda,1} \qquad i = 1,2. \\ u_{f_1} = A_1\varphi_{\lambda,0} + A_2\varphi_{\lambda,1} \\ u_{f_2} = B_2\varphi_{\lambda,0} + B_1\varphi_{\lambda,1} \end{cases} \tag{4.17}$$

It is easy to see that the continuity conditions (4.12) as well equation (4.14), are satisfied.

It remains to verify condition of zero-flux (4.13). By substituting (4.17) into (4.13),

$$\begin{cases} (3+t_0)_1\varphi'_{\lambda,0}(0) + \bar{F}(\theta)B_1\varphi'_{\lambda,1}(0) + t_0A_2\varphi'_{\lambda,1}(0) = 0 \\ F(\theta)A_1\varphi'_{\lambda,0}(1) + (3+t_0)B_1\varphi'_{\lambda,1}(1) + t_0B_2\varphi'_{\lambda,0}(1) = 0 \\ -t_0A_1\varphi'_{\lambda,0}(1) + (3\varphi'_{\lambda,0}(0) - t_0\varphi'_{\lambda,1}(1))A_2 + \bar{F}(\theta)B_2\varphi'_{\lambda,1}(0) = 0 \\ -t_0B_1\varphi'_{\lambda,1}(0) + F(\theta)A_2\varphi'_{\lambda,0}(1) + (3\varphi'_{\lambda,1}(1) - t_0\varphi'_{\lambda,0}(0))B_2 = 0 \end{cases}, \tag{4.18}$$

where $F(\theta) := 1 + e^{-i\theta_1} + e^{-i\theta_2}$ and $\bar{F}(\theta)$ its complex conjugate. By (4.16), we have that $\varphi'_{\lambda,0}(1) = -\varphi'_{\lambda,1}(0)$ and $\varphi'_{\lambda,0}(0) = -\varphi'_{\lambda,1}(1)$. Thus the system (4.18) is equivalent to

$$\begin{cases} -(3+t_0)A_1\varphi'_{\lambda,1}(1) + \bar{F}(\theta)B_1\varphi'_{\lambda,1}(0) + t_0A_2\varphi'_{\lambda,1}(0) = 0 \\ -F(\theta)A_1\varphi'_{\lambda,1}(0) + (3+t_0)B_1\varphi'_{\lambda,1}(1) - t_0B_2\varphi'_{\lambda,1}(0) = 0 \\ t_0A_1\varphi'_{\lambda,1}(0) - (3+t_0)A_2\varphi'_{\lambda,1}(1)) + \bar{F}(\theta)B_2\varphi'_{\lambda,1}(0) = 0 \\ -t_0B_1\varphi'_{\lambda,1}(0) - F(\theta)A_2\varphi'_{\lambda,1}(0) + (3+t_0)B_2\varphi'_{\lambda,1}(1)) = 0 \end{cases}. \tag{4.19}$$

Since $\varphi'_{\lambda,1}(0) \neq 0$, the quotient $\eta(\lambda) := \varphi'_{\lambda,1}(1)/\varphi'_{\lambda,1}(0)$ is well defined. Hence, dividing the system (4.19) by $\varphi'_{\lambda,1}(0)$ and multiplying the second and fourth lines by -1, we obtain

$$\begin{cases} -(3+t_0)\eta(\lambda)A_1 + \bar{F}(\theta)B_1 + t_0A_2 = 0 \\ F(\theta)A_1 - (3+t_0)\eta(\lambda)B_1 + t_0B_2 = 0 \\ t_0A_1 - (3+t_0)\eta(\lambda)A_2 + \bar{F}(\theta)B_2 = 0 \\ t_0B_1 + F(\theta)A_2 - (3+t_0)\eta(\lambda)B_2 = 0 \end{cases}. \tag{4.20}$$

The matrix form of the system (4.20) is

$$\mathcal{M}_2^{\mathrm{AA}}(\lambda,\theta)X = 0, \tag{4.21}$$

where $X = \begin{bmatrix} A_1 & B_1 & A_2 & B_2 \end{bmatrix}^\intercal$ and

$$\mathcal{M}_2^{\mathrm{AA}}(\lambda,\theta) = \begin{bmatrix} -T_1\eta & \bar{F} & t_0 & 0 \\ F & -T_1\eta & 0 & t_0 \\ t_0 & 0 & -T_1\eta & \bar{F} \\ 0 & t_0 & F & -T_1\eta \end{bmatrix}, \tag{4.22}$$

where $T_1 = 3 + t_0$, $F = F(\theta)$ and $\eta = \eta(\lambda)$. From now on, we will omit the dependence of θ in the matrix $\mathcal{M}_2^{\mathrm{AA}}(\lambda)$. Note that $\det(\mathcal{M}_2^{\mathrm{AA}}(\lambda)) = 0$ is a quartic polynomial in $\eta(\lambda)$.

Hence, if there exists a $\theta \in \mathcal{B}$ such that $\det(\mathcal{M}_2^{\mathrm{AA}}(\lambda)) = 0$, that is, $\eta(\lambda)$ is one of the four roots of $\det(\mathcal{M}_2^{\mathrm{AA}}(\lambda)) = 0$, it follows that the representation (4.17) solves the eigenvalue problem (4.8). Therefore by (4.7) it follows that $\lambda \in \sigma(H_2^{\mathrm{AA}})$.

Trilayer graphene

We now analyze the odd case $n = 3$; $\mathcal{G}_3^{\mathrm{AA}}$ consists of three graphene sheets G_1, G_2 and G_3. Similarly to the case $n = 2$, lets us write out the conditions (4.4), (4.5) and (4.6) on the fundamental domain $\mathcal{W}_3^{\mathrm{AA}}$ (see Figure 4.2). Since

$$u_{a_{i2}}(1) = e^{i\theta_1} u_{a_{i1}}(1) \quad \text{and} \quad u_{a_{i3}}(1) = e^{i\theta_2} u_{a_{i1}}(1), \quad i = 1, 2, 3,$$

it follows that the continuity condition (4.4) is equivalent to

$$\begin{cases} u_{a_{11}}(0) = u_{a_{12}}(0) = u_{a_{13}}(0) = u_{f_{11}}(0) := A_1 \\ u_{a_{11}}(1) = e^{i\theta_1} u_{a_{12}}(1) = e^{i\theta_2} u_{a_{13}}(1) = u_{f_{12}}(1) := B_1 \\ u_{a_{21}}(0) = u_{a_{22}}(0) = u_{a_{23}}(0) = u_{f_{11}}(1) = u_{f_{21}}(1) := A_2 \\ u_{a_{21}}(1) = e^{i\theta_1} u_{a_{22}}(1) = e^{i\theta_2} u_{a_{23}}(1) = u_{f_{12}}(0) = u_{f_{22}}(0) := B_2 \\ u_{a_{31}}(0) = u_{a_{32}}(0) = u_{a_{33}}(0) = u_{f_{21}}(0) := A_3 \\ u_{a_{31}}(1) = e^{i\theta_1} u_{a_{32}}(1) = e^{i\theta_2} u_{a_{33}}(1) = u_{f_{22}}(1) := B_3 \end{cases}, \tag{4.23}$$

and the zero-flux condition (4.5) is equivalent to

$$\begin{cases} u'_{a_{11}}(0) + u'_{a_{12}}(0) + u'_{a_{13}}(0) + t_0 u'_{f_{11}}(0) = 0 \\ u'_{a_{11}}(1) + e^{i\theta_1} u'_{a_{12}}(1) + e^{i\theta_2} u'_{a_{13}}(1) + t_0 u'_{f_{12}}(1) = 0 \\ u'_{a_{21}}(0) + u'_{a_{22}}(0) + u'_{a_{23}}(0) - t_0 u'_{f_{11}}(1) - t_0 u'_{f_{21}}(1) = 0 \\ u'_{a_{21}}(1) + e^{i\theta_1} u'_{a_{22}}(1) + e^{i\theta_2} u'_{a_{23}}(1) - t_0 u'_{f_{12}}(0) - t_0 u'_{f_{22}}(0) = 0 \\ u'_{a_{31}}(0) + u'_{a_{32}}(0) + u'_{a_{33}}(0) + t_0 u'_{f_{21}}(0) = 0 \\ u'_{a_{31}}(1) + e^{i\theta_1} u'_{a_{32}}(1) + e^{i\theta_2} u'_{a_{33}}(1) + t_0 u'_{f_{22}}(1) = 0 \end{cases}. \tag{4.24}$$

Let $\lambda \notin \sigma(H^D)$ and let $\varphi_{\lambda,0}$ and $\varphi_{\lambda,1}$ be the two linearly independent solutions of the problem (4.14) that satisfies (4.15) and (4.16). If we write

$$\begin{cases} u_{a_{i1}} = A_i\varphi_{\lambda,0} + \beta_i B_{\lambda,1} \\ u_{a_{i2}} = A_i\varphi_{\lambda,0} + e^{-i\theta_1}B_i\varphi_{\lambda,1} \\ u_{a_{i3}} = A_i\varphi_{\lambda,0} + e^{-i\theta_2}B_i\varphi_{\lambda,1} \\ u_{f_{11}} = A_1\varphi_{\lambda,0} + A_2\varphi_{\lambda,1} \qquad i = 1,2,3, \\ u_{f_{12}} = B_2\varphi_{\lambda,0} + B_1\varphi_{\lambda,1} \\ u_{f_{21}} = A_3\varphi_{\lambda,0} + A_2\varphi_{\lambda,1} \\ u_{f_{22}} = B_2\varphi_{\lambda,0} + B_3\varphi_{\lambda,1} \end{cases} \tag{4.25}$$

the continuity condition (4.23), as well as the problem (4.8), are satisfied. It remains to verify the zero-flux condition (4.24). By substituting (4.25) into (4.24),

$$\begin{cases} (3+t_0)\varphi_0'(0)A_1 + \bar{F}\varphi_1'(0)B_1 + t_0\varphi_1'(0)A_2 = 0 \\ F\varphi_0'(1)A_1 + (3+t_0)\varphi_1'(1)B_1 + t_0\varphi_0'(1)B_2 = 0 \\ -t_0\varphi_0'(1)A_1 + (3\varphi_0'(0) - 2t_0\varphi_1'(1))A_2 + \bar{F}\varphi_1'(0)B_2 - t_0\varphi_0'(1)A_3 = 0 \\ -t_0\varphi_1'(0)B_1 + F\varphi_0'(1)A_2 + (3\varphi_1'(1) - 2t_0\varphi_0'(0))B_2 - t_0\varphi_1'(0)B_3 = 0 \\ t_0\varphi_1'(0)A_2 + (3+t_0)\varphi_0'(0)A_3 + \bar{F}\varphi_1'(0)B_3 = 0 \\ t_0\varphi_0'(1)B_2 + F\varphi_0'(1)A_3 + (3+t_0)\varphi_1'(1)B_3 = 0 \end{cases}$$

where $F = F(\theta) = 1 + e^{i\theta_1} + e^{i\theta_2}$, $\bar{F}$ its complex conjugate and $\varphi_i = \varphi_{\lambda,i}$. Since $\varphi_0'(1) = -\varphi_1'(0)$ and $\varphi_0'(0) = -\varphi_1'(1)$, multiplying the even equations for -1 and dividing the whole above system by $\varphi_1'(0) \neq 0$, it follows that

$$\begin{cases} -T_1\eta A_1 + \bar{F}B_1 + t_0A_2 = 0 \\ FA_1 - T_1\eta B_1 + t_0B_2 = 0 \\ t_0A_1 - T_2\eta A_2 + \bar{F}B_2 + t_0A_3 = 0 \\ t_0B_1 + FA_2 - T_2\eta B_2 + t_0B_3 = 0 \\ t_0A_2 - T_1\eta A_3 + \bar{F}B_3 = 0 \\ t_0B_2 + FA_3 - T_1\eta B_3 = 0 \end{cases}, \tag{4.26}$$

where $T_1 := 3 + t_0$, $T_2 := 3 + 2t_0$ and $\eta = \eta(\lambda) = \varphi'_{\lambda,1}(1)/\varphi'_{\lambda,0}(0)$. The matrix form of the obtained system in this case is

$$\mathcal{M}_3^{\mathrm{AA}}(\lambda)X = 0,$$

where $X = \begin{bmatrix} A_1 & B_1 & A_2 & B_2 & A_3 & B_3 \end{bmatrix}^\intercal$ and

$$\mathcal{M}_3^{\mathrm{AA}}(\lambda) = \begin{bmatrix} M_{T_1T_2}^{\mathrm{AA}} & (\tilde{m}_{t_0}^{\mathrm{AA}})^\intercal \\ \tilde{m}_{t_0}^{\mathrm{AA}} & N_{T_1}^{\mathrm{AA}} \end{bmatrix}, \tag{4.27}$$

with (denote, for $i = 1, 2$, $S_i = T_1, T_2$)

$$M_{S_1S_2}^{\mathrm{AA}} = \begin{bmatrix} -S_1\eta & \bar{F} & t_0 & 0 \\ F & -S_1\eta & 0 & t_0 \\ t_0 & 0 & -S_2\eta & \bar{F} \\ 0 & t_0 & F & -S_2\eta \end{bmatrix}, \tag{4.28}$$

$$\tilde{m}_{t_0}^{\mathrm{AA}} = \begin{bmatrix} 0 & 0 & t_0 & 0 \\ 0 & 0 & 0 & t_0 \end{bmatrix} \quad \text{and} \quad N_{T_1}^{\mathrm{AA}} = \begin{bmatrix} -T_1\eta & \bar{F} \\ F & -T_1\eta \end{bmatrix}. \tag{4.29}$$

Note that $\mathcal{M}_2^{\mathrm{AA}}(\lambda) = M_{T_1T_1}^{\mathrm{AA}}$. Thus, if there exists $\theta \in \mathcal{B}$ such that $\det(\mathcal{M}_3^{AA}(\lambda)) = 0$, the representation (4.25) solves the eigenvalue problem (4.8) and so $\lambda \in \sigma(H_3^{AA})$.

Multilayer graphene

We now consider n sheets of AA-stacked graphene. Let $\lambda \notin \sigma(H^D)$. Similarly to the cases $n = 2, 3$, we have performed calculations for larger values of n and, by writing out the conditions (4.4), (4.5) and (4.6) on the fundamental domain $\mathcal{W}_n^{\mathrm{AA}}$; useful patterns have arisen, which have allowed us to get an expression for the general case.

Write the functions u_{a_j} and $u_{f_{i,k}}$ as linear combinations of $\varphi_{\lambda,0}$ and $\varphi_{\lambda,1}$ in such way that these representations satisfy the vertex conditions (4.4) and (4.5) and solve the eigenvalue problem in each vertex of $\mathcal{W}_n^{\mathrm{AA}}$. However, we have found that important properties depend on whether n is even or odd. If $n \geq 4$ is even, we have

$$\mathcal{M}_n^{\mathrm{AA}}(\lambda) = \begin{bmatrix} M_{T_1T_2}^{\mathrm{AA}} & (m_{t_0}^{\mathrm{AA}})^\intercal & 0 & \dots & 0 & 0 \\ m_{t_0}^{\mathrm{AA}} & M_{T_2T_2}^{\mathrm{AA}} & (m_{t_0}^{\mathrm{AA}})^\intercal & \dots & 0 & 0 \\ 0 & m_{t_0}^{\mathrm{AA}} & M_{T_2T_2}^{\mathrm{AA}} & \dots & 0 & 0 \\ \vdots & \vdots & \vdots & \ddots & \vdots & \vdots \\ 0 & 0 & 0 & \dots & M_{T_2T_2}^{\mathrm{AA}} & (m_{t_0}^{\mathrm{AA}})^\intercal \\ 0 & 0 & 0 & \dots & m_{t_0}^{\mathrm{AA}} & M_{T_2T_1}^{\mathrm{AA}} \end{bmatrix}, \tag{4.30}$$

and if $n \geq 5$ is odd, the matrix $\mathcal{M}_n^{AA}$ is given by

$$\mathcal{M}_n^{\mathrm{AA}}(\lambda) = \begin{bmatrix} M_{T_1T_2}^{\mathrm{AA}} & (m_{t_0}^{\mathrm{AA}})^\intercal & 0 & \dots & 0 & 0 \\ m_{t_0}^{\mathrm{AA}} & M_{T_2T_2}^{\mathrm{AA}} & (m_{t_0}^{\mathrm{AA}})^\intercal & \dots & 0 & 0 \\ 0 & m_{t_0}^{\mathrm{AA}} & M_{T_2T_2}^{\mathrm{AA}} & \dots & 0 & 0 \\ \vdots & \vdots & \vdots & \ddots & \vdots & \vdots \\ 0 & 0 & 0 & \dots & M_{T_2T_2}^{\mathrm{AA}} & (\tilde{m}_{t_0}^{\mathrm{AA}})^\intercal \\ 0 & 0 & 0 & \dots & \tilde{m}_{t_0}^{\mathrm{AA}} & N_{T_1}^{\mathrm{AA}} \end{bmatrix}, \tag{4.31}$$

where

$$m_{t_0}^{\mathrm{AA}} = \begin{bmatrix} 0 & 0 & t_0 & 0 \\ 0 & 0 & 0 & t_0 \\ 0 & 0 & 0 & 0 \\ 0 & 0 & 0 & 0 \end{bmatrix}. \tag{4.32}$$

AA-stacked graphite

Finally, we consider the AA-stacked graphite. Similarly to the other cases, we describe the conditions (4.4), (4.5) and (4.6) on the set $\mathcal{W}_{\mathrm{g}}^{\mathrm{AA}}$ (see Figure 4.2). By (4.4) and (4.6),

$$\begin{cases} u_{a_1}(0) = u_{a_2}(0) = u_{a_3}(0) = u_{f_{1,\pm}}(0) := A \\ u_{a_1}(1) = e^{i\theta_1} u_{a_2}(0) = e^{i\theta_2} u_{a_3}(0) = u_{f_{2,\pm}}(1) := B \end{cases} \tag{4.33}$$

and, by the vanishing flux condition (4.5), it follows that

$$\begin{cases} u'_{a_1}(0) + u'_{a_2}(0) + u'_{a_3}(0) + t_0 u'_{f_{1,+}}(0) + t_0 u'_{f_{1,-}}(0) = 0 \\ u'_{a_1}(1) + e^{i\theta_1} u'_{a_2}(1) + e^{i\theta_2} u'_{a_3}(1) + t_0 u'_{f_{2,+}}(1) + t_0 u'_{f_{2,-}}(1) = 0 \end{cases}. \tag{4.34}$$

Since, by Floquet condition (4.6),

$$u_{f_{1,\pm}}(1) = e^{\pm i\theta_3} u_{f_{1,\pm}}(0) \quad \text{and} \quad u_{f_{2,\pm}}(0) = e^{\mp i\theta_3} u_{f_{2,\pm}}(1),$$

we can write out, for $\lambda \notin \sigma(H^D)$,

$$\begin{cases} u_{a_1} = A\varphi_0 + B\varphi_1 \\ u_{a_2} = A\varphi_0 + e^{-i\theta_1} B\varphi_1 \\ u_{a_3} = A\varphi_0 + e^{-i\theta_2} B\varphi_1 \\ u_{f_{1,\pm}} = A\varphi_0 + e^{\pm i\theta_3} A\varphi_1 \\ u_{f_{2,\pm}} = e^{\mp i\theta_3} B\varphi_0 + B\varphi_1 \end{cases}, \tag{4.35}$$

where φ_0 and φ_1 are the two linearly independent solutions of the eigenvalue problem (4.14) that satisfies (4.15) and (4.16). Analogously to the calculations in the cases $n = 2, 3$, by using the representation (4.35) in the systems (4.33) and (4.34), we obtain the equation

$$\mathcal{M}_{\mathrm{g}}^{\mathrm{AA}}(\lambda) X = 0,$$

where $X = \begin{bmatrix} A & B \end{bmatrix}^{\intercal}$ and

$$\mathcal{M}_{\mathrm{g}}^{\mathrm{AA}}(\lambda) = \begin{bmatrix} -T_2\eta + 2t_0\cos\theta_3 & \bar{F} \\ F & -T_2\eta + 2t_0\cos\theta_3 \end{bmatrix}, \tag{4.36}$$

with $T_2 = 3 + 2t_0$, $\eta = \eta(\lambda)$ and $F = F(\theta) = 1 + e^{i\theta_1} + e^{i\theta_2}$.

Spectra

For all the above cases, we have got the following result:

Proposition 4.2.1. *Let $\lambda \notin \sigma(H^D)$ and $t_0 \in (0, 1)$. Then, for $\varrho = n, \mathrm{g}$, $\lambda \in \sigma(H_\varrho^{\mathrm{AA}})$ if and only if there exists $\theta \in \mathcal{B}$ such that*

$$\det(\mathcal{M}_\varrho^{\mathrm{AA}}(\lambda)) = 0. \tag{4.37}$$

Note that $\det(\mathcal{M}_n^{\mathrm{AA}}(\lambda)) = 0$ is a polynomial of degree n in $\eta(\lambda)$. By Proposition 4.2.1, the spectra $\sigma(H_n^{\mathrm{AA}})$ is basically determined if we know the range of all n roots $\eta(\lambda, \theta)$ of $\det(\mathcal{M}_n^{\mathrm{AA}}(\lambda)) = 0$. Obviously, it is not a simple task to find the roots of such polynomials.

However, for the cases $n = 2, 3$ we can explicitly calculate the roots of (4.37). For $n = 2$, we use the Laplace's formula for matrix determinants in $\mathcal{M}_2^{\mathrm{AA}}(\lambda)$, given by (4.22), to obtain

$$\begin{aligned} \det(\mathcal{M}_2^{\mathrm{AA}}(\lambda)) &= T_1^4\,\eta^4(\lambda) - 2T_1^2\left(t_0^2 + F(\theta)\bar{F}(\theta)\right)\eta^2(\lambda) \\ &+ \left(F(\theta)\bar{F}(\theta) - t_0^2\right)^2 = 0. \end{aligned} \tag{4.38}$$

Note that we can easily turn the quartic equation (4.38) into a quadratic equation in the variable η^2. Thus the four roots are

$$\eta_{\pm}^{\pm}(\lambda,\theta) = \pm\sqrt{\frac{F(\theta)\bar{F}(\theta) + t_0^2 \pm 2\sqrt{t_0^2 F(\theta)\bar{F}(\theta)}}{T_1^2}}. \tag{4.39}$$

Here, the subscript $\pm$ refers to the corresponding outside symbol of the first square root, whereas the superscript $\pm$ refers to the inside one.

For the case $n = 3$, applying Laplace's formula to (4.27), we obtain

$$\begin{aligned} \det(\mathcal{M}_3^{\mathrm{AA}}(\lambda)) &= T_1^4T_2^2\,\eta^6 - \left(4T_1^3T_2t_0^2 + (T_1^4 + 2T_1^2T_2^2)(F\bar{F})^2\right)\eta^4 \\ &+ \left(4T_1T_2t_0^2F\bar{F} + (T_1^2 + T_2^2)(F\bar{F})^2 + T_1^2(F\bar{F} - 2t_0^2)^2\right)\eta^2 \\ &- F\bar{F}\left(F\bar{F} - 2t_0^2\right)^2. \end{aligned} \tag{4.40}$$

The roots of $\det(\mathcal{M}_3^{\mathrm{AA}}(\lambda)) = 0$ are the following:

$$\tilde{\eta}_{\pm}^{\pm}(\lambda,\theta) = \pm\sqrt{\frac{G(\theta,t_0) \pm \sqrt{G(\theta,t_0)^2 - 4T_1^2T_2^2(F\bar{F} - 2t_0^2)^2}}{2T_1^2T_2^2}}, \tag{4.41}$$

$$\bar{\eta}_{\pm}(\lambda,\theta) = \pm\sqrt{\frac{F\bar{F}}{T_1^2}}, \tag{4.42}$$

where $G(\theta,t_0) = 4T_1T_2t_0^2 + (T_1^2 + T_2^2)F\bar{F}$. Note that the procedure to find the exact roots (4.41) and (4.42) of $\det(\mathcal{M}_3^{\mathrm{AA}}(\lambda)) = 0$ is the same described in Remark 3.2.1, for the AB-stacked trilayer graphene case.

It is easier to find the two roots of $\det(\mathcal{M}_{\mathrm{g}}^{\mathrm{AA}}(\lambda)) = 0$, which are

$$\eta_{\pm}^{\mathrm{g}}(\lambda,\theta) = \frac{2t_0\cos\theta_3 \pm \sqrt{F\bar{F}}}{T_2}. \tag{4.43}$$

In order to state the characterization theorem of the spectra of $H_{\varrho}^{\mathrm{AA}}$, we shall notice that:

- Lemma 3.2.2 (for Bernal-stacked graphene, see Section 3.2) that relates the functions $\eta(\lambda)$ and the discriminant $\mathcal{D}(\lambda)$ of the Hill operator, still holds for the AA-stacked

multilayer graphene and for the AA-stacked graphite. Thus, we have the following relation:

$$\eta(\lambda) = \frac{1}{2}\mathcal{D}(\lambda). \tag{4.44}$$

Hence, we are able to relate the spectra $\sigma(H^{\mathrm{per}})$ and $\sigma(H_{\varrho}^{\mathrm{AA}})$ (see Theorem 4.2.1).

- In the AA-stacked multilayer graphene and AA-stacked graphite, it is also true that a Dirichlet eigenvalue $\lambda \in \sigma(H^D)$ is an infinite multiplicity eigenvalue of $H_{\varrho}^{\mathrm{AA}}$, that is, the Lemma 3.2.1 still holds in this case.

We are ready to characterize the spectrum of $H_{\varrho}^{\mathrm{AA}}$. The proof of the next theorem follows the same arguments presented in the proof of Theorem 2.2.1, Theorem 7 in [12] and Theorem 3.6 in [23].

Theorem 4.2.1. *For the AA-stacked multilayer graphene and AA-stacked graphite Schrödinger operator* (4.3)*, we have:*

(i) The singular continuous spectrum of the $H_{\varrho}^{\mathrm{AA}}$ is empty.

(ii) The dispersion relation of $H_{\varrho}^{\mathrm{AA}}$ consists of two parts:

- *the pairs (λ, θ) $(\lambda \notin \sigma(H^D))$ such that*

$$\mathcal{D}(\lambda) = 2\eta(\lambda), \tag{4.45}$$

where $\eta(\lambda)$ are the roots of the equation $\det(\mathcal{M}_{\varrho}^{\mathrm{AA}}(\lambda)) = 0$;

- *the collection of flat branches $\lambda \in \sigma(H^D)$, that is, the pairs (λ, θ) for any $\theta \in \mathcal{B}_{\varrho}$.*

(iii) The absolutely continuous spectrum $\sigma_{\mathrm{ac}}(H_{\varrho}^{\mathrm{AA}})$ coincides, as a set, with $\sigma(H^{\mathrm{per}})$, that is, it has band-gap structure and

$$\sigma_{\mathrm{ac}}(H_{\varrho}^{\mathrm{AA}}) = \{\lambda \in \mathbb{R} : |\mathcal{D}(\lambda)| \leq 2\}. \tag{4.46}$$

(iv) The pure point spectrum $\sigma_{\mathrm{pp}}(H_{\varrho}^{\mathrm{AA}})$ of $H_{\varrho}^{\mathrm{AA}}$ coincides with $\sigma(H^D)$, and each $\lambda \in \sigma(H^D)$ is an eigenvalue of infinite multiplicity of $H_{\varrho}^{\mathrm{AA}}$.

(v) The spectrum $\sigma(H_{\varrho}^{\mathrm{AA}})$ has gaps if and only if $\sigma(H^{\mathrm{per}})$ has gaps.

In particular, for the AA-stacked bilayer graphene operator H_2^{AA}, (4.45) of the dispersion relation is

$$\mathcal{D}(\lambda) = \pm\frac{2}{3+t_0}\sqrt{F(\theta)\bar{F}(\theta) + t_0^2 \pm 2t_0\sqrt{F(\theta)\bar{F}(\theta)}},$$

and for the AA-stacked trilayer graphene operator H_3^{AA}, (4.45) takes the form

$$\mathcal{D}(\lambda) = \pm\frac{2}{\sqrt{2}\,T_1T_2}\sqrt{G(\theta,t_0) \pm \sqrt{G(\theta,t_0)^2 - 4T_1^2T_2^2(F\bar{F}-2t_0^2)^2}}, \pm\frac{2}{T_1}\sqrt{F\bar{F}}.$$

Similarly, the dispersion relation (4.45) for the AA-stacked graphite is

$$\mathcal{D}(\lambda) = \frac{2}{T_2}\left(t_0\cos\theta_3 \pm \sqrt{F(\theta)\bar{F}(\theta)}\right).$$

4.3 Dirac cones

Now we prove our main result about Dirac cones (see Definition 2.3.1) in the dispersion relation of the AA-stacked multilayer graphene Schrödinger operator, given by Theorem 4.2.1*(ii)*. Before the theorem, we shall make some remarks.

Remark 4.3.1. *1. In order to check (2.39) for the D-point candidates θ_D, we use (4.45) and expand in Taylor's series $\mathcal{D}(\lambda(\theta))$ around $\lambda(\theta_D)$ and $\eta(\lambda,\theta)$ around θ_D. Theorem 4.3.1 proves that, for $n = 2, 3$ and for the AA-stacked graphite, every root $\eta(\lambda,\theta)$ of $\det(\mathcal{M}_\varrho^{\mathrm{AA}}(\lambda)) = 0$ have a (nonzero) linear component $\pm\gamma|\theta-\theta_D|$.*

2. For $n \geq 4$, we employ approximations by vanishing some selected instances of t_0 in $\mathcal{M}_n^{\mathrm{AA}}(\lambda)$; to distinguish such instances we denote them by c; $c = 0$ corresponds to the approximation, whereas $c = t_0$ recovers the full model. In Theorem 4.3.1, we show the existence of the linear component $\pm\gamma_1|\theta-\theta_D|$ for the approximations of η (i.e., $c = 0$), which estimate the full model up to a correction $\mathcal{O}(c^2)$. Then we verify that, independently of t_0, the parameter γ_1 does not vanish as $c \to 0$ (and so, by continuity, it does not vanish for all t_0 small enough); therefore, the linear component $\pm\gamma|\theta-\theta_D|$ of $\eta(\lambda,\theta)$ survives in the full model, at least for small values of $t_0 > 0$.

Theorem 4.3.1. *Let n be a positive integer, and recall that H_ϱ^{AA} denotes the AA-stacked multilayer graphene operator, for $\varrho = n$, and the AA-stacked graphite operator, for $\varrho = \mathrm{g}$. Then:*

(i) For $n = 1, 2, 3$, the dispersion relation of H_n^{AA} have Dirac cones in the Brillouin zone.

(ii) Given $n \geq 4$, for $t_0 > 0$ small enough, the dispersion relation H_n^{AA} have Dirac cones in the respective Brillouin zone.

(iii) The dispersion relation of the graphite operator $H_{\mathrm{g}}^{\mathrm{AA}}$ have Dirac cones in the Brillouin zone $\mathcal{B}_{\mathrm{g}}$.

Proof. (i) Single layer: The case of a single sheet of graphene was discussed in [23] and in Theorem 2.3.1, with $\alpha_N = \alpha_B = 0$. For completeness, and as a warm up to the other cases, we present here a detailed argument. By (4.45) of Theorem 4.2.1, the dispersion relation of the graphene is given by $\mathcal{D}(\lambda) = 2\eta_{\pm}(\lambda, \theta)$, for $\lambda \notin \sigma(H^D)$, where (see [23])

$$\eta_{\pm}(\lambda, \theta) = \pm \frac{\sqrt{F(\theta)\bar{F}(\theta)}}{3}, \tag{4.47}$$

with $F(\theta) = 1 + e^{i\theta_1} + e^{i\theta_2}$. Note that as in Chapter 3, it is suffices to consider $\theta \in \mathcal{B}_d := \{\theta \in \mathcal{B} : \theta_1 = -\theta_2\}$, the diagonal of the Brillouin zone. Hence, $F(\theta) = 1 + 2\cos(\theta_1)$ and we can rewrite $\eta_{\pm}(\lambda, \theta)$ as

$$\eta_{\pm}(\lambda, \theta) = \pm \frac{|F(\theta)|}{3}.$$

Now we expand $\eta_{\pm}(\lambda, \theta)$ in Taylor's series around $\theta_D := \pm 2\pi/3$. Since

$$\cos\theta_1 = -\frac{1}{2} \mp \frac{\sqrt{3}}{2}(\theta_1 - \theta_D) + \mathcal{O}((\theta_1 - \theta_D)^2),$$

it follows that

$$|F(\theta)| = \sqrt{3}|\theta_1 - \theta_D| + \mathcal{O}(|\theta_1 - \theta_D|^2).$$

Hence

$$\eta_{\pm}(\lambda, \theta) - \eta_{\pm}(\lambda, \theta_D) = \pm\gamma_{1,D}|\theta - \theta_D| + \mathcal{O}(|\theta_1 - \theta_D|^2), \tag{4.48}$$

where $\gamma_{1,D} = \sqrt{3}/3$.

It remains to analyze $\mathcal{D}(\lambda(\theta))$. Since $\mathcal{D}'(\lambda) \neq 0$ in the spectral bands of $\sigma(H_n^{\mathrm{AA}})$, then expanding $\mathcal{D}(\lambda)$ in Taylor's series around $\lambda(\theta_D)$, we obtain

$$\mathcal{D}(\lambda(\theta)) - \mathcal{D}(\lambda(\theta_D))) = \mathcal{D}'(\lambda(\theta_D))(\lambda(\theta) - \lambda(\theta_D)) + \mathcal{O}((\lambda(\theta) - \lambda(\theta_D))^2). \tag{4.49}$$

Hence, the possible presence of Dirac cones in (2.39) is regulated by the expansion of $\eta_{\pm}$. In particular, in the free case, i.e., $q_0 = 0$, since $\mathcal{D}(\lambda(\theta)) = 2\cos\sqrt{\lambda(\theta)}$ (see [12, 23]), then

$$\mathcal{D}'(\lambda(\theta_D)) = -\frac{\sin(\sqrt{(\lambda(\theta_D))})}{\sqrt{\lambda(\theta_D)}}.$$

Therefore, from (4.48) and (4.49), (2.39) follows with $\gamma = \gamma_{1,D}/\mathcal{D}'(\lambda(\theta_D))$.

Bilayer graphene: Now we study the Dirac cones for $n = 2$ by making explicit the values of γ in each cone. In this case, in fact for all $n \geq 2$, it is enough to work with the right hand side of (2.39), since the discussion for the left hand side of (2.39) repeats the single layer case done above in (4.49). First note that by a simple explicit calculations we conclude:

Lemma 4.3.1. *Let $\eta_{\pm}^{\pm}(\lambda, \theta)$, given by (4.39). As a function of $\theta \in \mathcal{B}$, we have the ranges:*

$$\operatorname{img}(\eta_{+}^{+}(\lambda,\theta)) = \left[\frac{t_0}{3+t_0}, 1\right], \quad \operatorname{img}(\eta_{-}^{+}(\lambda,\theta)) = \left[-1, -\frac{t_0}{3+t_0}\right], \tag{4.50}$$

$$\operatorname{img}(\eta_{+}^{-}(\lambda,\theta)) = \left[0, \frac{3-t_0}{3+t_0}\right], \quad \operatorname{img}(\eta_{-}^{-}(\lambda,\theta)) = \left[-\frac{3-t_0}{3+t_0}, 0\right]. \tag{4.51}$$

Moreover,

(i) $\max \eta_{+}^{+}(\lambda,\theta) = 1$ *and* $\min \eta_{+}^{+}(\lambda,\theta) = \frac{t_0}{3+t_0}$, *attained at* $(0,0)$ *and* $\pm(2\pi/3, -2\pi/3)$, *respectively.*

(ii) $\max \eta_{-}^{+}(\lambda,\theta) = -\frac{t_0}{3+t_0}$ *and* $\min \eta_{-}^{+}(\lambda,\theta) = -1$, *attained at* $\pm(2\pi/3, -2\pi/3)$ *and* $(0,0)$, *respectively.*

(iii) $\max \eta_{+}^{-}(\lambda,\theta) = \frac{3-t_0}{3+t_0}$ *and* $\min \eta_{+}^{-}(\lambda,\theta) = 0$, *attained at* $(0,0)$ *and* $\pm(\arccos(\frac{\pm t_0 - 1}{2}), -\arccos(\frac{\pm t_0 - 1}{2}))$, *respectively.*

(iv) $\max \eta_{-}^{-}(\lambda,\theta) = 0$ *and* $\min \eta_{-}^{-}(\lambda,\theta) = -\frac{3-t_0}{3+t_0}$, *attained at* $\pm(\arccos(\frac{\pm t_0 - 1}{2}), -\arccos(\frac{\pm t_0 - 1}{2}))$ *and* $(0,0)$, *respectively.*

As in the graphene case, it is suffices to consider $\theta \in \mathcal{B}_d$. Then we can rewrite $\eta_{\pm}^{\pm}(\lambda,\theta)$ as

$$\eta_{\pm}^{\pm}(\lambda,\theta) = \pm\frac{||F(\theta)| \pm t_0|}{3+t_0}. \tag{4.52}$$

Let $\theta_{2,D} := \pm 2\pi/3$ and recall that $T_1 = 3+t_0$. Expanding in Taylor's series $\eta_{+}^{\pm}(\lambda,\theta)$ around $\theta_{2,D}$, we get

$$\eta_{+}^{\pm}(\lambda,\theta) = \frac{\left|\sqrt{3}|\theta - \theta_{2,D}| \pm t_0\right|}{T1} + \mathcal{O}(|\theta_1 - \theta_{2,D}|^2),$$

that is,

$$\eta_{+}^{\pm}(\lambda,\theta) - \eta_{+}^{\pm}(\lambda,\theta_{2,D}) = \eta_{+}^{\pm}(\lambda,\theta) - \frac{t_0}{T_1} = \pm\gamma_{2,D}|\theta_1 - \theta_{2,D}| + \mathcal{O}(|\theta_1 - \theta_{2,D}|^2),$$

with $\gamma_{2,D} = \sqrt{3}/T1$. Note that $\lim_{t_0\to 0}\gamma_{2,D} = \gamma_{1,D}$. Analogously, we get

$$\eta_-^{\pm}(\lambda,\theta) - \eta_-^{\pm}(\lambda,\theta_{2,D}) = \eta_-^{\pm}(\lambda,\theta) + \frac{t_0}{T_1} = \mp\gamma_{2,D}|\theta-\theta_{2,D}| + \mathcal{O}(|\theta_1-\theta_{2,D}|^2),$$

Let $\theta_{2,D_\pm} := \arccos(\frac{\pm t_0-1}{2})$. We now expand $\eta_\pm^-(\lambda,\theta)$ around $\theta_{2,D_\pm}$. Since

$$F(\theta) = \pm t_0 - (\theta_1-\theta_{2,D_\pm})b_\pm + \mathcal{O}((\theta_1-\theta_{2,D})^2),$$

where $b_\pm = 2\sin(\theta_{2,D_\pm})$, it follows that

$$|F(\theta)| = \pm|\theta-\theta_{2,D_\pm}||b_\pm| + t_0 + \mathcal{O}(|\theta_1-\theta_{2,D}|^2).$$

Then,

$$\eta_\pm^-(\lambda,\theta) - \eta_\pm^-(\lambda,\theta_{2,D_\pm}) = \pm\gamma_{2,D_\pm}|\theta_1-\theta_{2,D_\pm}| + \mathcal{O}(|\theta_1-\theta_{2,D})^2|,$$

with $\gamma_{2,D_\pm} = |b_\pm|/T_1$. Since $\theta_{2,D_\pm}\to 2\pi/3$ as $t_0\to 0$, it follows that $\lim_{t_0\to 0}\gamma_{2,D_\pm} = \gamma_{1,D}$. The same calculations can be done by taking $-\theta_{2,D_\pm}$. This proves the theorem for $n=2$ (see Figure 4.3).

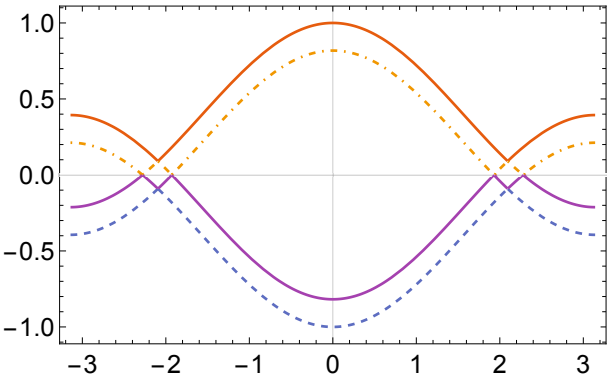

Figure 4.3: Dispersion relation for AA-stacked bilayer graphene restricted to $\mathcal{B}_d$ and $\theta_1 \in [-\pi,\pi]$; the curves are calculated for $t_0 = 0.3$.

Trilayer graphene: Now we study the Dirac cones for $n=3$. To do so, we analyze $\tilde{\eta}_\pm^\pm$ and $\bar{\eta}_\pm$, given by (4.41) and (4.42), respectively, and explicit the γ's of each cone. Analogously to the case $n=2$, Lemma 4.3.1 can be proven for $\tilde{\eta}_\pm^\pm$ with some differences:

- $\tilde{\eta}_+^+(\lambda,\theta) = \tilde{\eta}_+^-(\lambda,\theta) = \sqrt{\frac{2t_0^2}{T_1T_2}}$, for $\theta = \pm(2\pi/3,-2\pi/3)$;
- $\tilde{\eta}_+^-(\lambda,\theta) = \tilde{\eta}_-^-(\lambda,\theta) = 0$, for $\theta = \pm\left(\arccos(\frac{\pm\sqrt{2}t_0-1}{2}), -\arccos(\frac{\pm\sqrt{2}t_0-1}{2})\right)$;
- $\tilde{\eta}_-^+(\lambda,\theta) = \tilde{\eta}_-^-(\lambda,\theta) = -\sqrt{\frac{2t_0^2}{T_1T_2}}$, for $\theta = \pm(2\pi/3,-2\pi/3)$.

As in the case $n = 2$, let $\theta \in \mathcal{B}_d$. Since t_0 is close to zero, we can suppose that $T_1 = T_2$ to simplify (4.41). Recall that $G(\theta, t_0) = 4T_1T_2t_0^2 + (T_1^2 + T_2^2)F\bar{F}$. It follows that

$$G(\theta, t_0) = 4T_1^2t_0^2 + 2T_1^2F(\theta)^2$$

and

$$G^2 - 4T_1^2T_2^2(F\bar{F} - 2t_0^2) = 32T_1^4t_0^2F^2.$$

Then (4.41) turns to

$$\tilde{\eta}_{\pm}^{\pm}(\lambda, \theta) = \pm\frac{||F| \pm \sqrt{2}t_0|}{\sqrt{T_1T_2}}. \tag{4.53}$$

Note that we keep just one "T_2" in the denominator for convenience. Now we expand in Taylor's series $\tilde{\eta}_{+}^{\pm}(\lambda, \theta)$ around $\theta_{3,D} = \pm 2\pi/3$. Analogously to the case $n = 2$, it follows that

$$\tilde{\eta}_{+}^{\pm}(\lambda, \theta) - \tilde{\eta}_{+}^{\pm}(\lambda, \theta_{3,D}) = \tilde{\eta}_{+}^{\pm}(\lambda, \theta) - \sqrt{\frac{2t_0^2}{T_1T_2}} = \pm\tilde{\gamma}_{3,D}|\theta - \theta_{3,D}| + \mathcal{O}(|\theta_1 - \theta_{3,D}|^2),$$

where $\tilde{\gamma}_{3,D} = \sqrt{3/T_1T_2}$. Similarly we obtain

$$\tilde{\eta}_{-}^{\pm}(\lambda, \theta) - \tilde{\eta}_{-}^{\pm}(\lambda, \theta_{3,D}) = \tilde{\eta}_{-}^{\pm}(\lambda, \theta) + \sqrt{\frac{2t_0^2}{T_1T_2}} = \mp\tilde{\gamma}_{3,D}|\theta - \theta_{3,D}| + \mathcal{O}(|\theta_1 - \theta_{3,D}|^2).$$

Let $\theta_{3,D_\pm} = \arccos(\frac{\pm\sqrt{2}t_0 - 1}{2})$. Then

$$F(\theta) = \pm\sqrt{2}t_0 + \tilde{b}_{\pm}(\theta_1 - \theta_{3,D_\pm}) + \mathcal{O}((\theta_1 - \theta_{3,D_\pm})^2),$$

where $b_\pm = 2\sin\theta_{3,D_\pm}$, which implies

$$|F(\theta)| = \pm|b_\pm||\theta_1 - \theta_{3,D_\pm}| + \sqrt{2}t_0 + \mathcal{O}(|\theta_1 - \theta_{3,D_\pm}|^2).$$

Hence, by (4.53), it follows that

$$\tilde{\eta}_{\pm}^{-}(\lambda, \theta) - \tilde{\eta}_{\pm}^{-}(\lambda, \theta_{3,D_\pm}) = \pm\tilde{\gamma}_{3,D_\pm}|\theta_1 - \theta_{3,D_\pm}| + \mathcal{O}(|\theta_1 - \theta_{3,D\pm}|^2), \tag{4.54}$$

with $\tilde{\gamma}_{3,D_\pm} = |b_\pm|/\sqrt{T_1T_2} \to \gamma_{1,D}$ as $t_0 \to 0$. It remains to analyze (4.42). For $\theta \in \mathcal{B}_d$, we have that $\bar{\eta}(\lambda, \theta) = \pm|F(\theta)|/T_1$. However, this case is completely analogous to the case $n = 1$, but in this case we obtain $\gamma = \sqrt{3}/T_1$. Therefore, H_3^{AA} have Dirac cones (see Figure 4.4) and (i) is proven.

(ii) To study the existence of Dirac cones for H_n^{AA}, for $n \geq 4$, we consider suitable approximations of $\mathcal{M}_n^{\mathrm{AA}}(\lambda)$ by block diagonal matrices. We replace m_{t_0} and $m_{t_0}^{\intercal}$ by zero

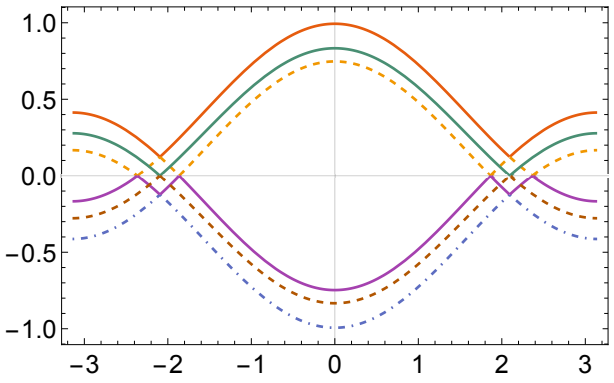

Figure 4.4: Dispersion relation for AA-stacked trilayer graphene restricted to $\mathcal{B}_d$ and $\theta_1 \in [\pi, \pi]$; the curves are calculated for $t_0 = 0.3$.

in the matrix $\mathcal{M}_n^{\mathrm{AA}}(\lambda)$, for even n, and $m_{t_0}, m_{t_0}^{\intercal}, \tilde{m}_{t_0}$ and $\tilde{m}_{t_0}^{\intercal}$ by zero, for odd n. In both cases the resulting matrix $\tilde{\mathcal{M}}_n^{\mathrm{AA}}(\lambda)$ is a block diagonal matrix with determinant given by

$$\det(\tilde{\mathcal{M}}_n^{\mathrm{AA}}(\lambda)) = (\det(M_{T_1T_2}))^2 \, (\det(M_{T_2T_2}))^m \,, \tag{4.55}$$

for even $n = 2m + 2$, and

$$\det(\tilde{\mathcal{M}}_n^{\mathrm{AA}}(\lambda)) = \det(M_{T_1T_2}) \, (\det(M_{T_2T_2}))^m \det(N_{T_1}), \tag{4.56}$$

for odd $n = 2m + 1$, with $m = m(n) \in \mathbb{N}$.

Now we show that, for any $n \geq 3$,

$$\det(\mathcal{M}_n^{\mathrm{AA}}(\lambda)) - \det(\tilde{\mathcal{M}}_n^{\mathrm{AA}}(\lambda)) = \mathcal{O}(t_0^2). \tag{4.57}$$

As already mentioned, we denote the t_0 variable in $m_{t_0}, m_{t_0}^{\intercal}, \tilde{m}_{t_0}$ and $\tilde{m}_{t_0}^{\intercal}$ by c, and by $\det_c(\mathcal{M}_n^{\mathrm{AA}}(\lambda))$ the determinant of this representation. Clearly, for $c = t_0$ and $c = 0$ we recover the original determinants, that is,

$$\det_{t_0}(\mathcal{M}_n^{\mathrm{AA}}(\lambda)) = \det(\mathcal{M}_n^{\mathrm{AA}}(\lambda)) \quad \text{and} \quad \det_0(\mathcal{M}_n^{\mathrm{AA}}(\lambda)) = \det(\tilde{\mathcal{M}}_n^{\mathrm{AA}}(\lambda)).$$

If $\frac{\mathrm{d}}{\mathrm{d}c}\det_c(\mathcal{M}_n^{\mathrm{AA}}(\lambda)) = 0$, for $c = 0$, then expanding $\det_c(\mathcal{M}_n^{\mathrm{AA}}(\lambda))$ in Taylor's series around $c = 0$, we get

$$\det_c(\mathcal{M}_n^{\mathrm{AA}}(\lambda)) = \det_0(\mathcal{M}_n^{\mathrm{AA}}(\lambda)) + \frac{c^2}{2}\frac{\mathrm{d}^2}{\mathrm{d}c^2}\det_c(\mathcal{M}_n^{\mathrm{AA}}(\lambda)) + \ldots,$$

that is, (4.57) holds. So, our task is reduced to check that $\frac{\mathrm{d}}{\mathrm{d}c}\det_c(\mathcal{M}_n^{\mathrm{AA}}(\lambda)) = 0$, for $c = 0$. Note that for any $n \geq 3$, either for even $n = 2m + 2$ or odd $n = 2m + 1$, $\mathcal{M}_n^{\mathrm{AA}}(\lambda)$ contains

$2m$ pairs of c's (for instance, for $n = 3, 4$, $m = 1$). Hence,

$$\frac{\mathrm{d}}{\mathrm{d}c}\det{}_c(\mathcal{M}_n^{\mathrm{AA}}(\lambda)) = \sum_{i=0}^{4m} \delta_i(c),$$

where $\delta_i(c)$ is the determinant of the matrix obtained by taking derivative of the column of $\mathcal{M}_n^{\mathrm{AA}}(\lambda)$ that contains the i-th c. Using the Laplace's formula in $\delta_i(0)$, we obtain matrices with either a row or a column of zeros. Then $\delta_i(0) = 0$, for $i = 1, \ldots, 4m$. Therefore, $\frac{\mathrm{d}}{\mathrm{d}c}\det_c(\mathcal{M}_n^{\mathrm{AA}}(\lambda)) = 0$, for $c = 0$, and (4.57) follows.

By taking t_0 close enough to 0, to analyze the Dirac cones for H_n^{AA}, $n \geq 4$, it suffices to analyze the Dirac cones on the roots of $\det(\tilde{\mathcal{M}}_n^{\mathrm{AA}}(\lambda)) = 0$, by (4.57). First, recall that $M_{S_1S_2}$ is given by (4.28) and N_{T_1} by (4.29). Hence,

$$\det(M_{S_1S_2}) = S_1^2 S_2^2\, \eta^4 - [2S_1S_2t_0^2 + (S_1^2 + S_2^2)F\bar{F}]\, \eta^2 + (F\bar{F} - t_0^2)^2 \tag{4.58}$$

and

$$\det(N_{T_1}) = T_1^2\eta^2 - F\bar{F}, \tag{4.59}$$

with $S_i = T_1, T_2$, with $i = 1, 2$, depending on each case. We have proven, in the case $n = 2$, that the roots of $\det M_{T_1T_1} = 0$ has Dirac cones. In a similar way, we conclude that the roots of $\det M_{T_2T_2} = 0$ has Dirac cones as well. In the case $n = 3$, we showed that the roots of $\det M_{T_1T_2} = 0$ and $\det N_{T_1} = 0$ have Dirac cones. Since the obtained γ values, which are equal or a variation of $\gamma_{i,D}$ and $\gamma_{j,D_\pm}$ (by changing T_1 by T_2), $i = 1, 2, 3$ and $j = 2, 3$, do not vanish as $c \to 0$, then we conclude that the dispersion relation of H_n^{AA} have Dirac cones in the Brillouin zone and (ii) is proven.

(iii) Finally, we analyze the dispersion relation of AA-stacked graphite operator $H_{\mathrm{g}}^{\mathrm{AA}}$. Let $\theta \in \mathcal{B}_{\mathrm{g}}^d := \{\theta = (\theta_1, \theta_2, \theta_3) \in \mathcal{B}_{\mathrm{g}} : \theta_1 = -\theta_2\}$. Then (4.43) can be rewritten as

$$\eta_\pm^{\mathrm{g}}(\lambda, \theta) = \frac{2t_0 \cos\theta_3 \pm |F(\theta)|}{T_2}; \tag{4.60}$$

recall that $F(\theta) = 1 + 2\cos\theta_1$ and $T_2 = 3 + 2t_0$. Analogously to the single graphene sheet case, we conclude that

$$\eta_\pm^{\mathrm{g}}(\lambda, \theta) - \eta_\pm^{\mathrm{g}}(\lambda, \theta_D^{\mathrm{g}}) = \pm\gamma^{\mathrm{g}}|\theta - \theta_D^{\mathrm{g}}| + \mathcal{O}(|\theta - \theta_D^{\mathrm{g}}|^2),$$

with $\gamma^{\mathrm{g}} = \sqrt{3}/T_2$ and $\theta^{\mathrm{g}} = (\pm 2\pi/3, \mp 2\pi/3, \theta_3)$, that is, the dispersion relation of the graphite operator $H_{\mathrm{g}}^{\mathrm{AA}}$ has Dirac cones (see Figure 4.5). This completes the proof of the theorem. □

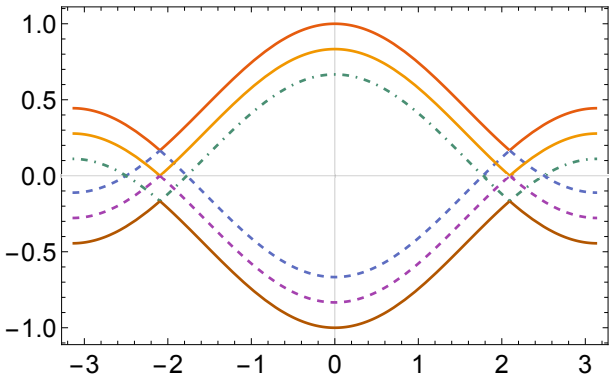

Figure 4.5: Dispersion relation for AA-stacked graphite restricted to $\mathcal{B}_{\mathrm{g}}^{d}$ and $\theta_1 \in [-\pi, \pi]$ with $t_0 = 0.3$. Three values of θ_3 were taken: $\theta_3 = 0, \pi/2$ and π. Any $\theta_3 \in (-\pi, \pi)$ generates a similar curve (in fact, interpolating).

4.4 Conclusions

We have proposed an extension of the single sheet quantum graph graphene model, discussed in [23], to the AA-stacked multilayer graphene, for any number of layers; a parameter t_0 in the zero flux boundary condition controls the intensity of the interaction between consecutive layers. The case of infinitely many layers, indexed by the integer numbers along the "z-axis" extends the model to the graphite and is periodic in the z-axis as well. An advantage of these models is that the dispersion relations are not so complicated to be found. The spectra of all such Hamiltonian operators are characterized and, in particular, eigenvalues of infinite multiplicity (the eigenvalues of the Dirichlet Hamiltonian in a single edge) are also present for all number of sheets.

With respect to Dirac cones, our results qualitatively recover theoretical and experimental findings for bilayer (see Figure 5 in [39]) and trilayer (see Figure 1(d) in [2]) graphene. In [28] the authors have concluded that AA-stacked bilayer graphene are similar to single graphene layer; we have in fact found Dirac cones for any number of AA-stacked layers and that they keep similarities to the single layer one. Our rigorous results on energy bands are also compatible with 3- and 4-layer graphene calculations by physicists (see Figure 5 in [33]), through a π-orbital continuum model with nearest-neighbor interactions. It is worth mentioning that for bilayer and trilayer graphene we have got explicit expressions for the discriminants of the Hill operators.

For the bulk graphite we have found Dirac cones parametrized by the quasimomentum $\theta_3 \in [-\pi, \pi]$, which is supported by experimental findings of Dirac fermions in

graphite [45] as well. We have indications that the Dirac cones for n-layer graphene can be approximated by selected θ_3 values for the Dirac cones in graphite; however, more investigations should be performed to prove such kind of assertion.

Chapter 5

Final Conclusions

In this work we employed quantum graph models to study the spectral characterization and (possible) presence of Dirac cones for materials with hexagonal structure. With respect to Dirac cones, our results qualitatively recover theoretical and experimental findings in all the following cases:

Boron Nitride and Dirac Operator: First, we have modelled bidimensional honeycomb materials with at most two kind of atoms by a relativistic graph model; furthermore, we have used Robin boundary conditions at vertices, so with two real parameters δ_N and δ_B, one for each vertex of the fundamental domain. All results are qualitatively valid for the (nonrelativistic) Schrödinger case.

Such Robin parameters recover the usual Neumann conditions by taking $\delta_N = \delta_B = 0$ and include a more general model of graphene (the same kind of atom at all vertices) by taking $\delta_N = \delta_B = \delta_C$. Moreover, a model for the hexagonal boron nitride was proposed by taking $\delta_N \neq \delta_B$. We have got that Dirac cones are present if, and only if, we have just one kind of atom, so generalizing results of [23] for the case of Neumann conditions (for Schrödinger operators).

For the BN case we have got a positive gap between the valence and conducting band, which agrees with results from the experimental and theoretical literature. An important point here is that such gap occurs as soon as $\delta_N \neq \delta_B$, and quantitative results depend on specific values of such parameters.

Finally, by taking $c \to \infty$, we have formally recovered the nonrelativistic parameters from the relativistic ones (at least in case of zero potential).

AB-Stacked Bilayer and Trilayer Graphene: We extend the spectral results of [23],

which propose a quantum graph model for a single sheet of graphene, to bilayer and trilayer Bernal-stacked graphene. We considered the Schrödinger operator with the stardard Neumann boundary conditions at vertices and modelled the weak interaction between the layers of graphene with a (small) parameter $t_0 > 0$ in the vanishing total flux condition. It was possible to obtain exact expressions to the dispersion relation for these materials.

In the bilayer case, it was observed that the dispersion relation is gapless with a quadratic touching and does not have any Dirac cones. On the other hand, the presence of Dirac cones was observed in the trilayer case, in the same points which occurs the quadratic touching of the bilayer graphene. For the trilayer graphene, we have found that the existence and location of D-points is independent of the value of the interlayer interaction parameter t_0. It would be interesting to investigate whether this occurs for, say, tight-binding models, at least for a range of interaction parameters; we have not found any result in this direction in the literature.

AA-Stacked Multilayer Graphene and Graphite: Finally, a similar study to the Bernal-stacked graphene was performed for the AA-stacked graphene and graphite. As in AB-stacked graphene, we got exact expressions for the dispersion relation of bilayer and trilayer graphene and it was possible to prove the existence of Dirac cones in both cases. Approximations were employed to obtain the Dirac cones for multilayer graphene, that is, $n \geq 4$. The case of infinitely many layers, indexed by the integer numbers along the "z-axis" extends the model to the graphite and is periodic in the z-axis as well. An advantage of these models is that the dispersion relations are not so complicated to be found.

Bibliography

[1] Amovilli, C., Leys, F. and March, N. Electronic energy spectrum of two-dimensional solids and a chain of C atoms from a quantum network model. *J. Math. Chem.* **36** (2004) 93–112.

[2] Bao, C., Yao, W., Wang, E, Chen, C., Avila, J., Asensio, M. C. and Zhou, S. Stacking-dependent electronic structure of trilayer graphene resolved by nanospot angle-resolved photoemission spectroscopy. *Nano Lett.* **17** (3) (2017), 564–1568

[3] Benguria, R. D., Fournais, S., Stockmeyer, E. and Van Den Bosch,H. Self-adjointness of two-dimensional Dirac operators on domains. *Ann. Henri Poincaé* **18** (2017), 1371–1383.

[4] Berkolaiko, G. and Kuchment, P. *Introduction to Quantum Graphs*. American Mathematical Society, 2012, 290 p.

[5] Brown, M. B., Eastham, M. S. P. and Schmidt, K. M. *Periodic Differential Operators*. Birkhäuser, Basel, 2013.

[6] Campos, L.C., et al. Landau level splittings, phase transitions, and nonuniform charge distribution in trilayer graphene. *Phys. Rev. Lett.* **117** (2016), 066601

[7] Castro Neto, A. H., Guinea, F., Peres, N. M. R., Novoselov, K. S. and Geim, A. K. The electronic properties of graphene. *Rev. Mod. Phys.* **81** (2014), 109–162.

[8] Coulson, C. A. Note on the applicability of the free-electron network model to metals. *Proc. Phys. Soc. A* **67** (1954), 608–614.

[9] Das Sarma, S., Adam, S., Hwang, E. H. and Rossi, E. Electronic transport in two-dimensional graphene. *Rev. Mod. Phys.* **83** (2011), 407–470.

[10] de Andres, P. L., Ramírez, R. and Vergés, J. A. Strong covalent bonding between two graphene layers. *Phys. Rev. B.* **77** (2008), 045403

[11] DiVincenzo, D. P. and Mele, E. J. Self-consistent effective mass theory for intralayer screening in graphite intercalation compounds. *Physical Review B* **29** (1984), 1685–1694.

[12] Do, N. T. and Kuchment, P. Quantum graph spectra of a graphyne structure. *Nanoscale Systems MMTA* **2** (2013), 107-123

[13] Eastham, M. S. P. *The Spectral Theory of Periodic Differential Equations.* Scottish Acad. Press, Edinburgh, 1973.

[14] Fefferman, C. L. and Weinstein, M. I. Honeycomb lattice potentials and Dirac cones. *J. Amer. Math. Soc.* **25** (2012), 1169–1220.

[15] Fefferman, C. L. and Weinstein, M. I. Wave packets in honeycomb structures and two-dimensional Dirac equations. *Commun. Math. Phys.* **326** (2014), 251–286.

[16] Freitas, P. and Siegl, P. Spectra of graphene nanoribbons with armchair and zigzag boundary conditions. *Rev. Math. Phys.* **26** (2014), 1450018.

[17] Hunt, B., et al. Massive Dirac fermions and Hofstadter butterfly in a van der Waals heterostructure. *Science* **340** (2013), 1427–1430.

[18] Jakubský, V. and Krejčiřík, D. Qualitative analysis of trapped Dirac fermions in graphene. *Ann. Phys.* **349** (2014), 268–287.

[19] Katsnelson, M. I. Graphene: carbon in two dimensions. *Materials Today* **10** (2007), 20–27.

[20] Kostrykin, V. and Schrader, R. Kirchhoff's rule for quantum wires. *J. Phys. A Math. Gen.* **32** (1999), 595–630

[21] Kuchment, P. *Floquet Theory for Partial Differential Equations.* Birkhäuser, New York, 1993.

[22] Kuchment, P. Quantum Graphs I. Some Basic Structures. *Waves Random Media* **14** (2004), S107–S128.

[23] Kuchment, P. and Post, O. On the spectra of carbon nano-structures. *Commun. Math. Phys.* **275** (2007), 805–826.

[24] Latil, S. and Henrard, L. Charge carriers in few-layer graphene films. *Phys. Rev. Lett.* **97** (2006), 036803

[25] Levitan, B. M. and Sargsjan, I. S. *Sturm-Liouville and Dirac Operators.* Kluwer Academic, Dordrecht, 1991.

[26] Liu, H., Jiang, H. and Xie, X. C. Intrinsic superconductivity in ABA-stacked trilayer graphene. *AIP Advances* **2** (2012), 041405

[27] Li, L. H. and Chen, Y. Atomically thin boron nitride: Unique properties and applications. *Advanced Functional Materials* **26** (2016), 2594–2608.

[28] Liu, Z., Suenaga, K., Harris, P. J. F. and S. Iijima. Open and Closed Edges of Graphene Layers. *Phys. Rev. Lett.* **102** (2009), 015501

[29] Magnus, W. and Winkler, S.: *Hill's Equation.* Wiley, New York (1966)

[30] McCann, E., Abergel, D. S. L. and Fal'ko., V. I. The low energy electronic band structure of bilayer graphene. *Eur. Phys. J. Special Topics* **148** (2007), 91–103

[31] McCann, E. and Fal'ko, V. I. Landau-level degeneracy and quantum Hall effect in a graphite bilayer. *Phys. Rev. Lett.* **96** (2006), 086805

[32] McCann, E. and Koshino, M. The electronic properties of bilayer graphene. *Rep. Progr. Phys.* **76** (2013), 056503

[33] Min, H. and MacDonald, A. H. Eletronic structure of multilayer graphene. *Prog. Theor. Phys. Suppl.* **176** (2008), 227–252

[34] Novoselov, K. S., et al. Unconventional quantum Hall effect and Berry's phase of 2π in bilayer graphene. *Nature Phys.* **2** (2006), 177–180

[35] Partoens, B. and Peeters, F. M. From graphene to graphite: Electronic structure around the K point. *Phys. Rev. B* **74** (2006), 075404

[36] Paton, K. R. Scalable production of large quantities of defect-free few-layer graphene by shear exfoliation in liquids. *Nature Materials* **13** (6) (2014), 624–630

[37] Pauling, L. The diamagnetic anisotropy of aromatic molecules. *J. Chem. Phys.* **4** (1936), 673–677

[38] Reed, M. and Simon, B. *Methods of Modern Mathematical Physics IV: Analysis of Operators*. Academic Press, New York, 1978.

[39] Rozhkova, A. V., Sboychakova, A. O., Rakhmanova, A. L. and Nori, F. Electronic properties of graphene-based bilayer systems. *Physics Reports* **648** (2016), 1–104

[40] Ruedenberg, K. and Scherr, C. W. Free-electron network model for conjugated systems. I. Theory. *J. Chem. Phys.* **21** (1953), 1565–1581.

[41] Shcherbakov, A. O. Regularized Trace of the Dirac Operator. *Mathematical Notes* **98** (2015), 168–179.

[42] Thaller, B. *The Dirac Equation*. Springer, Heidelberg, 1992.

[43] Wallace, P. R. The band theory of graphite. *Phys. Rev.* **71** (1947), 622–634.

[44] Watanabe, K., Taniguchi, T. and Kanda, H. Direct-bandgap properties and evidence for ultraviolet lasing of hexagonal boron nitride single crystal. *Nature Mater* **3** (2004), 404–409.

[45] Zhou, S. Y., et al. First direct observation of Dirac fermions in graphite. *Nature Phys.* **2** (2006), 595–599.